DEVELOPMENT OF AN AUTOMATIC SYSTEM TO MONITOR THE PERFORMANCE OF A DENSE MEDIUM (MINERAL) SEPARATION PROCESS

PREPARED FOR: The department of Electrical and Electronics Engineering at the University of Cape Town.

PREPARED BY: Mr P.A. Alberts
B.Sc Eng (Elec) UCT

Submitted to the University of Cape Town in partial fulfilment of the requirements for the degree of Master of Science in Engineering.

September 1989

DECLARATION

I declare that this thesis is my own, unaided work. It is being submitted for the degree of Master of Science in Engineering in the University of Cape Town. It has not been submitted for any degree or examination in any other University.

29th day of September 1989

Signed by candidate

ACKNOWLEDGEMENTS

The author is indebted to Prof B.J. Downing for his supervision, assistance and encouragement during this project, and to Dr. D. Salter (De Beers Diamond Research Laboratory, Johannesburg) for his enlightened technical input.

I would also like to thank Mr N. Wright, Mr P. Daniels and Mr A. Vinnecombe, for their help in the construction of some of the components used in this thesis.

ABSTRACT

Dense Medium Separation (DMS) is a process used extensively in the minerals processing industry to separate dense from less dense material in a dense fluid. It may be considered to be a simple "sink-float" separation process. DMS is used on a large scale in South African coal, iron ore and diamond operations.

There are, however, no commercially available systems that can determine the separation efficiency of a DMS process on-line. This presents severe problems to those operating DMS processes. The present study attempts to provide a measurement technique for on-line application.

The technique is based on the use of density tracers. These are colour coded, uniformly sized plastic beads of known density which have been used to monitor DMS processes for many years. Their distribution between the "sink" and "float" products, upon being discharged from the DMS process provides a measure of its separation efficiency. Unfortunately, they can only be used when a DMS process is not treating any material and, as such, they only provide an approximate measure of the separation efficiency.

Density tracers are fed into, and collected from, DMS processes manually. An automatic means of feeding and detecting these tracers on-line would therefore satisfy the needs of DMS operators. (The feeding mechanism was not considered as part of this study since it is a relatively simple piece of engineering.)

Active, or powered, tracers were discounted as being impractical. Metal doped tracers with an associated metal detection system were ruled out because of false signals from the ubiquitous tramp metal in DMS feed streams. Passive microwave corner reflectors proved to be equally unreliable because of similiar-strength reflections produced by the DMS products.

The solution to the tracer problem was for the tracers to receive an applied signal and to re-radiate passively a modified signal. Reception of the modified signal therefore indicates the presence of the tracer.

Frequency mixing and multiplication techniques were considered for the tracer application. Both rely on the fact that a mixer diode will produce harmonics of an incident signal, if the transmitted signal is strong enough. Frequency mixing was discounted, however, because of the need for complex, expensive, high frequency crystal locked oscillators.

The system chosen for development uses frequency multiplication. Each tracer contains a dual-frequency cross-dipole antenna with a suitable Schottky mixer diode and RF choke. The applied frequency is received by one dipole antenna causing the mixer diode to produce harmonics of this fundamental frequency. The tracer's second dipole antenna is matched, however, to radiate only the second harmonic.

Initial tests were conducted using a 500 MHz-1 GHz system. Following the success of these tests, a 3 GHz-6 GHz system was developed. The development, design and evaluation of this system is described in detail.

LIST OF TABLES PAGE

LIST OF FIGURES PAGE

GLOSSARY

Corner reflector	- right angled pyramids made of metal, designed to reflect signals independent of orientation.
Cyclone	- device for separating dense from less dense material.
DAST	- Division of Aeronautics & Systems Technology (CSIR).
density tracer	- pieces of plastic with exact specific gravities used in cyclones to measure their separation efficiencies.
diode	- semiconductor device used to rectify RF signals. It can also be used to mix two independent signals.
dipole	- device used to launch and receive electromagnetic signals.
directional coupler	- microwave component used to insert a signal from one transmission line, to an adjacent one, by inductive and capacitive coupling.
microstrip	- guiding substrate for microwave signals.
microwave freq.	- signals with a wavelength from 1 m to 1 mm.

notch filters	- device used to attenuate a certain selected frequency band.
power splitter	- device used to split a signal into two or more paths.
spiral antennas	- overmoded dipole antenna. The elements are wrapped around the feed point with the wavelength of radiation related to the diameter of the spiral.

TABLE OF CONTENTS PAGE

CHAPTER 1

INTRODUCTION

1.1 Dense Medium Separation

Dense medium separation (DMS) is a process used by the minerals processing industry to separate dense from less dense material in a dense fluid. The technique relies on the principle that two particles of different density can be separated completely if they are immersed in a liquid with a density intermediate to these two [1]. This is provided that there is sufficient settling time.

A variety of DMS equipment types exists. One of the most commonly used, especially for treating material smaller than 32 mm, is the DMS cyclone. Figure 1 shows a typical dense medium cyclone.
The cyclone consists of a cylindrical section connected to a conical section. Feed contained in a fluid medium enters the cyclone through a tangentially mounted inlet pipe in the cylindrical section.

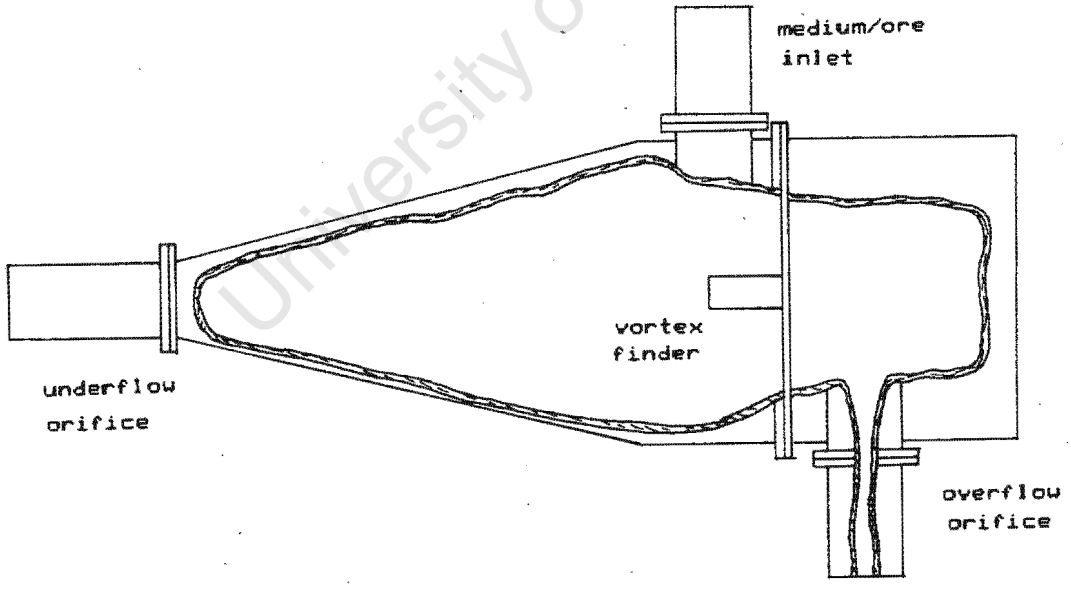

Figure 1. Cutaway view of a cyclone

High density particles are forced, under action from the centrifugal force, to move through the medium to the walls of the cyclone. They then spiral down to the underflow orifice.

Lower density particles are caught up in the air core inside the cylone, forced through the vortex pipe, and expelled through the overflow orifice at the top of the cylindrical section.

Figure 2(a) is a photograph of a typical dense medium cyclone Figure 2(b) shows a dismantled version of the cyclone.

Figure 2(a). Dense medium cyclone

Figure 2(b). Dismantled cyclone (indicating over and underflow orifices)

The fluid medium used is typically composed of powdered ferrosilicon dispersed in water. The fluid so formed has a typical density of 2700 kgm^{-3}, although under the dynamic conditions in a cyclone a pseudo density of approximately 3100 kgm^{-3} is attained.

Material that has been separated is then sent to shaking screens, where it is washed to recover the ferro silicon. The washed material falls off the edge of the screen and proceeds to futher treatment. The ferro silicon has a high magnetic susceptibility and is concentrated means of a magnetic separator for reuse. The complete dense medium separation system is shown in figure 3.

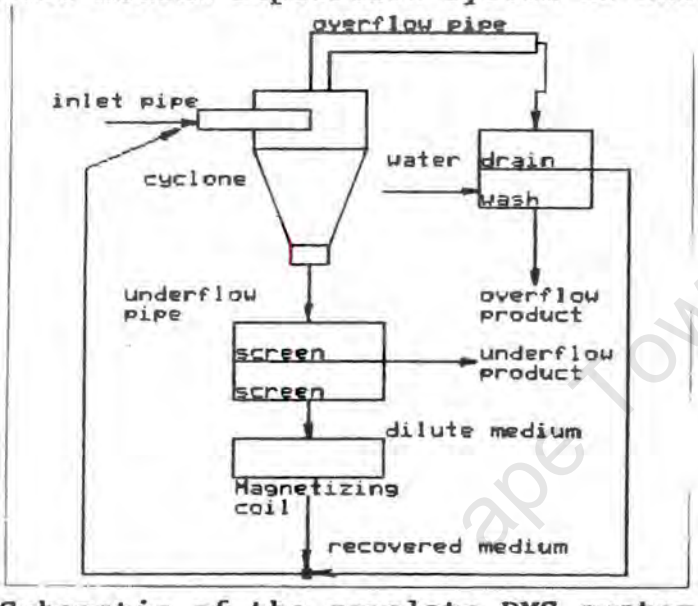

Figure 3. Schematic of the complete DMS system

Figure 4 indicates a shaking screen (underflow product).

Figure 4. Photograph of an underflow shaking screen

1.2 The Tromp Curve-measuring the efficiency of the cyclone

It is important [2] to determine the separating efficiency of a cyclone, since it gives an indication of the operable state of the cyclone. Low separation efficiencies could be caused by a variety of circumstances. The result would be a change in the operating specific gravity of the cyclone. This would cause product destined for the underflow orifice to report to the overflow orifice, and vice-versa.

This is obviously not desirable from an economic point of view.

It is thus important to be able to measure the separation efficiency of the cyclone, to timeously detect problems with the cyclone.

An indicator of the separation efficiency of a cyclone is the slope of a Tromp curve. This curve shows the percentage of feed material of a specific density collected at the underflow orifice, against specific gravity. Figure 5 indicates a typical Tromp curve.

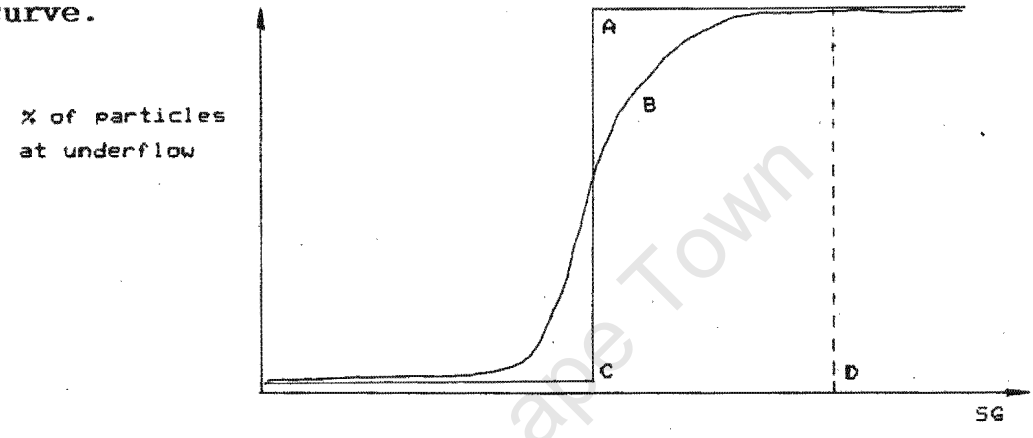

Figure 5. A typical Tromp curve

The curve shows that below a certain cut-off specific gravity C, few particles report to the underflow orifice. Above this point, it is found that most of the particles report to the underflow orifice. If a particle of specific gravity D is required to be processed, then it must be ensured that the system cut-off specific gravity C, is sufficiently low to allow the particle to report with 100% certainty, to the underflow.

It is expected [3] that the Tromp curve should have a pattern as shown in curve A in figure 5. However, particles which have a specific gravity approaching the specific gravity of the medium, will not have sufficient time to reach either the overflow (or the underflow) orifice and will report to the other product. For this reason the Tromp curve appears as curve B in figure 5. Particles which have the same specific gravity as the medium,

have an equal chance of being expelled through either the underflow or overflow pipes.

1.3 The density tracer

The material inside a cyclone is a complex mixture of ore and a fluid medium mix. It is difficult to measure the density of this mixture or how efficiently the cyclone is separating the dense from less dense particles. One widely used technique [4],[5] is to construct a Tromp curve with the aid of density tracers, and determine the separation efficiency from the slope of the curve.

Density tracers are colour coded, uniformly sized plastic beads which have a range of known densities. The beads are usually weighted with heavy metal salts to obtain the density required. These density tracers are added to the fluid medium before it enters the cyclone. Only the medium is present, and ore from the mine is not included in the feed.

The density tracers are collected by hand from the overflow and underflow screens. They are then sorted into various specific gravity categories, according to their colour. From these results a Tromp curve can be drawn and the separation efficiency determined.

Density tracers can thus provide a quick and accurate estimation of system performance. Unfortunately, they can only be used when a DMS process is not treating any material and, as such, they only provide an approximate measure of the true separation efficiency.

1.4 Problem statement

A problem arises when attempting to measure the efficiency of the cyclone on line while ore is being treated. It is not possible to count the tracers, as they are generally buried under a layer of ore particles and ferro silicon. They will thus be difficult to

collect as many could be removed with some of the larger ore particles. The others would be processed with the finer particles.

This problem of identification prompted the following question: Could a system be devised which would automatically count density tracers used in diamond and coal mineral processing?

The advantages of a system which can count density tracers remotely, while ore is being treated, are as follows:

1) Since the efficiency of separation can be measured while the ore is being treated, the cyclone does not have to be off-line to the rest of the plant.

2) The density tracers are counted by computer, not by hand. This means that the processing time of the information is increased, and consequently the response time to the information.

3) The cyclone and the automatic counting system can be connected in a closed loop control system to ensure that the cyclone is operating at its maximum efficiency. Control can be achieved by altering the density of the fluid medium used and determining its affect on the separation efficiency.

A completely new type of density tracer is required to enable it to be detected by some remotely situated system. Analysis of ore treatment operations gave the following criteria for the tracers.

1) They must comparable in size to the ore being processed. In the diamond mining industry, the maximum size would be 32 mm.

2) The cost per density tracer must be less than R1.50.

3) There must be little upkeep. This would imply that the density

tracers contain no battery driven components. Thus, a passive means of detecting the density tracer must be employed.

4) The density tracer must be able to exist in the harsh environment of the dense medium cyclone.

1.5 Objective of thesis

The aim of this thesis is to investigate various passive detection techniques for counting density tracers, and construct a prototype of the most suitable scheme.

The system must comply with the above specifications.
An analysis of possible detection techniques is presented. A suitable scheme is then recommended. The method is commented on, and experimental procedures and results are discussed. The design, construction and testing of a prototype is described.

Recommendations are given with regard to the final integration of the product in the dense medium separation system. Conclusions are drawn as to the suitability of the system.

CHAPTER 2

DETECTION OF THE DENSITY TRACER

2.1 Passive & Active detection

The terms passive and active detection are chosen to indicate the targets status in the detection process. A passive detection technique can be defined as one where the target has no means of signalling its presence. It uses a physical phenomenon , such as reflection, to indicate its location. An example of this would be an object detected by radar. The object can be detected, and to an extent identified, by its reflectivity at radar frequencies. Identification can be estimated from the amplitude of the reflected signal or the radar cross section.

Active detection involves a target indicating its presence by signalling, in some manner, on request. A typical example of this are transponder system on aircraft or spacecraft. The aircraft will transmit a sequence of codes, identifying itself, on receipt of a specific signal from an airport radar.

In choosing which type of detection system will be used, it is important to see the advantages and disadvantages of both techniques.

Active detection is a simpler technique. A transmitter could be mounted into a density tracer. The signal could then be received, indicating the presence of a density tracer. The receiver would also not have to be as sensitive as that used in a passive detection system. This is because an active detection system relies on a $1/r^2$ rule as opposed to the $1/r^4$ rule observed by passive detection.

Active detection systems have the disadvantage that they require an energy source to power their transponder systems. The

practical result of this in the density tracer detection scheme would be an increase in the time spent servicing such a device. Active detection density tracers would be more expensive than those for a passive detection system, since the miniature transmitter circuits would be expensive to design and build.

Passive density tracers are cheaper to build and require less upkeep than active density tracers. However, they need more powerful transmitters and more sensitive receivers.

Since cost and upkeep are of primary interest for this application, a passive detection system will be used.

2.2 Examination of various passive detection techniques

2.2.1 Metal Detection

2.2.1.1 Theory of metal detection

Metal detection relies on the fact that an object with a high magnetic susceptibility , will cause an increase in the flux linkage between two neighbouring coils. See figure 6. The increase in the flux linkage between the coils will cause an increase in the induced voltage in coil B (figure 6).

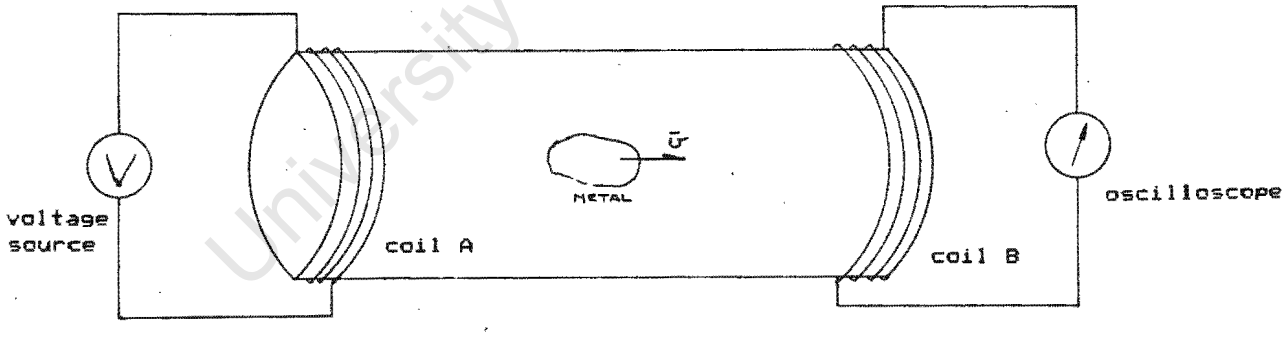

Figure 6. Metal detection test rig

If these coils were now mounted below the underflow shaking screen, as shown in figure 7., a metal density tracer would indicate its presence by an increase in coil B's induced voltage.

The density tracers could thus be counted by determining the number of times the voltage level rose above a certain threshold.

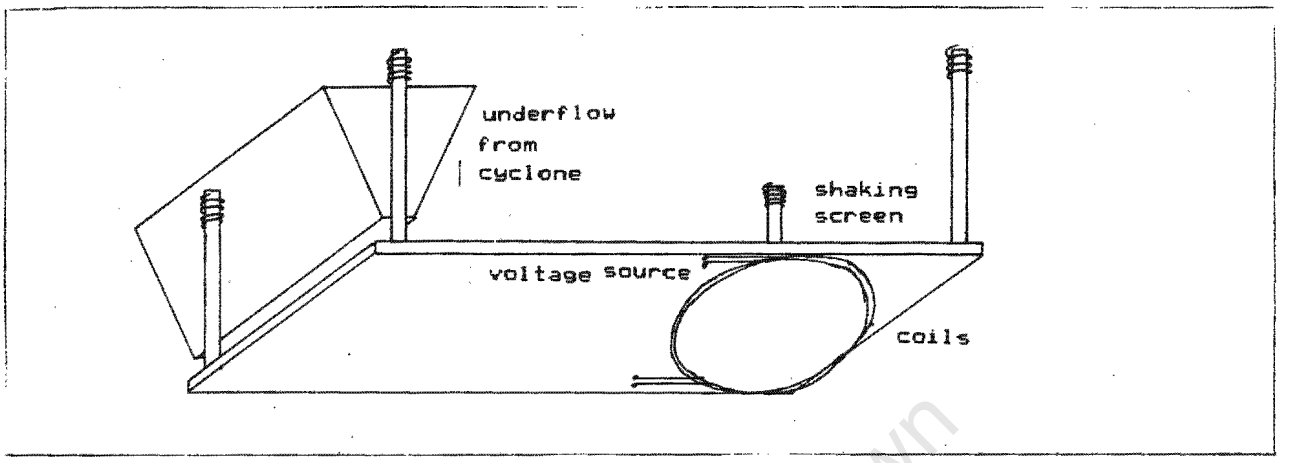

Figure 7. Coil positions under shaking screen

A problem with this system, however, is that since it has a low resolution (difficult to focus magnetic fields) it is difficult to discriminate between different metal types or sizes. Accompanying the ore from the mine is a substantial amount of extraneous metallic material, hammer heads, pieces of girders, copper wire etc.

2.2.1.2 Conclusions

It would be difficult to determine the difference between a metallic density tracer and another piece of metal. It has also been proven too expensive to remove the extraneous metal from the ore. Metal detection is thus not a viable technique to count density tracers.

2.2.2 Investigating Microwave corner reflectors as density tracers

2.2.2.1 Theory of corner reflector operation

For the role of a density tracer it is desirable to have a small radar target with a large radar cross section [6]. The larger the

radar cross section, the greater the signal return. A flat metal plate could be used, its radar cross section is given by:

$$\sigma_p = 4 * \pi * A^2/\lambda^2 \qquad ..(2.1)$$

where σ_p = radar cross section in m^2

A = area of metal plate in m^2

λ = wavelength in m

The reflection from a metal plate is very orientation dependent, the radar cross section drops rapidly as the sheet is rotated. The return is strongest along the normal.

A construction that provides better orientation dependance with good radar cross section, is the microwave corner reflector.

Microwave corner reflectors are devices that reflect input signals back along their incident paths. Figure 8 indicates a triangular corner reflector and the path of a beam entering the device.

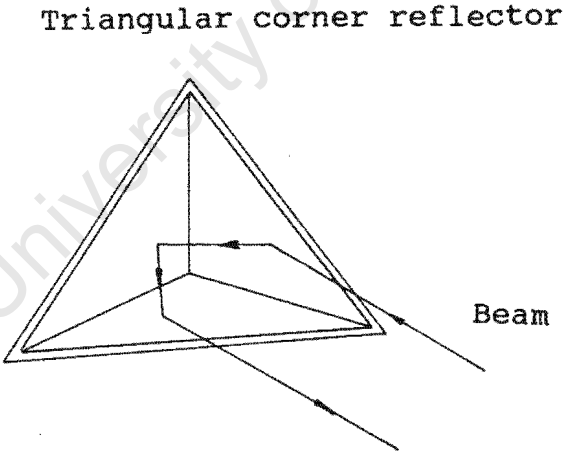

Figure 8. Microwave corner reflector

Microwave corner reflectors are simply three mutually perpendicular metallic plates. As a beam enters the corner reflector, it is reflected three times and returns along its incident path.

The cross sectional area of the triangular corner reflector can be obtained by equating the effective area of the flat plate to the maximum area of the triple reflections.

The maximum area of triple reflection is that afforded by the corner when it is viewed along its axis of symmetry. This area is a hexagon as shown in figure 9.

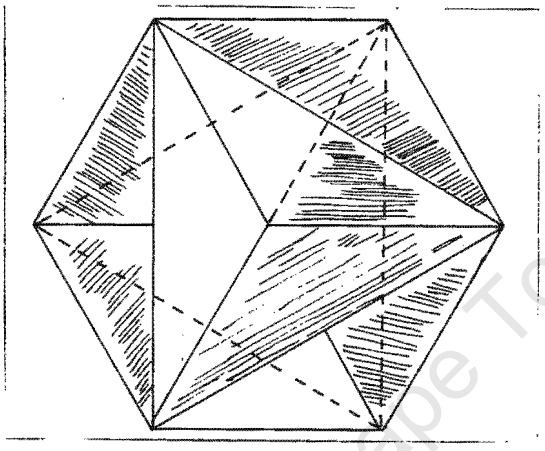

Figure 9. Maximum area of reflection from reflector

The maximum area of reflection of the triangular corner reflector is then given by:

$$A_{max} = a^2/\sqrt{3} \qquad ..(2.2)$$

where a = edge length of a corner reflector in m.

subst. (2.2) into (2.1) yields for triangular reflectors:

$$\sigma_t = 4*\pi*a^4/3*\lambda^2 \qquad ..(2.3)$$

2.2.2.2. Measuring reflected power from corner reflector

A microwave corner reflector was designed and constructed with an edge length of 50 mm. The corresponding radar cross section is 0.356 m^2 9 from eq. (2.3))

A test setup consisting of a 35 GHz transmitter and horn antenna, a 35 GHz receiver and horn antenna and spectrum analyser, is mounted 30 cm above a table of rocks. The antenna gains were approximately 28 dB. The test rig is shown in figure 10.

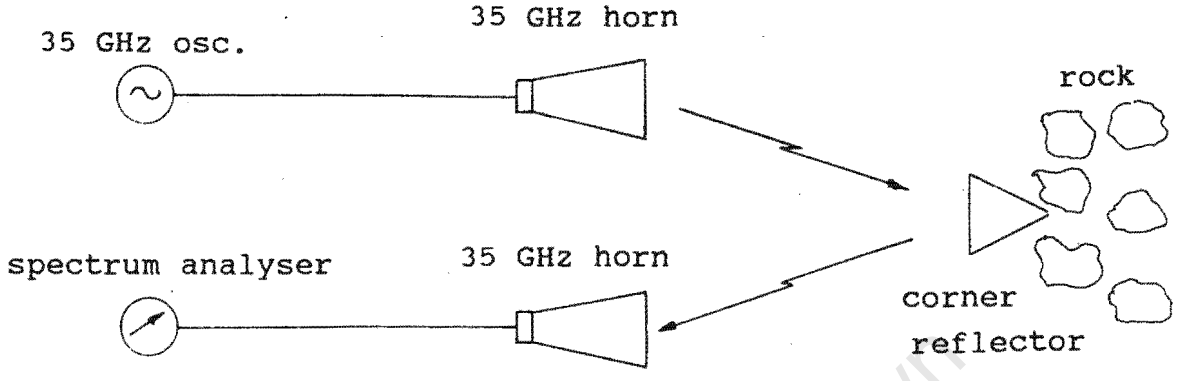

Figure 10. Test rig measuring reflections from corner reflector

2.2.2.3 Results

It was found that the reflected power from the rock mixture varied dramatically with rock orientation. The return signal varied between -40 dB and -60 dB as viewed on the spectrum analyser. The corner reflector was placed in the path of the signal, to ensure maximum possible signal return. At best this was found to be -40 dB.

Thus the best resolution available with a 100 mm diameter corner reflector at 35 GHz, is comparable to the return from certain rock orientations. The reason for this is that at 35 GHz, there will not be an appreciable specular reflection from these rocks. This means that seen along the normal a rock will appear to be a relatively flat plate.

A large corner reflector (side length 350 mm, radar cross section 855.567 m^2) was placed in the path of the 35 GHz signal. The assumption being that if there was an appreciably better signal return with a 350 mm edge corner reflector at 35 GHz, then the original 50 mm edge length corner reflector would work well at 350/50*35 GHz = 245 GHz. However, the maximum signal was

again measured to be -40 dB. This means that the corner reflector would not benefit from operating at a higher frequency.

The fact that increasing the radar cross section had no effect on the signal return can be explained as follows. The corner reflector is operating within the near field of the horn antennas. Thus the radar cross section is not valid here, and hence the reflected power is not linearly dependent on radar cross section or the inverse fourth power of distance. Further, for efficient operation the frequency would have to be increased to ensure specular reflections occurred from the rocks. At these high frequencies signal penetration through surface sludge or contamination is negligible and the corner reflector would have to be kept perfectly clean.

2.2.2.4 Conclusions

The reflections from rocks in certain orientations may be of the same magnitude as a corner reflector. For this reason corner reflectors are not suitable as density tracers.

CHAPTER 3

COUNTING DENSITY TRACERS BY FREQUENCY MIXING OR MULTIPLICATION

3.1 The technique of frequency mixing and multiplication

Another passive means of detection relies on frequency mixing or multiplication. A Schottky mixer diode has a non linear voltage current characteristic which produces harmonics of any sufficiently large signal incident on it. It can also accept two signals and produces their mixed components.

These characteristics provide two ways of detecting density tracers. In both cases a mixer diode is inserted into a density tracer. The frequency mixing technique will require two transmitters operating with frequencies A and B. The diode will produce a mixed component of frequency A-B, this signal will be detected by a receiver and will thus indicate the presence of a density tracer.

In the case of frequency multiplication, a single transmit frequency is used. The mixer diode receives the signal and produces harmonics. The second harmonic has the highest amplitude and will thus be the easiest to detect. The density tracers can thus be counted by noting the number of second harmonic pulses received.

3.2 Analysing the frequency mixing technique

As stated previously the mixing technique would require two transmitters/antenna combinations. The mixer diode would be mounted across the feed points of an antenna, as shown in figure 11, inside a density tracer. This antenna would be efficient at receiving the two transmit frequencies as well as transmitting their mixed component. A suitable antenna would be the spiral antenna.

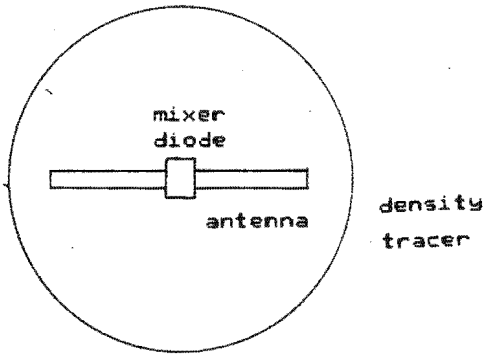

Figure 11. Mixer diode mounting

3.2.1 The spiral antenna

This antenna has a very wide bandwidth and is thus able to operate at the three frequencies required by the mixing technique. This antenna has the useful property that it is circularly polarised. The density tracer falls off the screen in any orientation, thus the signal it receives from the transmitter will be in an unknown plane of polarisation. With a circularly polarised antenna, the plane of polarisation would not be an issue. Generally the antenna efficiency would be 3 dB lower due to it being circularly polarised, but the benefits overshadow this slight loss in efficiency. The spiral antenna is shown in figure 12.

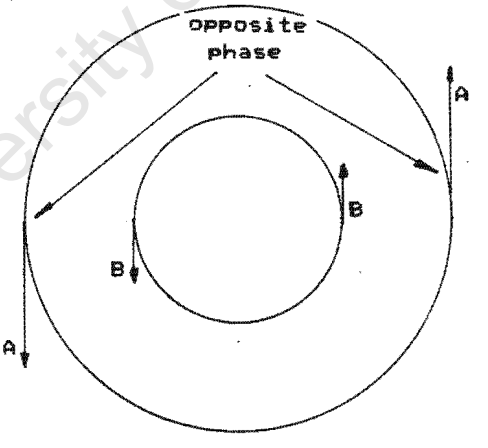

Figure 12. The spiral antenna

The spiral antenna will radiate when currents of opposite phase are exactly one wavelength apart. This means that the antennas

bandwidth will be determined by its width. For lower frequency signals the antenna will radiate near the edges (as in point A), higher frequency signals will tend to radiate near the center of the spiral (point B).

The relationship between the wavelength and the diameter of the spiral is:

$$\lambda = \pi * D \qquad ..(3.1)$$

where λ = wavelength of signal
D = diameter of spiral

Assuming that the maximum diameter of the density tracer is 32 mm, the wavelength of the lowest frequency is given by (3.1)

$$\lambda = \pi * D$$

$$= 3.1415 * 32$$

$$\lambda = 100.53 \text{ mm}$$

The frequency of operation is given by:

$$f = c/\lambda \qquad ..(3.2)$$
$$= 3*10^{-8}/100.53*10^{-3}$$
$$= 2.98*10^{9} \text{ Hz}$$

Thus 3 GHz is the lowest frequency and will be the mixed component in the system.

Assuming that one of the transmitters is operating at 4 GHz, the other would have to operate at 4+3 = 7 GHz.

3.2.2 The frequency mixer/counter system

Figure 13 indicates a density tracer counting system using frequency mixing.

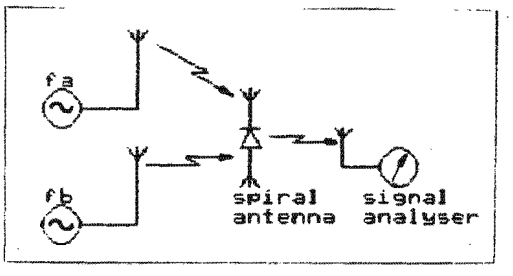

Figure 13. Frequency mixing/density tracer counter system

To ensure that the receiver is detecting the mixed signal, i.e. the mixed component, we will have to reference it to the transmitters. There are two ways of doing this.

1) Crystal locking the transmitter oscillators to form a stable reference for the mixed component.

2) Installing a sweep-and-lock circuit at the receiver. This circuit will sweep over a desired bandwidth and detect and lock onto a signal received from the mixer diode.

The problem with solution 1 is that crystal locked oscillators are expensive, especially at 7 GHz. This would not be an economically viable solution. Solution 2 also has its problems, as shown below.

It is assumed, as in figure 13, that the density tracer is detected in free fall over the shaking screen. There is a maximum range at which the density tracer/ mixer diode can be detected. If this is assumed to be 30 cm (suitable distance from edge of

screen to detection unit), then the time taken for the density tracer to fall through this distance is given by:

$$t = \sqrt{2*s*g} \qquad ..(3.3)$$
$$= \sqrt{2*30*10^{-2}*9.8}$$
$$= \underline{0.247 \text{ seconds}}$$

where s = distance in m
g = gravitational acceleration in m/s^2
t = time in s

Most sweep-and-lock circuits take longer than this to lock onto a received signal. The circuit used on the Plessey MRA-7 distance measuring survey instrument device locks after 0.5 s. Thus a sweep and lock circuit that could detect signals in time would need expensive and intricate circuitry.

To summarise then, the mixing technique has the disadvantage that it's transmitter needs two oscillator/antenna systems. Referencing the mixed component to the receiver, so as to ensure early detection, will require either expensive crystal locking oscillators or quick sweep and lock circuits.

3.2.3 Conclusions

Considering the various disadvantages and advantages it appears that frequency mixing is not a satisfactory technique from the point of view of economics. Frequency multiplication will be analysed in the next chapter, to see if it is a more cost effective means of counting density tracers.

CHAPTER 4

MICROWAVE FREQUENCY MULTIPLICATION

4.1 A description of a prototype multiplication system

It has already been described how density tracers can be counted by detecting the second harmonic reflected from a Schottky mixer diode.

A frequency multiplication system has proven to be a simpler technique, since only one transmitter/antenna system is necessary. It was decided to test this technique by using available components such as the HP 3595 RF plug in unit as a variable oscillator and a HP 8555 signal analyser as the detection unit.

For ease of construction a half wave dipole antenna constructed from round brass rods would be used for the transmitter and receiver units. A fundamental frequency [7],[8] of 500 MHz was chosen to test this principle, as this gave a manageable transmit antenna dipole length of:

$$l = \lambda/2 = c/(2*f) \qquad ..(4.1)$$
$$= 3*10^8/2*500*10^6$$
$$= 300 \text{ mm}$$

Figure 14 shows the dipole and its electrical length.

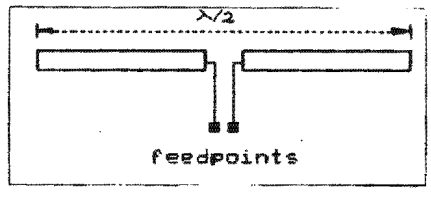

Figure 14. Electrical length of 500 MHz dipole

Further, it is less critical to end effects loading and feed point impedance discontinuity effects than a spiral antenna.

The receiver unit will detect the second harmonic of the fundamental frequency reflected from the mixer diode. It will thus require a receiver operating at 1 GHz. For simplicity another dipole antenna will be used, and constructed from brass.

All that is required is to decide upon a suitable mixer diode and the antenna which will receive the fundamental frequency and transmit the multiplied second harmonic.

It was decided to use a HP 5802-2800 Schottky mixer diode as they are readily available and they operated adequately over the bandwidth of the system.

The choice of antenna upon which the mixer diode is mounted, is important. It must be able to operate at the fundamental frequency as well as the second harmonic. The antenna must also have a wide beamwidth. The reason for this is that the density tracer can be in any orientation after rolling off the edge of the screen. The antenna may then present a null in its radiation pattern towards the receiver, which might result in the density not being detected.

In the previous chapter, it was shown how a spiral antenna was used in a frequency mixing technique. The mixer diode was mounted between the feedpoints of the spiral antenna. The spiral antenna being wide band would receive the two fundamental frequencies and transmit the mixed component. This antenna has the following characteristics.

a) wide bandwidth
b) circularly polarised

c) reasonable beamwidth
d) good radiation efficiency

This antenna would also be suitable for the frequency multiplication technique. The mixer diode could be mounted across the feedpoints of the antenna, as shown in figure 11. A spiral antenna could not be obtained which operated between 500 MHz and 1 GHz (DAST supplied spiral antennas which operated from 2 GHz to 18 GHz).

It was decided that an antenna would be chosen that could operate at both transmit and receive frequencies with a reasonable beamwidth . The antenna would have to be efficient at radiating at these frequencies (low return loss). The criterion of circular polarisation, would be dropped, as the system was a prototype, and the density tracer would be detected statically (density tracer would not be detected as it was falling). An antenna which fulfilled this requirement was the cross dipole antenna.

It will be described in the next section.

4.2 The cross dipole antenna

An [9],[10] antenna which satisfies the criterion of operating at two frequencies, is the cross dipole antenna (shown in figure 15).

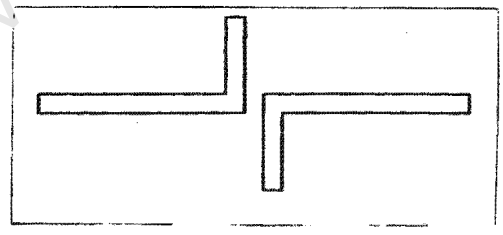

Figure 15. The cross dipole antenna

The elements of the dipoles are orthogonal to each other. This means that the electric fields of the two dipoles are at right

angles to each other, minimizing any coupling between the dipoles.

The elements lengths are in the ratio 2:1 since the antenna has to operate at both the fundamental and second harmonic. This improves the isolation for the following reasons. The longer element will appear as a resistive impedance across the feedpoints for the fundamental frequency (point A), but will be an open circuit for the second harmonic (point B). The voltage waveforms indicate this in figure 16(a). Similarly the shorter elements appear as a resistive impedance at the feedpoints at the second harmonic (point A figure 16(b)), but will be a high impedance at (point B) for the fundamental, as can be seen in figure 16(b).

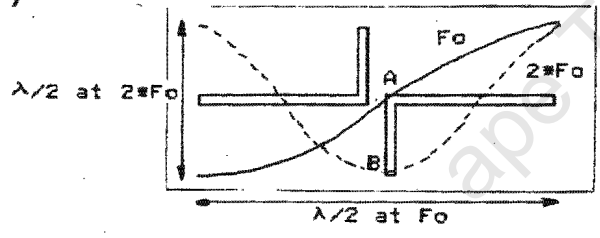

Figure 16(a). Operation of fundamental mode element

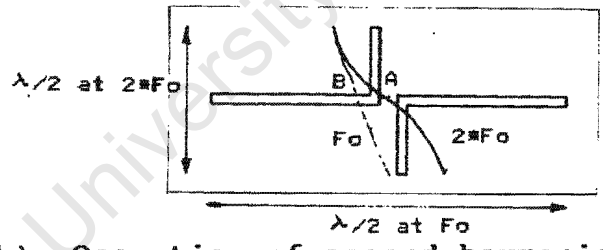

Figure 16(b). Operation of second harmonic mode element

This means that the antennas are isolated from each other and the fundamental frequency will radiate more efficiently through longer element. Thus the second harmonic frequency radiate more efficiently through the shorter elements.

4.3 Constructing the antennas for the prototype multiplication system

The prototype multiplication system requires the following antennas:

A 500 MHz transmit dipole

A 1 GHz receive dipole

A 500 MHz/ 1 GHz cross dipole

The dipoles would be constructed from brass rods (cross section 6 mm). Brass rods are easier to solder than the traditional antenna material, aluminium.

Two dipoles were constructed, and their lengths reduced, until the resonant frequencies were approximately 500 MHz and 1 GHz. Figure 17 shows the return loss plots for the two antennas.

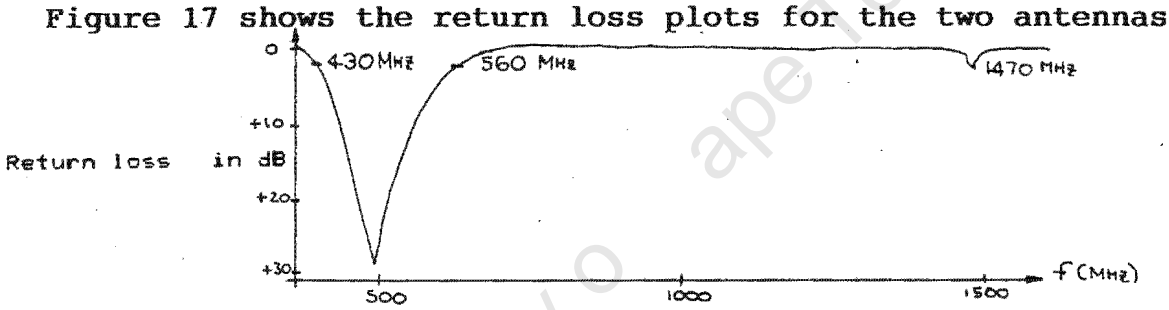

Figure 17(a). Return loss for transmit dipole

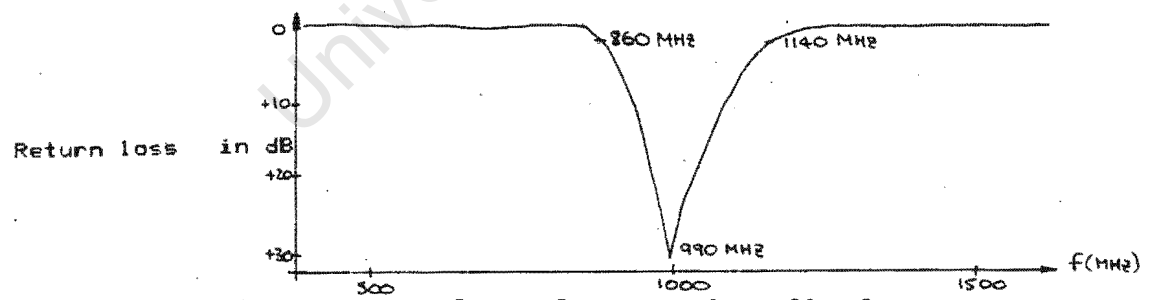

Figure 17(b). Return loss for receive dipole

Table 1 shows the characteristics more clearly.

Resonant frequency (MHz)	bandwidth (MHz)	Return loss (dB)
480	130	25
990	260	30

Table 1. Characteristics of transmit and receive dipoles

The 500 MHz/1 GHz cross dipole antenna was constructed using the same 6 mm brass rod. Element lengths of 144 mm and 60 mm were finally chosen. The dipole elements were soldered together and an SMA-coax adapter was soldered to the feedpoint.

The return loss plot was obtained and can be seen in figure 18.

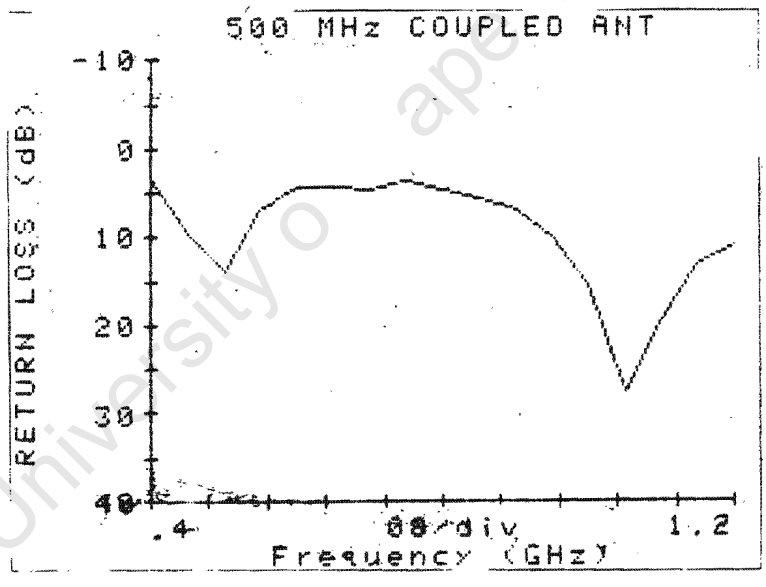

Figure 18. Return loss for 500 MHz/1 GHz cross dipole antenna

Table 2 shows the characteristics of this antenna as obtained from the network analyser.

Resonant Frequency (MHz)	Bandwidth (MHz)	Return loss (dB)
500	150	15
1030	270	25

Table 2. Characteristics of cross dipole antenna

4.3.1 Choosing the correct choke for the cross dipole antenna

The mixer diode placed across the feedpoint required a reference bias voltage. Since we are using a schottky diode, the reference voltage is zero voltage. All that is needed then is to place a choke across the diode, to provide a closed DC path for rectified current to flow. The mounting of the choke is shown in figure 19.

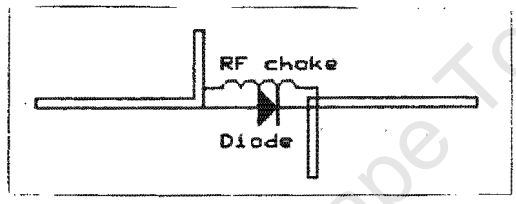

Figure 19. Choke mounting on cross dipole antenna

It is important to choose a choke with a sufficient number of turns. An unsuitable choke will effect the match of the antenna, as well as its resonant frequency.

Chokes were designed using 0.2 mm diameter copper wire. It was found that the resonant frequency decreased as the number of turns of the choke was increased. When too few turns were used, the amplitude of the reflection coefficient was reduced. A choke with 12 turns was chosen. Figure 20 shows the return loss of the loaded cross dipole antenna.

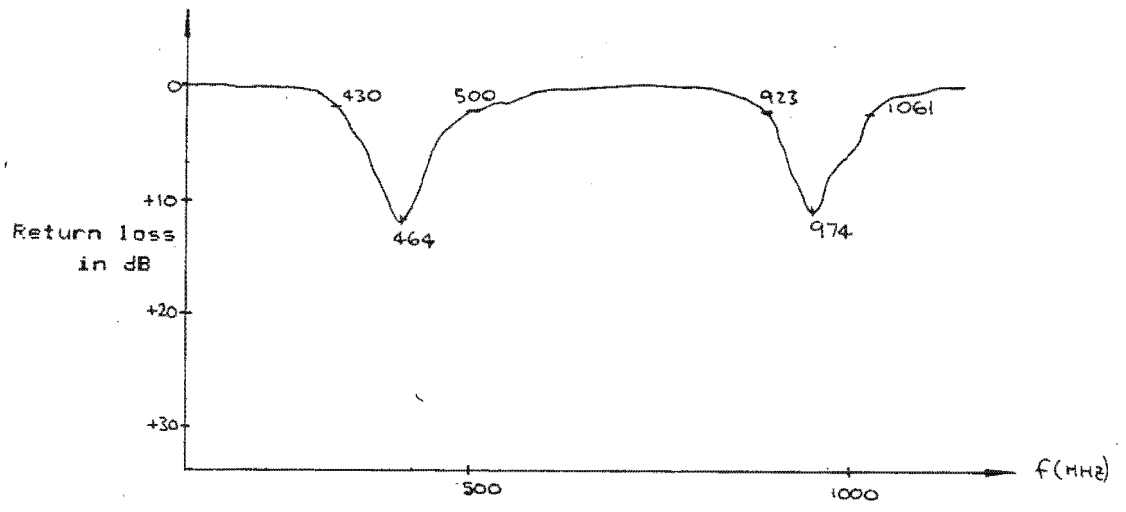

Figure 20. Return loss of cross dipole with 12 turn choke

4.4 Filtering the RF plug in's second harmonic

An HP 3595 plug in was used as a transmitter. It was found that the oscillator produced the second harmonic 20 dB below the fundamental frequency. It is important to reduce the amplitude of the second harmonic from the oscillator,because it could be confused with the multiplied second harmonic from the mixer diode. A suitable filter would be a quarter wavelength cavity resonator (λ = 500 MHz).

4.4.1 Designing the quarter wavelength cavity resonator

A [11] quarter wavelength cavity resonator is a device which allows the fundamental and odd harmonics to propagate, while filtering the even harmonics (including the second harmonic).

It was decided that a circular coaxial cavity resonator be used. To obtain the maximum match (maximum Q-factor), the ratio of the radii r_1 and r_2 (as in figure 25) must be 3.6. Aluminium tubing with an outside diameter of 101.85 mm and an inner diameter of 94 mm, was obtained. A solid brass rod of with a diameter of 15.07 mm would be used for the inner conductor. The ratio of the radii is:

$$r_2/r_1 = (94.90/15.07)/2 \qquad ..(4.2)$$
$$= 3.8$$

The completed cavity resonator is shown in figure 21.

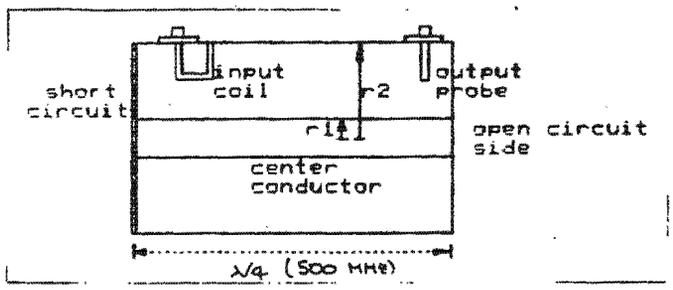

Figure 21. 500 MHz coaxial cavity resonator

It can be noted that the signals are propagated by a loop on the short circuit side of the cavity. A metal plate shorts the aluminum outer conductor to the brass inner conductor. Signals are received via the output probe at the open circuit side of the resonator.

Figure 22 shows the return loss and insertion losses for the cavity resonator.

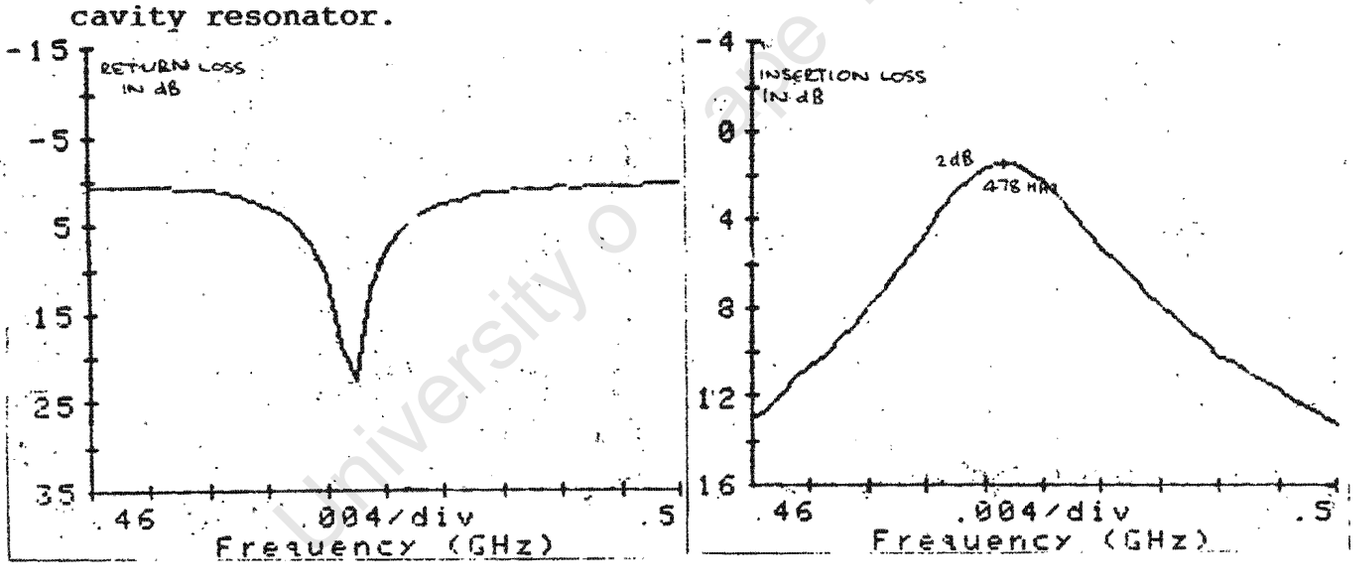

Figure 22. Return and insertion losses for the cavity resonator

From the figures it can be noted that the cavity resonator has an insertion loss of 2 dB at 478 MHz. From figure 23 it can also be seen that the insertion loss at 956 MHz is 30 dB.

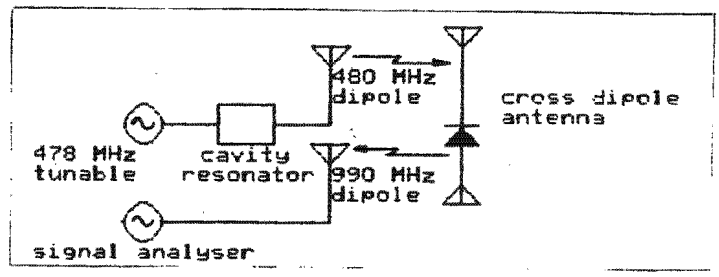

Figure 24. Frequency multiplication test setup

To obtain maximum benefit from the fact that the resonator operated at 478 MHz, the RF plug in was tuned to this frequency. The fact that the frequency is 22 MHz short of the expected fundamental frequency, is of little consequence. The antennas in the system have wide enough bandwidths to accept both the 478 MHz fundamental and its 956 MHz second harmonic.

The cavity resonator is attached to the RF plug in oscillator via the short circuit input coil. The transmit antenna is attached to the output probe of the cavity resonator. The receive antenna, connected to the signal analyser, was placed at right angles to the transmit antenna. This was to receive maximum isolation from the planar travelling wave from the transmit antenna, and hence any residual second harmonic component. The distance between the antennas was set at 20 cm.

An HP 5802-2800 schottky mixer diode and a 12 turn choke were placed across the feedpoints of the cross dipole antenna. It was then placed between the transmit and receive antennas.

4.5.1 Results

The sweep oscillator was set to a center frequency of 478 MHz, the power level of the RF plug in was set to 19.5 dBm. The signal analyser indicated that the fundamental frequency (478 MHz) had an amplitude of -30 dB.

It was found that the second harmonic rose from -50 dBm to -20 dBm as the cross dipole antenna was inserted between the transmit and receive antennas. The -50 dBm signal was that of the second harmonic from the filtered sweep oscillator. Thus the signal returned from the schottky diode was 30 dBm higher.

In a further experiment the choke was removed and an ammeter connected across the feedpoints. The ammeter acted as a low impedance hence satisfied the need for a DC path. It was found that the current rose from 0 to 1.5 mA when the cross dipole antenna was placed between the transmit and receive antennas. A diode turns on hard when it draws more than about 1 mA of rectified current. This thus confirms that the schottky diode has switched on, and is generating harmonic components.

4.5.2 Conclusions

From the results it can be seen that the frequency multiplication system operates satisfactorily. The diode switched on hard and provided a significantly large second harmonic to be detected by the receive system.

4.5.3 Recommendations

It has been proven that the 478 MHz/956 MHz frequency multiplication system works as anticipated. However, to fit into the density tracer, the antenna would require a smaller diameter of (32 mm), and hence a higher frequency than the 500 MHz/1 GHz system. Such a system could use spiral antennas. However, those obtained from DAST, which operated from 2 GHz to 18 GHz, were

still too large (45 mm) to use in the system.

The alternative was to scale down the cross dipole antenna used in the 500 MHz/1 GHz system, to a diameter of 32 mm.

A cross dipole antenna of 120 mm diameter was constructed, using brass rods, as for the 500 MHz/1 GHz system. The antenna would not operate in its dual frequency mode and was highly inefficient. The reason for this was that the element lengths were much shorter and the ratio of diameter of rod to element length, was effecting the match of the antenna.

The solution was to load the load the antenna with a dielectric backing, so that it could operate at a lower frequency. Another advantage was that the axial ratio (ratio of diameter to length of the antenna element) could be reduced so that the effect on the antennas match was less. The material used was printed circuit board (PCB).

It was found that although the dielectric constant was not as accurately defined for this material as RT-Duroid or other microstrip boards, it could still be used at frequencies up to 6 GHz.

Instead of designing an antenna with a diameter of 32 mm (and hence higher frequency), it was decided to design an antenna at an intermediate frequency of approximately 1 GHz (with the multiplied harmonic at 2 GHz).

The antenna would be etched onto PCB and the match and radiation pattern measured. The reason for this would be to determine if the antenna operated as two distinct, isolated dipoles. If they operated correctly, then the antenna size could be scaled down even further to the limit required by the density tracer counter circuit.

4.6 Testing a cross dipole antenna

A cross dipole antenna was required to indicate its performance as a dual frequency antenna. Frequencies of 1 and 2 GHz were chosen. As shown previously, the antenna would be etched onto PCB.

The simulation package "EESOF Linecalc" was used to obtain the lengths of each of the elements. The PCB had the following characteristics.

Dielectric constant ϵ_r = 4.8
Height of dielectric H = 1.6 mm
Thickness of copper t = 0.017 mm
Ratio of copper loss RGO = 0.84
Loss tangent = $9*10^{-4}$
Characteristic impedance = 50Ω

As can be seen from Appendix A, the lengths and widths of the lines are as summarised in Table 3.

freq (GHz)	length (mm)	width (mm)
1	39.607	2.83
2	19.73	2.81

Table 3. Dimensions of 1/2 GHz cross dipole antenna

Figure 25 shows the positive printed version of this antenna

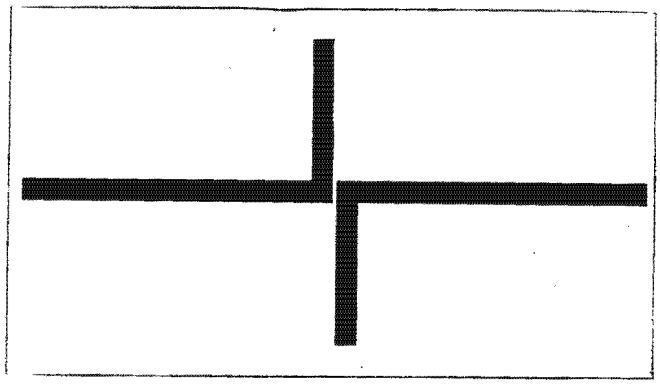

Figure 25 1/2 GHz cross dipole antenna

The antenna was drawn four times oversize and then photo reduced to improve accuracy.

4.6.1 Results of tests on 1/2 GHz cross dipole antenna

4.6.1.1 Measuring the return loss

A short length of copper coaxial-to-SMA line was soldered to the feedpoints of the antenna. The antenna was then connected up to the test arrangement, as shown in figure 26. The following equipment was used to test the match of the antenna:

HP 8350 B	sweep oscillator
HP 8410 C	network analyser
HP 8746 B	S-parameter test set
HP 3595 B	RF-plug in

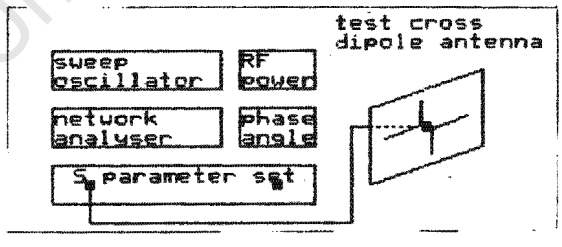

Figure 26. Test rig to measure antenna match

Figure 27 shows the return loss $(S11)^2$ characteristic for this

antenna. As can be seen the antenna is not resonating at exactly 1 and 2 Ghz. The fundamental frequency is 1.43 GHz with the second harmonic at 2.86 GHz. THe characteristics of this antenna can be seen in Table 4.

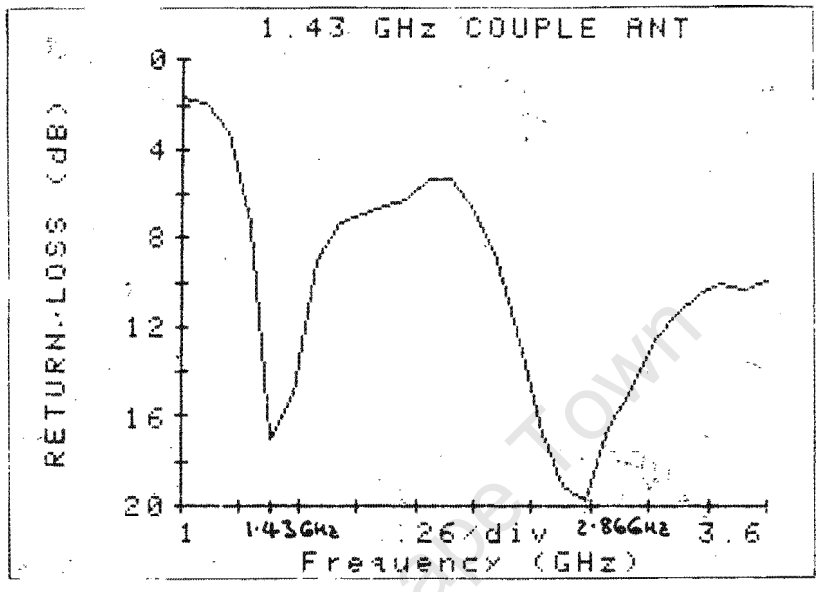

Figure 27. Return loss plot for the 1/2 GHz cross dipole

Center frequency (Ghz)	HPBW (MHz)	S11(dB)
1.43	330	-17
2.86	790	-20

Table 4. Loss characteristics for 1/2 GHz cross dipole

There are many factors which influence the resonant frequency of an antenna. It has been shown that the end effects, produced by the ratio of the diameter of the element to its length, cause the antenna to resonate at a lower frequency. However, their would be an increase in the resonant frequency due to the field in the immediate vicinity of the dipole elements being partly confined within the dielectric of the PCB. The wavelength then becomes:

$$\lambda_g = \lambda_o / \epsilon_r' \qquad ..(4.3)$$

where λ_g = wavelength through microstrip
λ_o = free space wavelength
ϵ'_e = effective dielectric constant of the PCB dielectric and air combination surrounding the dipoles.

This factor is, however, taken into account by the simulation package LINECALC.

The final factor which influences the resonant frequency of the antenna is the gap between the feedpoints. This was chosen at 0.5 mm, so as to accommodate miniature chip mixer diodes. This gap causes a certain amount of coupling between the two elements. The result is a distortion of the electric field around the feedpoint (where the electric field has a predominantly reactive component). This could explain the consequently higher resonant frequency.

4.6.1.2 Conclusions

The return loss plot shows that the antenna is operating at a higher fundamental frequency than initially designed. To ensure the antenna operated at the desired frequencies, the element lengths were increased.

4.6.1.3 Measuring the radiation pattern

To determine if the two dipoles were acting independently of one another, it was important to see if they produced satisfactory E and H radiation patterns at both the resonant frequencies. The antenna was sent to the Microwaves and Antennas Laboratory at the Division of Aeronautics and System Technology (DAST) of the Council for Scientific and Industrial Research (CSIR). The patterns were obtained using DAST's 1-4 GHz anechoic chamber. Figure 28 shows the anechoic chamber setup.

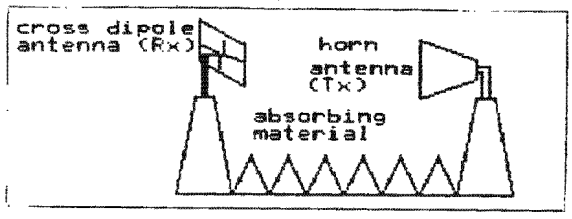

Figure 28. 1-4 GHz anechoic chamber setup

The E field plots at 1.43 and 2.86 GHz, which can be found in Appendix B, both show the distinctive [12] "figure eight" pattern. The 10 dB beamwidth appears to be 90° at 2.86 GHz. It is difficult to determine the beamwidth at 1.43 GHz. A possible reason for this could be that the horizontal portion of the coaxial-to-SMA cable interferes with the electric field. This is shown in figure 29, where position A indicates the horizontal portion of the cable.

The H planes at both 1.43 and 2.86 GHz, are omnidirectional. This was expected from a short dipole. The H-plane plots can also be found in Appendix B.

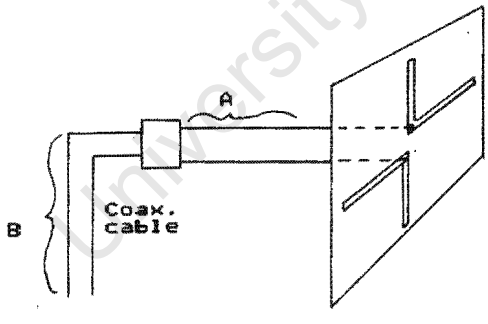

Figure 29. Cross dipole antenna showing coax feed cable

The slight oscillation in the H-plane plot at 2.86 GHz is caused by the vertical section of the coaxial cable. Position B in figure 29.

A solution to obtaining more accurate H plane plots is to place a reflective plate a distance l behind the antenna, covering the vertical portion of the coaxial cable. For the cross dipole antenna, the distance l was chosen as:

$$l = \lambda/8 \text{ at } 1.43 \text{ GHz}$$
$$= \lambda/4 \text{ at } 2.86 \text{ GHz}$$

Figure 30 shows the cross dipole antenna with its reflective plate.

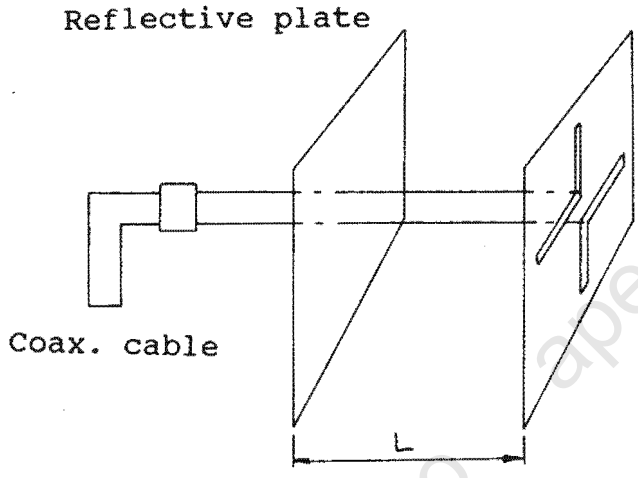

Figure 30. Cross dipole antenna with reflective plate

It must be noted that a balun was not used to match the antenna to the feedline. This was because the antenna was operating at two frequencies, and it is not possible to match an antenna to two frequencies using quarter wavelength sections. A quarter wavelength section at 1.43 GHz transforms to half wavelength at 2.86 GHz.

4.6.2 Conclusions

The radiation plots show that both dipoles are acting independently of each other. The E and H fields are exactly what

would be expected from a traditional short wire dipole. It must be noted that the cross dipole used in practice will not have the short section of coaxial cable to interfere with the radiation patterns. In conclusion then, the cross dipole antenna satisfies the criterion for the frequency multiplication method.

CHAPTER 5

DESIGNING THE ANTENNAS FOR THE FREQUENCY MULTIPLICATION SYSTEM

5.1 Design of the cross dipole antenna

The frequencies of the system are ultimately determined by the size of the density tracer. From section 4.6 it can be seen that a cross dipole antenna mounted on PCB, with a maximum diameter of 80 mm, will resonate at a fundamental frequency of 1.43 GHz. By simply scaling the dipole down in size it is possible to produce an antenna which has the correct diameter as specified. The antenna will now however be radiating at a higher fundamental and second harmonic frequency.

It was found that by reducing the antenna by a factor of two will produce a density tracer of diameter: 80/2 = 40 mm. The frequencies of operation should then be 2.86 GHz and 5.72 GHz.

If 3 GHz and 6 GHz are chosen as the frequencies of operation of the antenna, the scaling down factor would be 2/1.43 = 2.09. The maximum diameter of the density tracer would be approximately 40 mm (including feedpoint gap). This is larger than that specified (32 mm), which would have implied frequencies of 3.58 and 7.16 GHz for the antenna. After discussion with DRL it was decided that 3 and 6 GHz be chosen as the frequencies of the system, merely because of their ease of use components are available which operate specifically at these frequencies.

Working on these principles then, an antenna was designed by reducing the lengths by the factor 2.09. Figure 31 indicates the positive print of this antenna after it was photo reduced by twenty five percent.

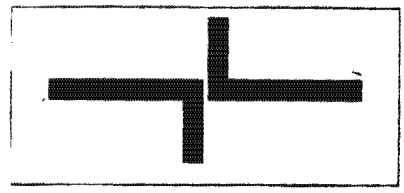

Figure 31. Positive print of 3/6 GHz cross dipole antenna

Figure 32 (a) and (b) indicates the match of this antenna over both bands of operation.

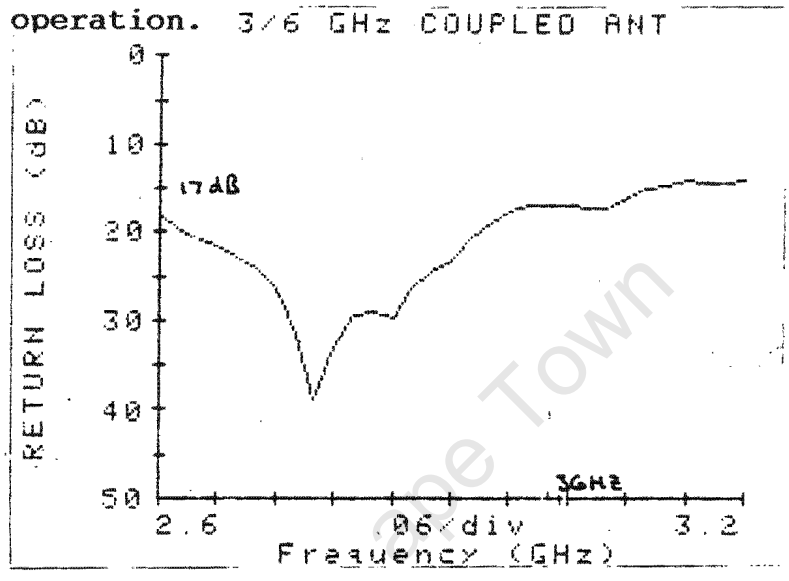

Figure 32(a). Return loss of cross dipole antenna centered on 3 GHz

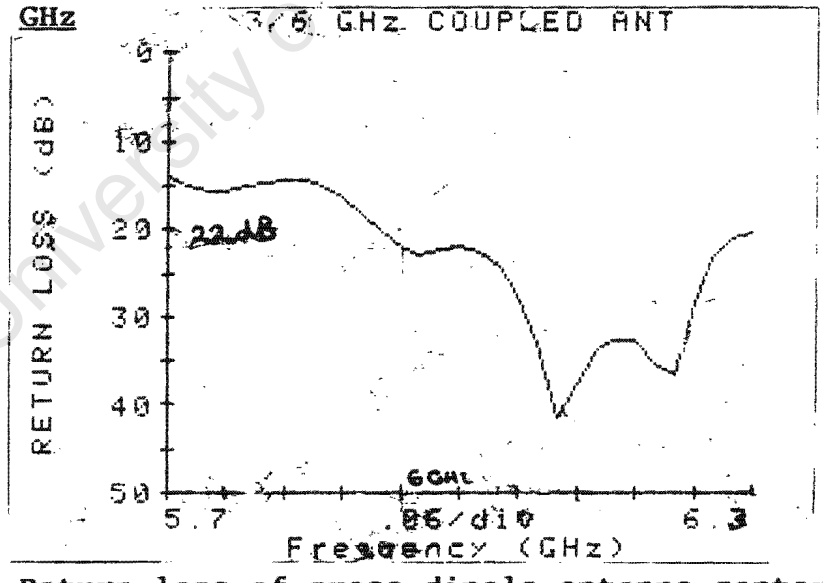

Figure 32(b). Return loss of cross dipole antenna centered on 6 GHz

As can be seen the antennas are well matched at 3 GHz and 6 GHz with return losses of 17 dB and 22 dB respectively. It can be seen that the antennas have better return losses at 2.76 and 6.16 GHz. It was found however that these troughs were susceptible to loading by objects placed in front of the antenna. Standing waves would be formed between the antenna and the object. The return loss correspondingly rose from 20 to 40 dB. The resonant frequencies at 3 GHz and 6 GHz remained more constant. It can thus be accepted that the antenna shown in figure 30 is a suitable cross dipole antenna at 3&6 GHz.

5.2 Designing a suitable DC biasing choke

It has been shown earlier (sect. 4.3.1) that a choke is important to provide a DC path for the mixer diode. It is also used as a self biasing unit, giving the diode a reference bias at zero volts.

It must be noted that the chokes are self resonant at certain frequencies and that their reactance increases with the frequency. The relationship between reactance and frequency is linear, as can be seen in eq. 5.1

$$Z_L = 2*\pi*f*L \qquad ...(5.1)$$

where Z_L = reactance of choke in
f = frequency in Hz
L = inductance of choke in H

An ideal choke must be passive and have no affect on the match of the system, other than to provide a DC path. As we have seen however, this is not entirely possible, since reactance increases with frequency.

The test bed in figure 33 shows how chokes with various turns can

be tested to see their affect the on the match of a system. A 50Ω line is etched onto microstrip, using the physical parameters from table 5. A patch of copper is etched and shorted to the ground plate via a screw. Two SMA launchers are then soldered onto the board and the test bed is connected to a network analyser. The return and insertion losses over a range of frequencies, for each choke, is measured.

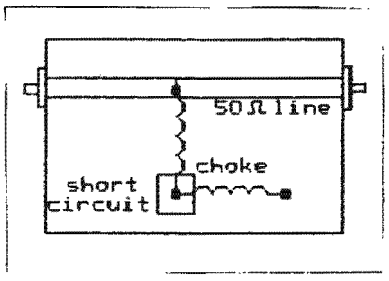

Figure 33. Choke reactance test bed

The principle is that as a choke becomes series resonant it will be a low impedance and reflect all of the energy incident upon on the 50Ω line. There will thus be a decrease in the return loss and in the transmitted power $(S12)^2$ absorbed by the mixer.

The effect of a 5 turn choke on the return loss is shown in figure 34 (a) and (b). 32 SWG copper wire was used in this experiment.

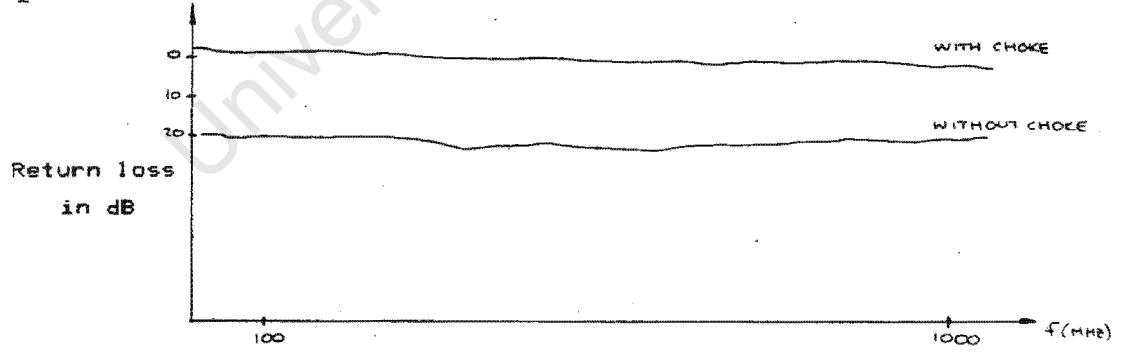

Figure 34(a). Return loss of 5 turn choke over 100 MHz-1 GHz band

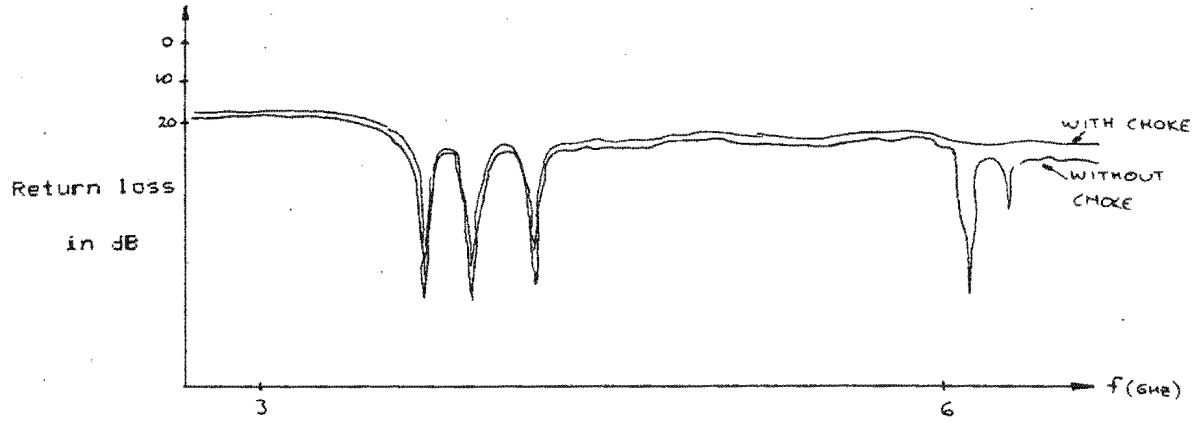

Figure 34(b). Return loss of 5 turn choke over 3 GHz - 6 GHz band

It can be seen that the choke is too low a reactive impedance and is reflecting ($X_L = 2*\pi*f*l$) most of the energy over the band 100 Mhz-1 GHz, but is a much higher inductive reactance, thus reflecting very little power over the range 3-6 GHz. Very little power is being reflected back to port 1.

5.2.1 Conclusions

A 5 turn choke using 32 SWG copper wire will be mounted across the mixer diode, since it will have little affect on the match of the cross dipole antenna.

5.3 Choosing a suitable mixer diode for the cross dipole antenna

The mixer diode used on the cross dipole has to conform to certain specifications. It must be a schottky barrier diode. The biasing voltage must be zero (no onboard power supplies). The device should be packaged as a chip, i.e. without leads and plastic containment, since these will cause capacitive parasitic loading at high frequencies. The chip must be small enough to fit across the feedpoints of the cross dipole antenna. Chip diodes are cheaper than encapsulated diodes. However bonding facilities must be available in order to mount the chip device into the density tracer.

The device chosen was an Alpha DMK 5068 Gallium Arsenide Schottky

barrier mixer diode. The characteristics of this diode can be found in Appendix C. Although the diode operates best over the Ku band (12.4-18 GHz), it will still operate successfully at 6GHz. For convenience the measurement reported here were performed using a packaged mixer diode, the package has dimensions of 1.4 mm by 1.27 mm. The gold contacts were 0.8 mm apart thus the unit will thus fit in perfectly between the feedpoints (0.5 mm separation).

5.4 Designing the 3&6 GHz transmit & receive antennas

As shown previously, the system will be operating with a 3 GHz fundamental frequency and a 6 GHz second harmonic, thus 3 GHz transmit and 6 GHz receive antennas are needed.

Metal fabricated dipoles at these frequencies would be very short, especially at 6 GHz where the antenna length l would be less than $3*10^8/6*109/2 = 25$ mm. A horn antenna would be a useful substitute. They have wide bandwidths and high gains, as required by the system.

5.4.1 The 3 Ghz horn antenna & waveguide-coaxial transformer

The frequency multiplication system requires horn antennas which have a high gain and a wide beamwidth 60°.

It has been shown [13] that there exist empirical formulas to calculate the 10 dB width as a function of aperture, for the average horn antenna. These are:

1) For the electric field:

$$\theta_E(10) = 88*\lambda/B \text{ degrees} \qquad B/\lambda < 2.5 \quad ..(5.2)$$

2) For the magnetic field:

$$\theta_H(10) = 31 + 79*\lambda/A \text{ degrees} \quad A/\lambda < 3 \quad ..(5.3)$$

B,A are the apertures in the electric and magnetic fields.

The system requires a 60° in the electric field, thus from eq(5.2), the horn antenna will require an aperture of:

$$B = 88*\lambda/\theta_E(10) \qquad ..(5.4)$$

Now the free space wavelength at 3 GHz is:

$$\lambda_o(3\ GHz) = c/f \qquad ..(5.5)$$
$$= 3*10^8/3*10^9$$
$$= \underline{100\ mm}$$

Therefore the aperture is:

$$B = 88*100/60 \qquad ..(5.6)$$
$$= \underline{147\ mm}$$

To simplify construction an aperture of 150 mm was used. It was decided that square pyramidal horns would be used, thus the beamwidth in the magnetic field would be:

$$\theta_H(10) = 31 + 79*\lambda/A \qquad ..(5.7)$$
$$= 31 + 79*100/150$$
$$= \underline{84°}$$

It has been noticed in a previous work that the beamwidth of an antenna is related to the aperture of the antenna, and as expected as the aperture increases in size, so the beamwidth narrows. Looking at this another way, as the horn length of an antenna with a given flare angle is increased, the aperture increases. This would cause the beam to narrow. It was found however that the effect of increasing the aperture is overshadowed by the phase error effects of the slant length of the horn. This phase error had to be determined and taken into

account for the design of the horn antenna.

Figure 35 shows a section of a horn antenna. δ represents the maximum departure of the wavefront r_2 from the aperture plane.

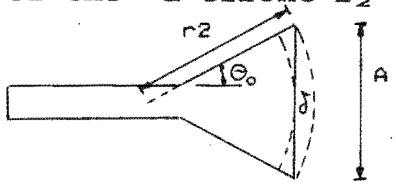

Figure 35 . Section of horn antenna with wave front

The phase difference between the center of the aperture and the edge, is given by $2*\pi*\delta/\lambda_g$. From figure 35 it can be seen that:

$$r_2*\cos(\theta_o) + \delta = r_2 \qquad ..(5.9)$$

$$\text{therefore} \qquad \delta = r_2(1-\cos(\theta_o))$$

$$\text{and} \qquad \delta / \lambda_g = r_2/ \lambda_g*(1-\cos(\theta_o))$$

When the flare angle is small, δ/λ_g is small and the wavefront approximates a plane wave. The field is thus more evenly spread across the aperture of the horn antenna. It has been shown that a suitable upper limit for δ/λ_g is 1/8.

A conservative estimate of δ/λ_g = 1/6 for the phase error was assumed. This phase error is shown in figure 36.

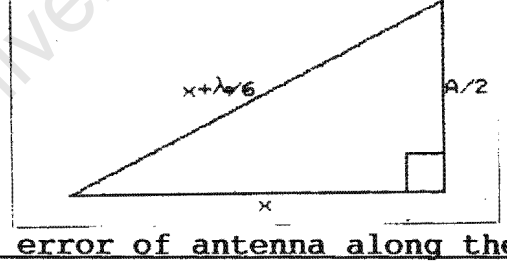

Figure 36. Phase error of antenna along the slant length

Now $\lambda_o/6$ = 100/6 = 16.67 mm
and A/2 = 150/2 = 75 mm
From Pythagoras then:

$$(x + \lambda_o/6)^2 = x^2 + 75^2 \qquad ..(5.10)$$

$$x^2 + 33.34*x + 277.89 = x^2 + 75^2$$

$$x = \underline{160.38 \text{ mm}}$$

The square pyramid will be constructed using four brass plates brazed onto a circular flange. The dimensions of this flange can be found in Appendix D. The flange is designed to work with a system operating between 2.60-3.95 GHz. Figure 37 shows the flange.

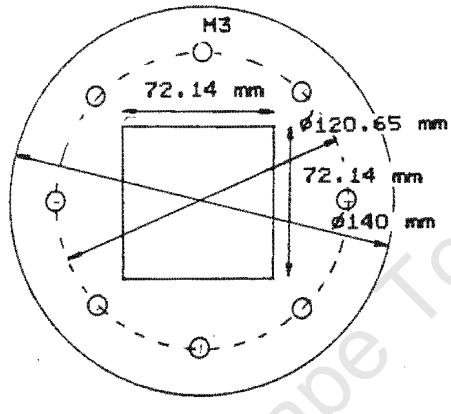

Figure 37. Dimensions of 3 GHz circular flange

As can be seen, the base of the pyramid has a width of 7.214 cm. The template from which the pyramid is made, is shown in figure 38.

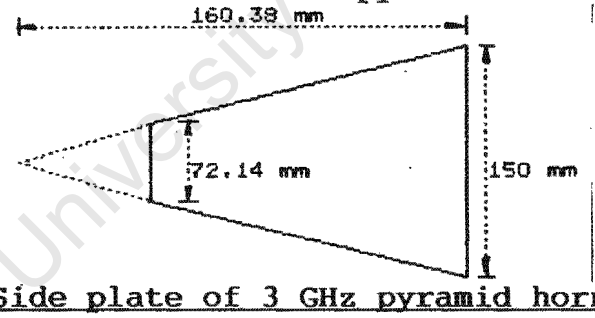

Figure 38. Side plate of 3 GHz pyramid horn

The length C is given by similar triangles:

$$75/160.38 = 36.07/C$$

$$C = \underline{77.132 \text{ mm}}$$

From this we obtain:

$$D = 160.38-77.132$$
$$= \underline{83.25 \text{ mm}}$$

Four plates of these dimensions are soldered to the flange in figure 38. A system of launching waves from the coaxial feed cable to the 3 GHz horn was required. A waveguide-coaxial transformer was constructed. From Appendix D, it was found that the transformer would have dimensions as indicated in figure 39.

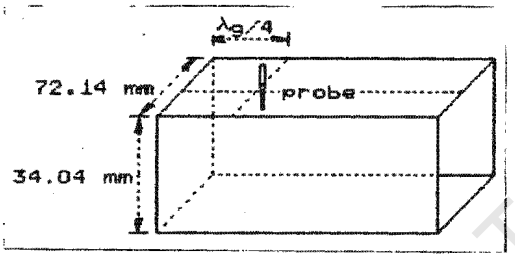

Figure 39. 3 GHz waveguide/coaxial transformer

Appendix D, it is found that the cut off frequency is:

$$f_c = 2.08 \text{ GHz}$$

, and that the transformer waveguide has the following dimensions:

72.14 mm * 34.04 mm

Free space wavelength is from (5.5)

$$\lambda_o = c/f$$
$$= 3*10^8/3*10^9$$
$$= \underline{100 \text{ mm}}$$

The wavelength of the cut-off frequency is:

$$\lambda_c = c/f_c \qquad ..(5.11)$$
$$= 3*10^8/2.08*10^9$$
$$= \underline{144.231 \text{ mm}}$$

The waveguide wavelength is given by:

$$1/\lambda_g^2 = 1/\lambda_o^2 - 1/\lambda_c^2 \qquad ..(5.12)$$

$$\lambda_g^2 = 19257.047$$

$$\lambda_g = \underline{138.77 \text{ mm}}$$

The point of the probe from the rear of the waveguide is:

$$\lambda_g/4 = \underline{34.693 \text{ mm}}$$

The probe, shown in figure 38, protrudes a length:

$$\lambda_o/4 = \underline{25 \text{ mm}}$$

into the transformer.

A transformer of these dimensions was constructed and soldered to a circular flange, as in figure 36. The transformer was bolted to the horn antenna, and then tested in the same manner as that in section 4.6.1.1

5.4.2 Testing the 3 GHz horn antenna & waveguide-coax transformer

The 3 GHz horn antenna was connected to port 1 of the network analyser. The return loss plot, shown in figure 40, indicates the match of the antenna at 3 GHz. As can be seen, the antenna has a loss of 11.3 dB at 3 GHz.

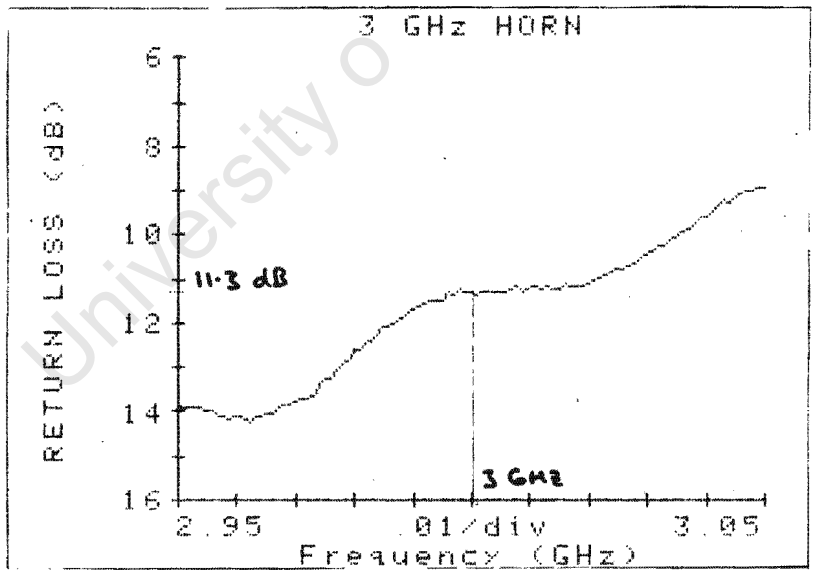

Figure 40. Return loss for 3 GHz horn antenna

The low efficiency of the antenna could be due to:

a) Probe not in maximum position to intercept maximum electric field.
b) Plate added to waveguide wall causes discontinuity in electric field.

5.4.3 Conclusions

The return loss plot indicates that the 3 GHz horn antenna will operate adequately in the system.

5.4.4 Designing the 6 GHz horn antenna & waveguide-coaxial transformer

The 6 GHz receive system requires a 6 GHz horn with a waveguide-coaxial transformer, similar to the 3 GHz unit. The dimensions for the antenna and its transformer are calculated below.

The beamwidth of the 6 GHz horn antenna was chosen to be 60°, the same as the 3 GHz horn antenna. The aperture of the antenna was determined as follows:

The free space wavelength at 6 GHz is obtained from eq (5.5)

$$\lambda_o = c/f$$
$$= 3*10^8/6*10^9$$
$$= 50 \text{ mm}$$

The aperture is then determined using eq (5.6).

$$B = 88*\lambda/\theta_E(10)$$
$$= 88*50/60$$
$$= 73.33 \text{ mm}$$

For convenience an aperture of 75 mm was chosen.
A phase error of $\lambda_o/6$ along the slant length of the pyramid, is assumed, as shown in figure 36.

Now $\lambda_o/6 = 50/6$

$= \underline{8.333 \text{ mm}}$

and A is chosen to be 75 mm, this implies that A/2 = 37.5 mm

x can now be determined using Pythagoras as in eq (5.11)

$$(x + \lambda_o/6)^2 = x^2 + (A/2)^2 \qquad ..(5.13)$$

$$(x + 8.333)^2 = x^2 + 37.5^2$$

$$x^2 + 16.67*x + 69.44 = x^2 + 1406.25$$

$$x = \underline{80.192 \text{ mm}}$$

It was then decided to build a rectangular pyramidal horn using the dimensions to fit the base of the 6 GHz. This would entail constructing two types of side plates for the horn.

From Appendix D, the dimensions of the waveguide are found to be:

40.39 mm * 20.19 mm

The circular flanges to be used on the 6 GHz horn and transformer, are shown in figure 41.

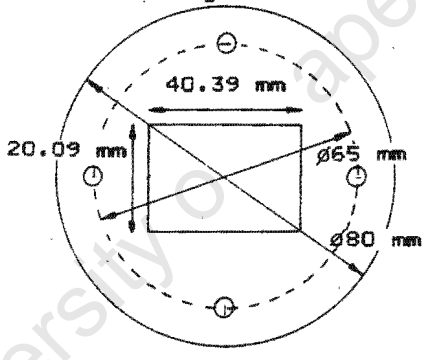

Figure 41. Dimensions of 6 GHz circular flange

The flange is designed to operate over the band 4.90-7.05 GHz.

From figure 41 it can be seen that two sides of the pyramidal base have dimensions of 40.39 mm while the other two sides have widths of 20.19 mm. The two side plates are shown in figure 42. The dimensions of the plate are calculated thereafter.

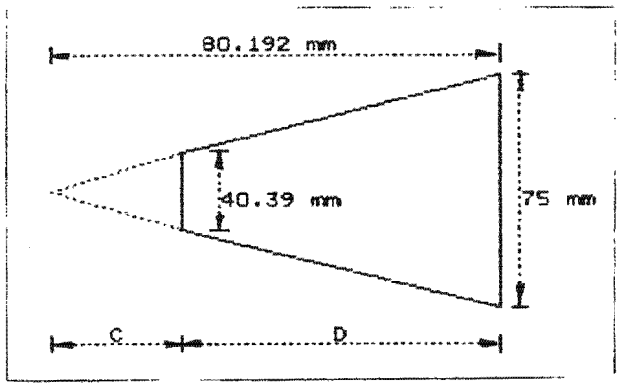

Plate 1

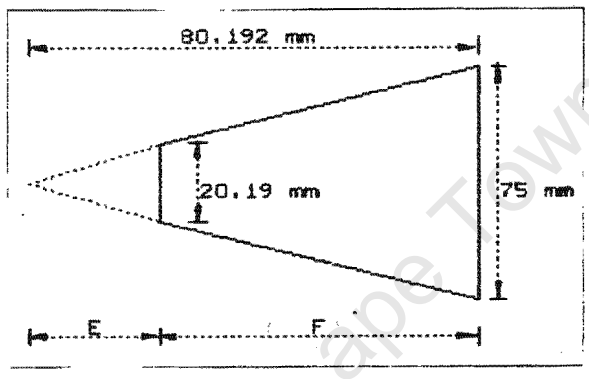

Plate 2

Figure 42. Side plates for the 6 GHz pyramidal horn

From the diagrams: 37.5/80.192 =20.195/C

thus C = 43.186 mm

and D = 80.192-43.186

= 37.006 mm

This gives plate 1 a slant length of:

$$l_1 = \sqrt{(37.5-20.195)^2 + 37.006^2}$$

$$= 40.852 \text{ mm}$$

Plate 2 will also have to have this slant length, to ensure that the side plates fit flush against each other. The length of this plate can then be calculated using this criterion.

$$F = \sqrt{(40.852)^2 - (37.5 - 10.095)^2}$$
$$= \underline{30.296 \text{ mm}}$$

The horn antenna was then constructed using these plates and soldered to the circular flange shown in figure 41.

A unit to launch waves into the horn was required. A suitable launcher is the quarter wavelength waveguide-coaxial transformer. The dimensions of the launcher are determined as follows.

From Appendix D we find that the flange dimensions are:

$\underline{40.39 \text{ mm} * 20.19 \text{ mm}}$

The waveguide is designed to operate over the band $\underline{4.90\text{-}7.05 \text{ GHz}}$, with a cut-off frequency of $\underline{3.71 \text{ GHz}}$.

Now the free space wavelength is: $\lambda_o = c/f = 3*10^8/6*10^9$ ..(5.14)
$= \underline{50 \text{ mm}}$

The cut off frequency wavelength is: $\lambda_c = c/f_c = 3*10^8/3.71*10^9$
$= \underline{80.86 \text{ mm}}$

From this the waveguide wavelength can be calculated.

$$1/\lambda_g^2 = 1/\lambda_o^2 - 1/\lambda_c^2 \qquad ..(5.15)$$
$$\lambda_g^2 = 4047.665$$
$$\lambda_g = \underline{63.62 \text{ mm}}$$

The coordinates of the probe position are given by:

$$\lambda_g/4 = 63.62/4$$
$$= \underline{15.905 \text{ mm}}$$
$$\lambda_o/4 = 50/4$$
$$= \underline{12.5 \text{ mm}}$$

The completed transformer is shown in figure 43.

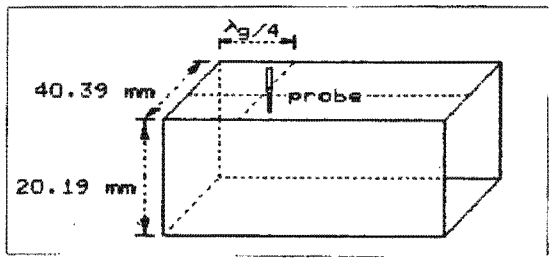

Figure 43. 6 GHz horn & waveguide-coaxial transformer

5.4.5 Testing the 6 GHz horn antenna & transformer

The 6 GHz horn antenna and transformer are attached to port 1 of the HP 8410 B network analyser. The return loss for the antenna was determined and then plotted. The results of the test can be seen in figure 44.

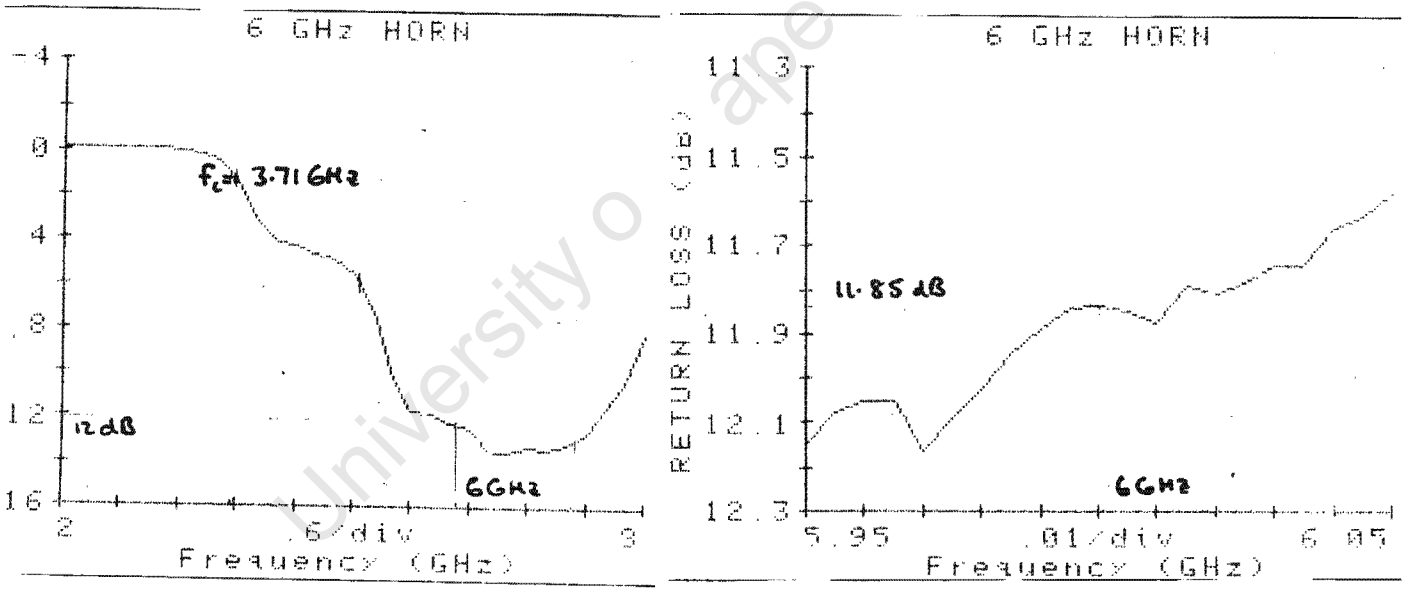

Figure 44(a) & (b). Return loss for 6 GHz horn & waveguide to coaxial transformer

Figure 44(a) shows the cut-off frequency at 3.71 GHz and that the antenna is operating well within the band of 4.90-7.05 GHz.

Figure 44(b) indicates that the return loss is approximately 11.85 dB at 6 GHz.

5.4.6 Conclusions

Figures 44(a)&(b) indicate that the antenna is operating adequately over the band, and satisfactory for the operation of the frequency multiplication system.

CHAPTER 6

CONFIGURATION OF 3/6 GHz FREQUENCY MULTIPLICATION SYSTEM

6.1 Problems with conventional receiver units

The simplified block diagram for the 3/6 GHz frequency multiplication system is shown in Figure 45.

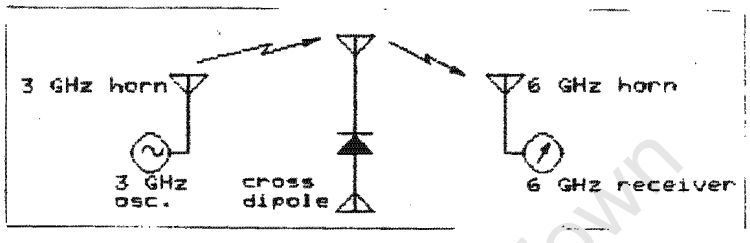

Figure 45. Block diagram of frequency multiplication system

The problem with this system lies primarily with the receiver unit. Receivers are generally wide band, and since we expect the 3 GHz signal to drift in frequency due to various physical factors, the second harmonic will not have a constant frequency either. This complicates detection. If the second harmonic had a stable position in the frequency domain, then a narrow filter could re placed in front of the receiver. This would narrow the bandwidth of the receiver, easing detection.

A solution might be to place a sweep and lock circuit in series with the receiver. This device sweeps a band frequencies and locks onto signals above a certain threshold. The system then locks onto this signal. It is then put through a narrow bandpass filter after which it is sent to a receiver.

Two problems exist with this system:
1) Amplitude of second harmonic

2) Time taken for circuit to sweep

1) The frequency multiplication system obeys a fourth order power law, similar to radar systems. It can thus be expected that the multiplied second harmonic will have a low amplitude. If the second harmonic level entering is lower in amplitude than the background noise of the receiver, the circuit will not lock.

2) The sweep and lock circuit takes a finite amount of time to lock onto a receiver tone. As stated earlier, a typical period is 0.5 seconds. After this period, the density tracer would have fallen out of the detection range.

One way to produce a stable source of second harmonic at the receiver, is to lock the 3 GHz oscillator. Crystal locking is expensive, however.

A better solution is to lock the receivers local oscillator to the second harmonic produced by the transmit oscillator.

The advantages are:
1) The transmitter can be free running
2) The sweep and lock circuit on the receivers local oscillator is continually locked onto the transmit oscillators second harmonic. The density tracer, with cross dipole antenna, does not have to be present.

6.2 The receiver local oscillator feedback loop

The full frequency multiplication system/density tracer counter unit is shown in figure 46.

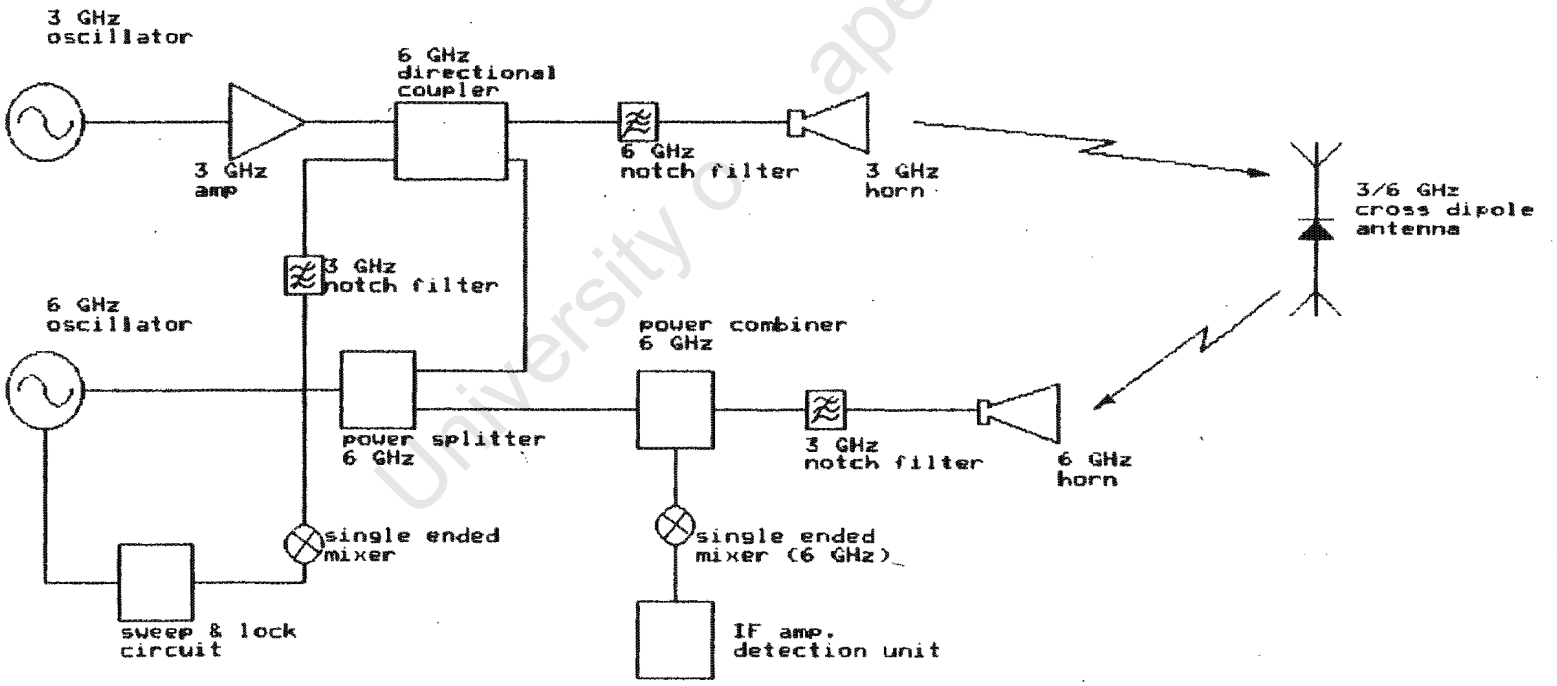

Frequency multiplication system (prototype

Size	Document Number	REV
A	Figure 46	1
Date: January 1, 1980	Sheet of	

The 3 GHz oscillator in the transmit unit generates a second harmonic at a lower amplitude. This second harmonic is coupled to the receivers local oscillator/ sweep and lock unit. The sweep and lock unit ensures that the local oscillator is locked onto the second harmonic. It also adds 10.7 MHz (FM intermediate frequency) to the second harmonic. This signal is power split into two paths. One closes the loop with the coupler and the sweep and lock circuit.

This feedback loop ensures that the sweep and lock circuit receives 10.7 MHz at its input. The signals are mixed by the single ended mixer to form this FM-IF tone. Figure 47 shows the sweep and lock loop.

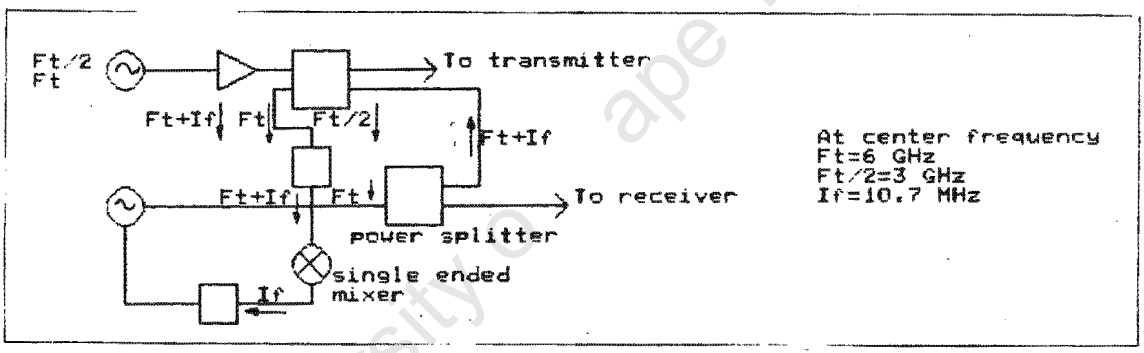

Figure 47. Sweep and lock feedback loop

From figure 46 it can be seen that the receiver unit, which is fed by the local oscillator, will have a continuous source of second harmonic available. This signal will have the same frequency as that multiplied by the mixer diode within the density tracer. It must be noted that the second harmonic does not have to sit at exactly 6Ghz, it is free to move within the bandwidth of the system. For this reason, the second harmonic has

been given the notation f_t. The need for the 10.7 MHz FM-IF will be explained later.

The 3 GHz notch filter removes the high power fundamental frequency from the feedback loop. This filter allows the second harmonic through with minor attenuation. The description of this filter is given in chapter 7 of this thesis.

6.3 The fundamental frequency transmitter and antenna

Figure 48 shows the transmitter unit consisting of oscillator, RF amplifier, directional coupler, 6 GHz notch filter and 3 GHz horn antenna/waveguide-coaxial transformer.

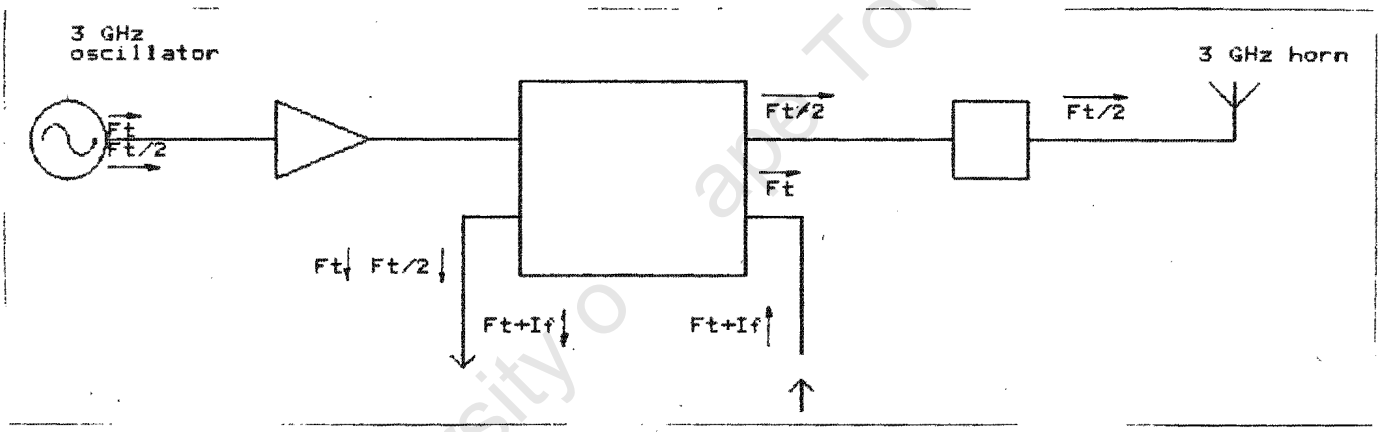

Figure 48. Block diagram of transmitter unit

The oscillator is chosen to produce a fundamental frequency centered at 3 GHz, with a lower amplitude 6 GHz component. A 3 GHz RF amplifier (the specifications of which will be given in chapter 10) is used to boost the power of the fundamental to produce 1 watt.

The directional coupler ensures signal flow to the sweep and lock circuit as well as to the transmit antenna. The signal from the

receiver local oscillator is also coupled to the seep and lock circuit at this point.

The 6 GHz notch filter attenuates the second harmonic while allowing most of the fundamental frequency to be transmitted. The second harmonic is attenuated to ensure that it is not erroneously detected by the receiver, as a density tracer.

The 3 GHz horn antenna/waveguide-coax transformer, transmits the fundamental frequency to the density tracer.

6.4 The receiver unit

Figure 49 shows the receiver unit consisting of power combiner, single ended mixer, 3 GHz notch filter, IF amplifier and 6 GHz horn antenna.

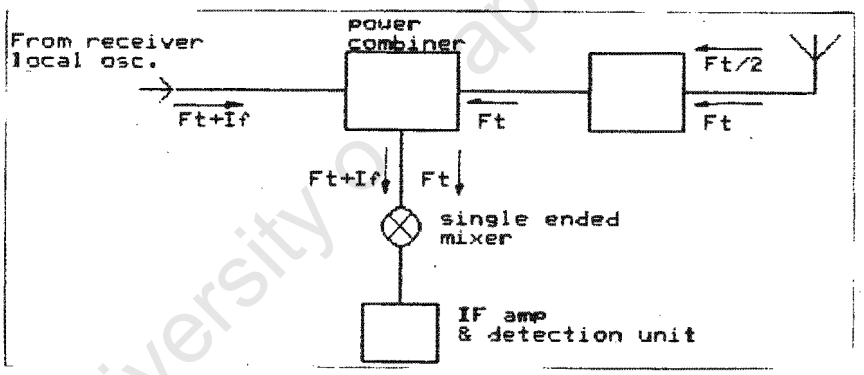

Figure 49. Block diagram of the receiver unit

The figure indicates how the tone (f_t + IF) from the receivers local oscillator enters the power combiner from the left. The 6 GHz horn antenna receives the second harmonic (f_t) from the mixer diode in the density tracer. There is a small amount of coupling between the two horn antennas so some 3 GHz component is also received. The 3 GHz notch filter attenuates most of this signal,

while allowing most of the multiplied second harmonic to the power combiner.

The power combiner then sends both of the RF(f_c) and LO(f_c+IF) signals to a single ended mixer where the difference component (IF) is removed and sent to an IF amplifier and bandpass filter.

The reason for using this complicated form of local oscillator/receiver system now becomes clear. Detection is made at IF frequency. In this case FM-IF (10.7 MHz). A very narrow bandpass filter (300 kHz) can be made thus reducing the noise bandwidth and increasing the receiver sensitivity. The intermediate frequency is then sent to a FM demodulator, for detection.

What becomes immediately obvious is that the second harmonic used in the receivers local oscillator and that multiplied by the mixer diode are the same. They will only vary in amplitude. These signals will drift with frequency in the same manner.

In summary then, on presentation of a density tracer containing a cross dipole antenna and mixer diode, the receiver will detect a pulse at 10.7 MHz. This pulse will last until the density tracer falls out of the detection range of the receiver.

This solution is very elegant since detection is done at a very low frequency. None of the oscillators need to be crystal locked, and there is no delay in detecting a density tracer while the circuit sweeps the frequency band.

The following chapters will discuss the design, construction and testing of each of the components of figure 46.

CHAPTER 7

DESIGN AND CONSTRUCTION OF THE NOTCH FILTERS

7.1 Analysing the stub notch filter

As shown in figure 46 there is a need for a 3 GHz notch filter which allows 6 GHz signals through with minimum attenuation, as well as a 6 GHz notch filter with minimum 3 GHz attenuation. For each filter, the bandwidths of the notch, must be sufficiently wide to accept drift of the oscillators. The nulls must be deep enough to provide adequate attenuation of the high amplitude fundamental frequency. Another criterion is that, in its pass band, the filter remain as flat as possible and have a transmission loss of as close to zero dB as possible.

A filter which satisfies the requirement is the quarter wavelength transmission line stub filter. The operation of a single stub will be reviewed and it will be shown how the notch filters was constructed using stubs.

From Appendix A we find that for RT duroid with the following characteristics,

ϵ_r = 2.2
H = 0.254 mm
t = 0.01778 mm
RHO = 0.84
RGH = 0

the width and length of a quarter wavelength of transmission line at 3 GHz is:

w = 0.76 mm l = 18.29 mm

The effect of an open circuit quarter wavelength stub at 3 GHz, on a transmission line, is now simulated by the package "EESOF Touchstone". Figure 50 shows the transmission line and stub.

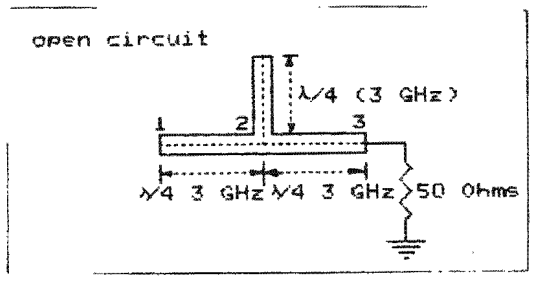

Figure 50. Open circuit stub at 3 GHz

The program (OPENIM.CKT) analyses this circuits operation, and can be found in Appendix E. The return loss and transmission loss for the circuit over a band of frequencies are shown in figure 51. Table 5 summarises the characteristics of the filter.

freq(GHz)	S11(dB)	S12(dB)
3	-0.157	-41.027
6	-49.853	-0.139

Table 5. Characteristics of 3 GHz open circuit stub

From the table it can be seen that the circuit reflects most of the power at 3 GHz:

$$\% \text{ reflection} = 100*\text{ALOG}(-0.157/10) \quad ..(7.1)$$
$$= 96\%$$

There is a small amount of reflection at 6 GHz (from eq. (7.1) we obtain 0.001%). Seen differently, the circuit allows almost all of the power (97%) at 6 GHz to be transmitted through it. The attenuation at 3 GHz is very high as only 0.008% is transmitted.

The problem that arises with this filter is that since a single stub is used the bandwidth is narrow (quarter wavelength). Techniques for increasing the bandwidth of the 3 and 6 GHz notch filters will be discussed in the next section.

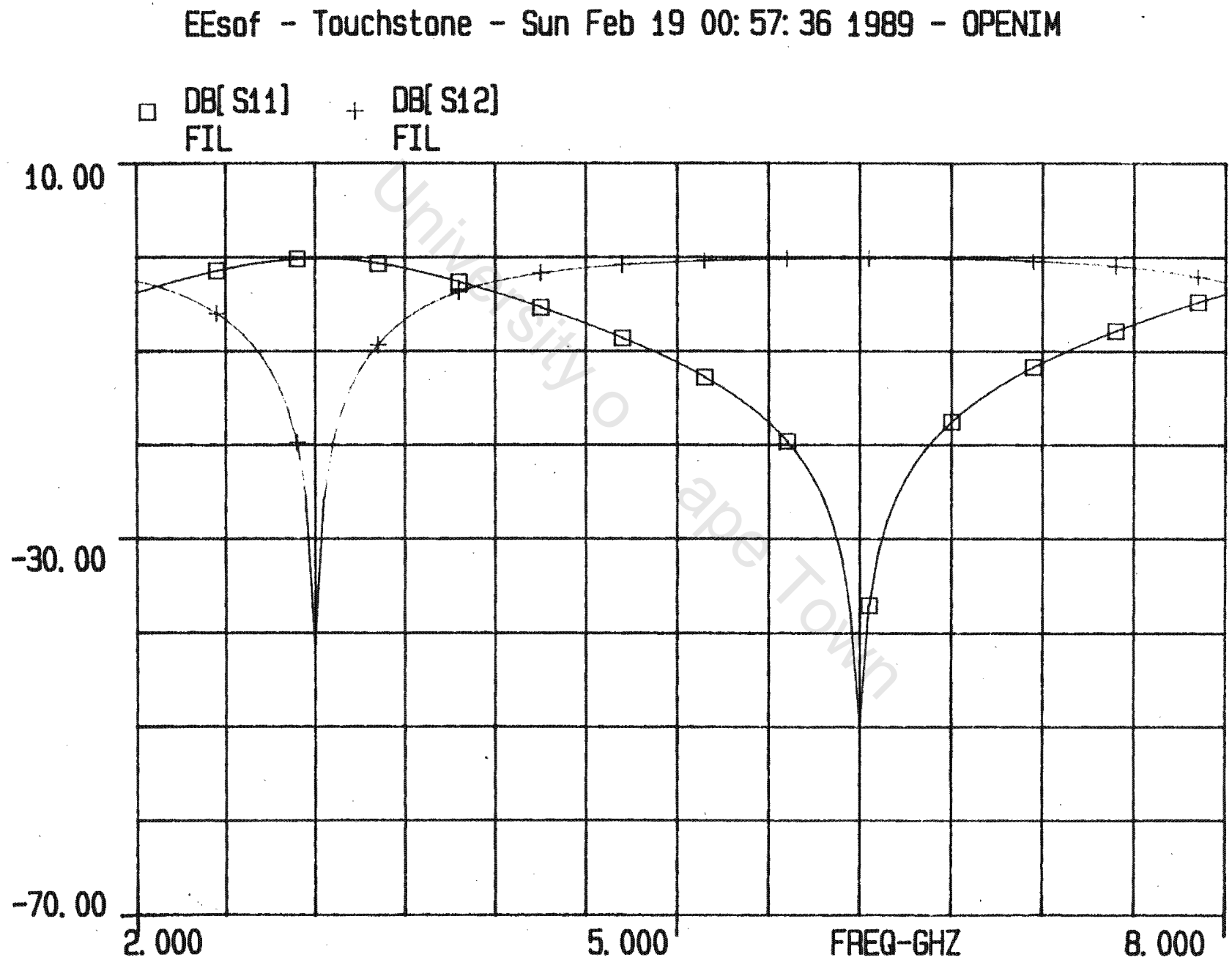

FIGURE 51

7.2 The design, construction and testing of the 3 GHz notch filters

As has been shown in the previous section, a quarter wavelength open circuit stub, makes a useful notch filter at the fundamental frequency and allows minor attenuation of the second harmonic. The problem lay with the depth and the narrow bandwidth of the null. One way to increase the bandwidth of the notch and to deepen it, is to increase the number of open circuit stubs. The spacing between stubs is set at a quarter wavelength at 3GHz.

A four stub filter was designed and a program to test the filter was written for the simulation package "Touchstone", which can be found in Appendix E. A plot of the return and transmission loss is shown in figure 52. Comparing figures 51 and 52, it can be seen that the depth of the notch has been dramatically increased from -40 dB to greater than -100 dB. The width of the null has also been increased from approximately 625 MHz (at 10 dB) to 1400 MHz.

This would appear to be a good solution to the problem of providing a wide band notch filter.

7.2.1 Analysing the operation of the filter

Figure 53 shows the 3 GHz notch filter

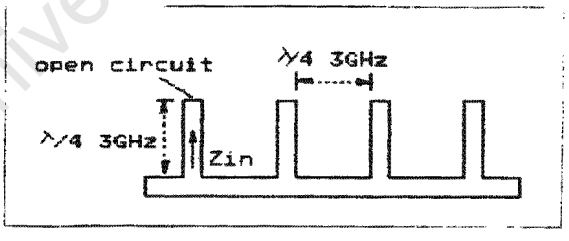

Figure 53. 3 GHz notch filter

This circuit can be analysed by using wave dynamics, to prove how the circuit rejects the 3 GHz components but allows transmission of any 6 GHz signal.

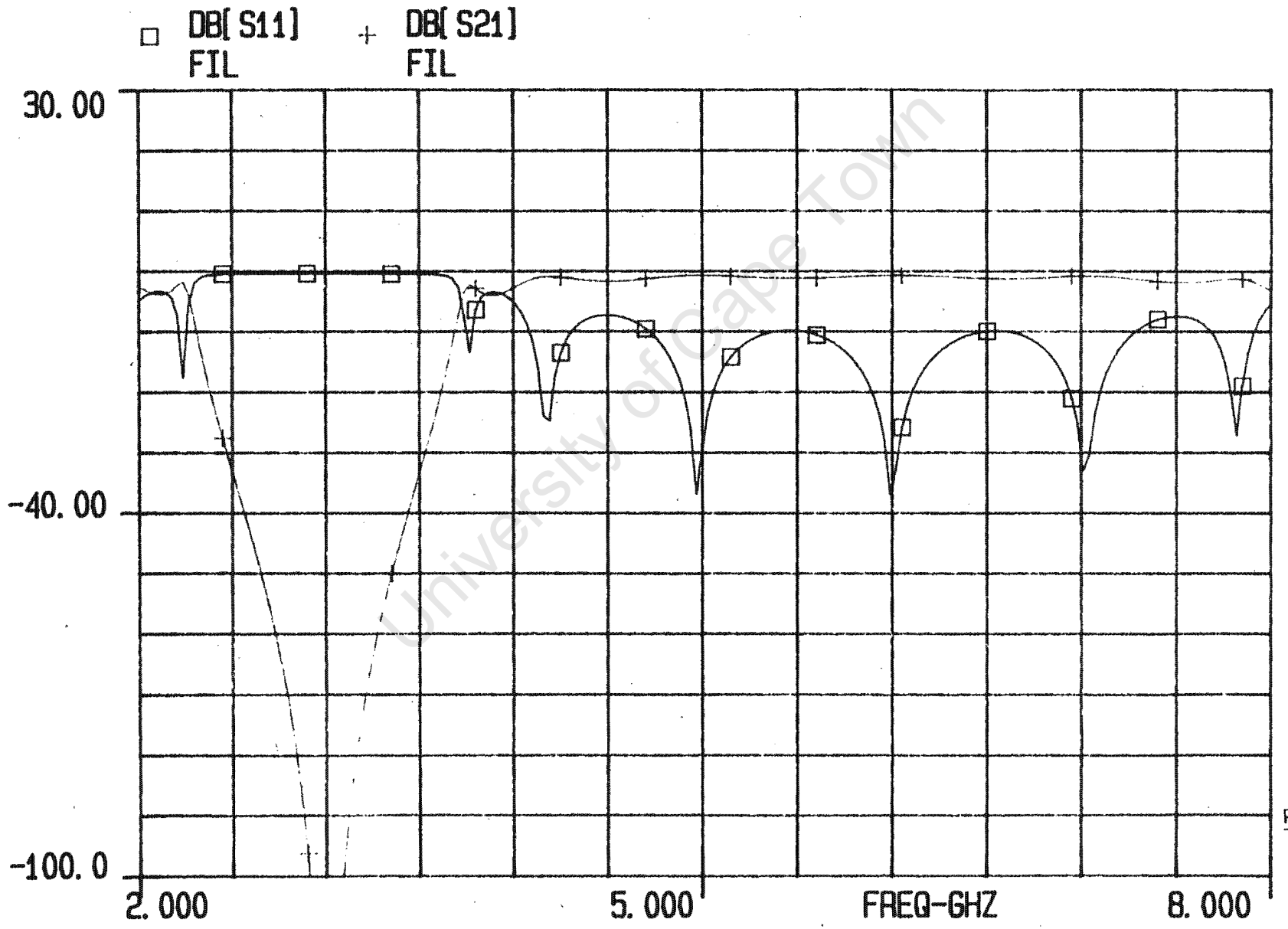

FIGURE 52

Analysing the stubs at 3 GHz we find that since the length of the stub are a quarter wavelength, the input impedance is given by:

$$Z_{in}(3GHz) = Z_o^2/Z_1 \qquad ..(7.2)$$
$$= 50^2/\infty$$
$$\longrightarrow \underline{0\Omega}$$

The open circuit $\lambda/4$ stubs thus present a zero impedance across the transmission line at 3 GHz. However, at 6 GHz it can be found that the input impedance is given by:

$$Z_{in}(6GHz) = Z_o * \frac{[Z_1*\cos(2*\pi*l/\lambda) + j*Z_o*\sin(2*\pi*l/\lambda)]}{[Z_o*\cos(2*\pi*l/\lambda) + j*Z_1*\sin(2*\pi*l/\lambda)]} \qquad ..(7.3)$$

Letting $l = \lambda/2$, since $\lambda(6) = \lambda(3)/2$, gives:

$$Z_{in}(6GHz) = Z_o * \frac{[Z_1*\cos(\pi) + j*Z_o*\sin(\pi)]}{[Z_o*\cos(\pi) + j*Z_1*\sin(\pi)]}$$
$$= Z_o * \frac{[-Z_1 + 0]}{[-Z_o + 0]}$$
$$= \underline{Z_1}$$

The load is thus reflected back to the input of the stub, since $Z_l \rightarrow \infty$ (open circuit), therefore $Z_{in}(6GHz) \rightarrow \infty$
The stub will thus present an open circuit across the transmission line at 6 GHz and will flow through the transmission line unaffected.

From Figure 53 it can be seen that the elements are $\lambda(3)/4$ apart. At 6 GHz the gap between the stubs is $\lambda(6)/2$, thus the 3 GHz signal has a maximum at the input to the stub. Since the 6 GHz signal is phase shifted by 180°, it will be transformed from the end of the filter to the beginning. Thus the filter will tend to minimize attenuation of the 6 GHz signal.

Appendix F provides another interesting way of analysing the 3 GHz open circuit stub, notch filter. The stubs are compared to PIN diodes which are used to protect mixer diodes on transmission lines.

7.2.2 Testing the 3 GHz notch filter

Two filters were constructed using RT-Duroid 5880 and given the dimensions used in figure 51. The completed version is shown in figure 54 (both filters were dimensionally identical, hence only one is produced here).

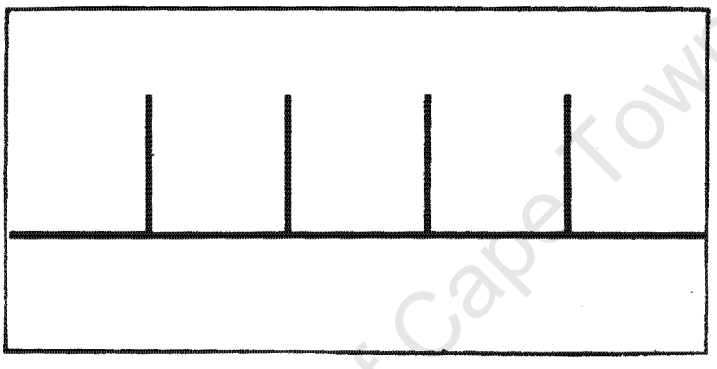

Figure 54. Positive print of 3 GHz notch filter

The filters were attached to the same test rig as in section 4.6.1.1. The return loss and transmission loss for both of them was obtained and can be found in figures 55 (a)..(f), (can be found on the following page). Comparing figure 55 to figure 52, it can be seen that the filters operate almost as well in practice as predicted by theory. Table 6 compares the theoretical and practical results.

	Freq(Ghz)	S12(dB)	notch bandwidth (Mhz)
Predicted	3	>100	1375
Actual	3	75	1350
predicted	6	+/-0	-
actual	6	0.8	-

Table 6. Characteristics of 3 GHz notch filter

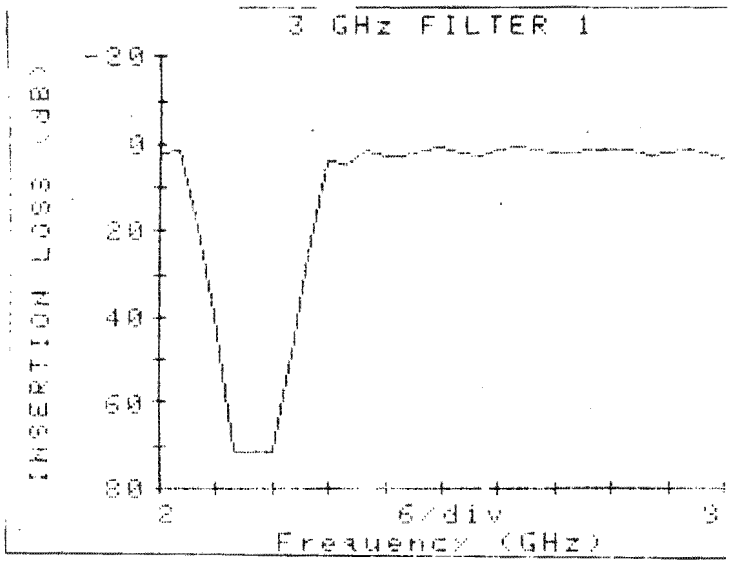

Fig. 55 (a)

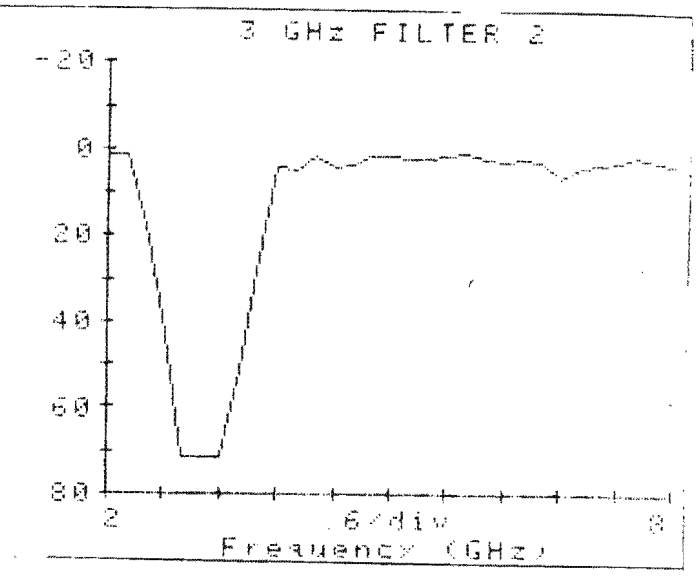

Fig. 55(b)

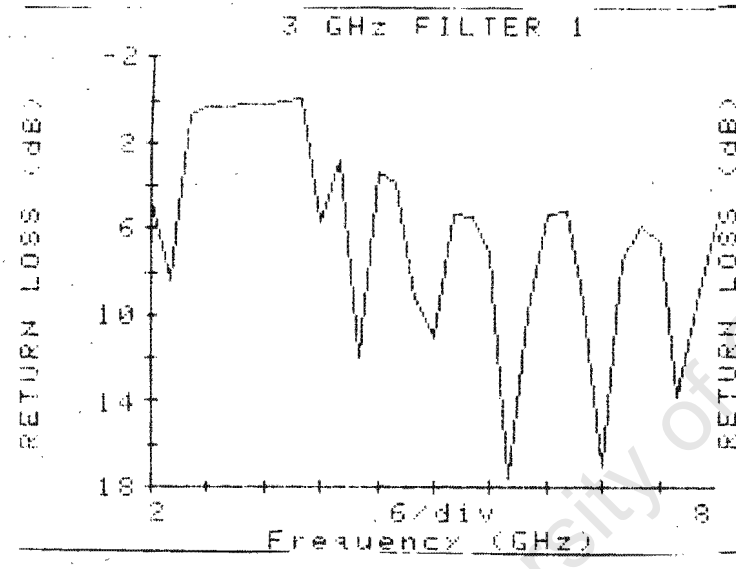

Fig. 55(c)

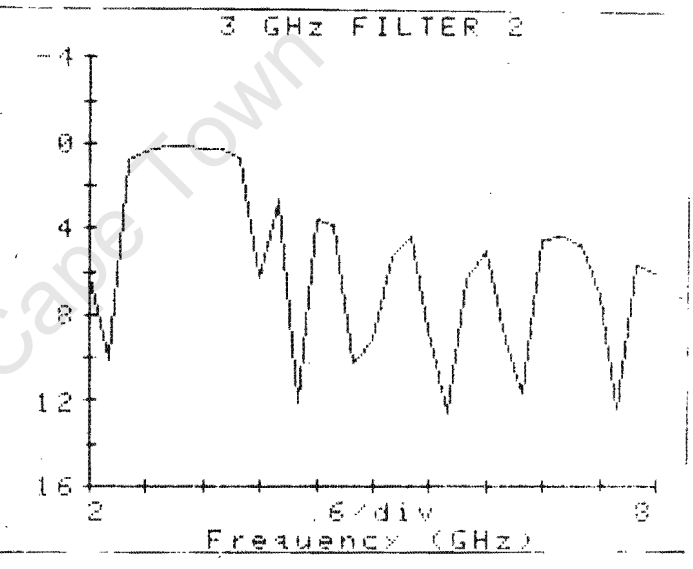

Fig. 55 (d)

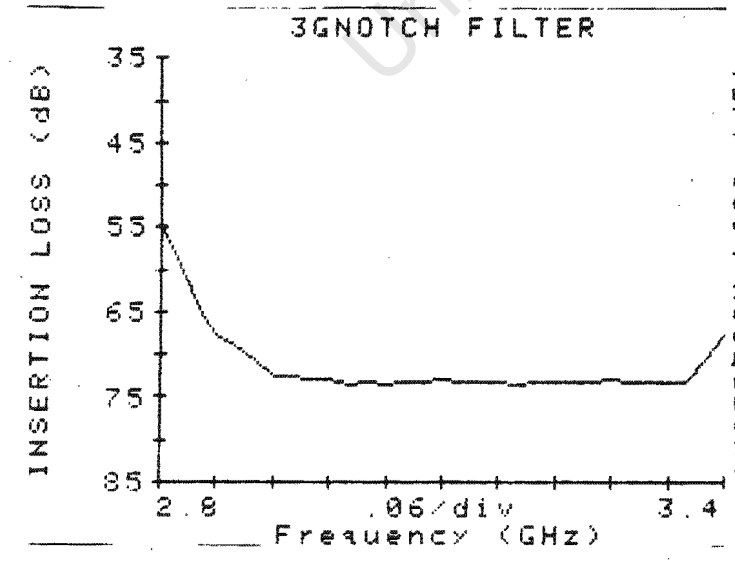

Fig. 55(e)

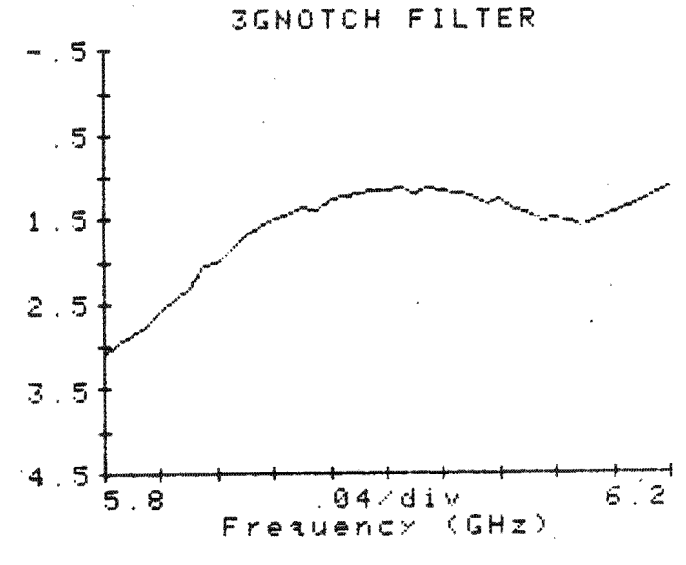

Fig. 55(f)

From the table it can be seen that the notch is 75 dB compared to the 100 dB predicted by Touchstone. In the program no algorithms were included that corrected for the microstrip propagation and radiation losses, this could be the reason for the errors in the prediction. The insertion loss at 6 GHz is approximately 0.8 dB which is satisfactory (83% of the power is transmitted through the filter).

7.2.3 Conclusions

The 3 GHz notch filter conforms adequately to what was predicted by theory. The notch is deep enough to ensure adequate attenuation of the fundamental frequency. A 1W signal at 3 GHz will be reduced to $3.16*10^{-8}$ W after passing through the filter.

7.3 Design, construction and testing of the 6 GHz notch filter

The 6 GHz notch filter is similar to the 3 GHz notch filter in appearance and operation. A major difference however is that the 6GHz notch filter uses short circuit stubs. The stubs are separated from each other by λ(6GHz)/4 sections. The lengths of the stubs are λ(3GHz)/4 as before.

"Touchstone" was used to analyse the notch filter. Appendix G contains a copy of the program entitled "6GNOTCH.CKT". Figure 56 indicates the return and transmissions loss of the filter. Comparing figure 56 with figure 42, it can be seen that they are almost identical but symmetric around the 5 GHz line. Touchstone predicts that the notch at 6 GHz has an amplitude of >-100 dB and that the bandwidth is approximately 1400 MHz (at 10 dB points). The transmission loss at 3 GHz is approximately zero. In practice open circuit stubs are easier to fabricate than short circuit stubs in microstrip.

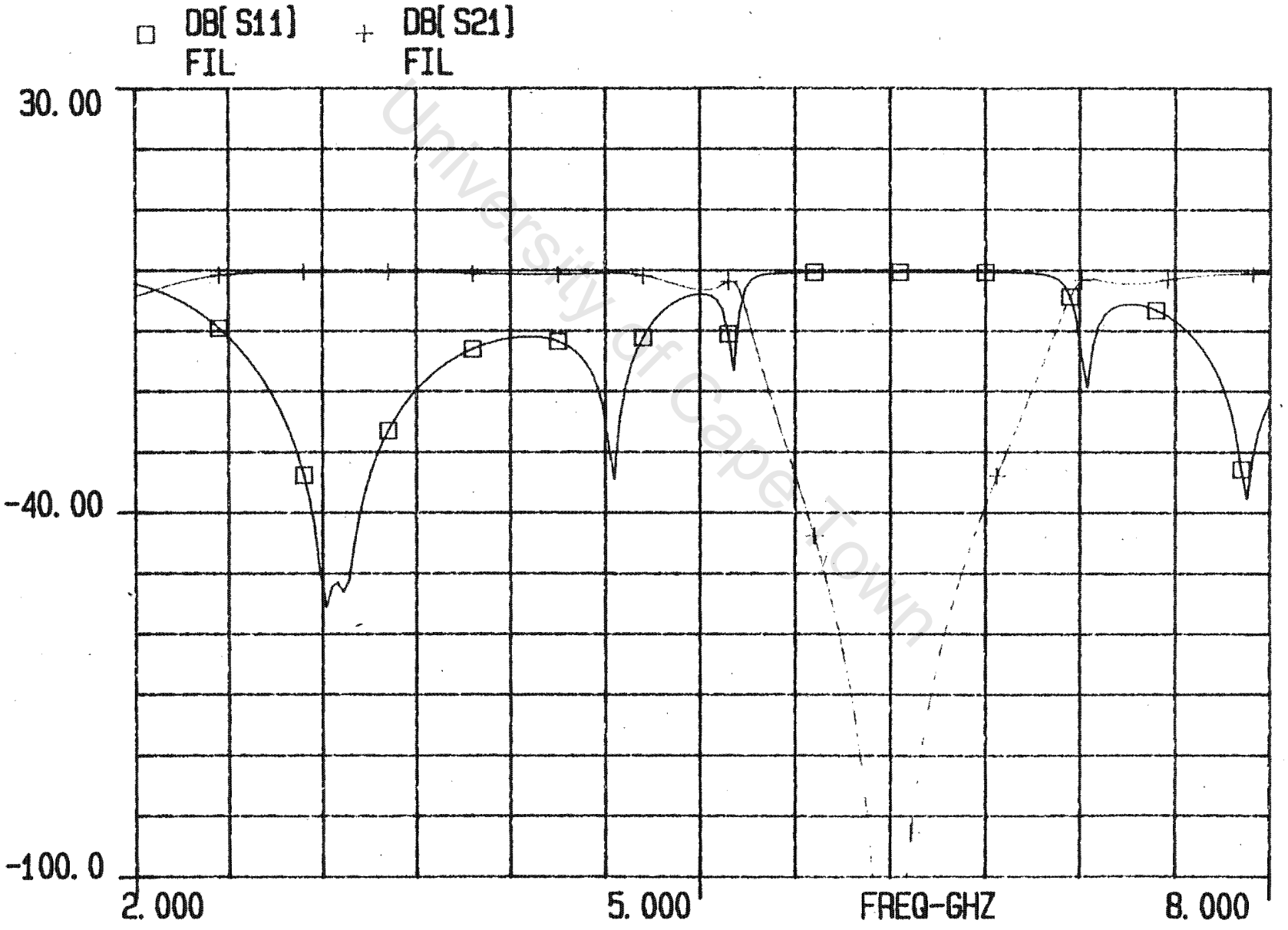

FIGURE 56

A program entitled "6GSNOTCH.CKT" was written, the objective was to determine the effect of the resistance of the short circuit stubs, which were fabricated using brass screws; on the characteristics of the filter. The program can be found in Appendix G. The microwave resistance of the screw was assumed to be 1Ω . The return loss and transmission loss for a four stub filter can be found in figure 57.

Comparing figures 56 and 57 it appears that the null is wider (1800 MHz as compared to 1400 MHz) and possibly deeper, if the screw resistance is taken into account. The transmission loss at 3 GHz appears to be deeper, it can thus be expected that slightly less 3 GHz signal will propagate.

7.3.1 Analysing the operation of the 6 GHz notch filter

Figure 58 shows dimensions of the filter.

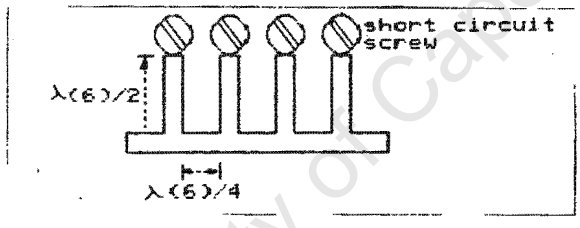

Figure 58. 6 GHz notch filter

At 6 GHz the short circuit stubs provide an input impedance of:

$$Z_{in}(6GHz) = Z_o * \frac{[Z_1*\cos(2*\pi*l/\lambda) + j*Z_o*\sin(2*\pi*l/\lambda)]}{[Z_o*\cos(2*\pi*l/\lambda) + j*Z_1*\sin(2*\pi*l/\lambda)]} \quad ..(7.4)$$

letting $l = \lambda/2$, this yields:

$$Z_in(6GHz) = Z_o * \frac{[Z_1*\cos(\pi) + j*Z_o*\sin(\pi)]}{[Z_o*\cos(\pi) + j*Z_1*\sin(\pi)]}$$

$$= Z_o * \frac{(-Z_1)}{(-Z_o)}$$

$$= Z_1$$

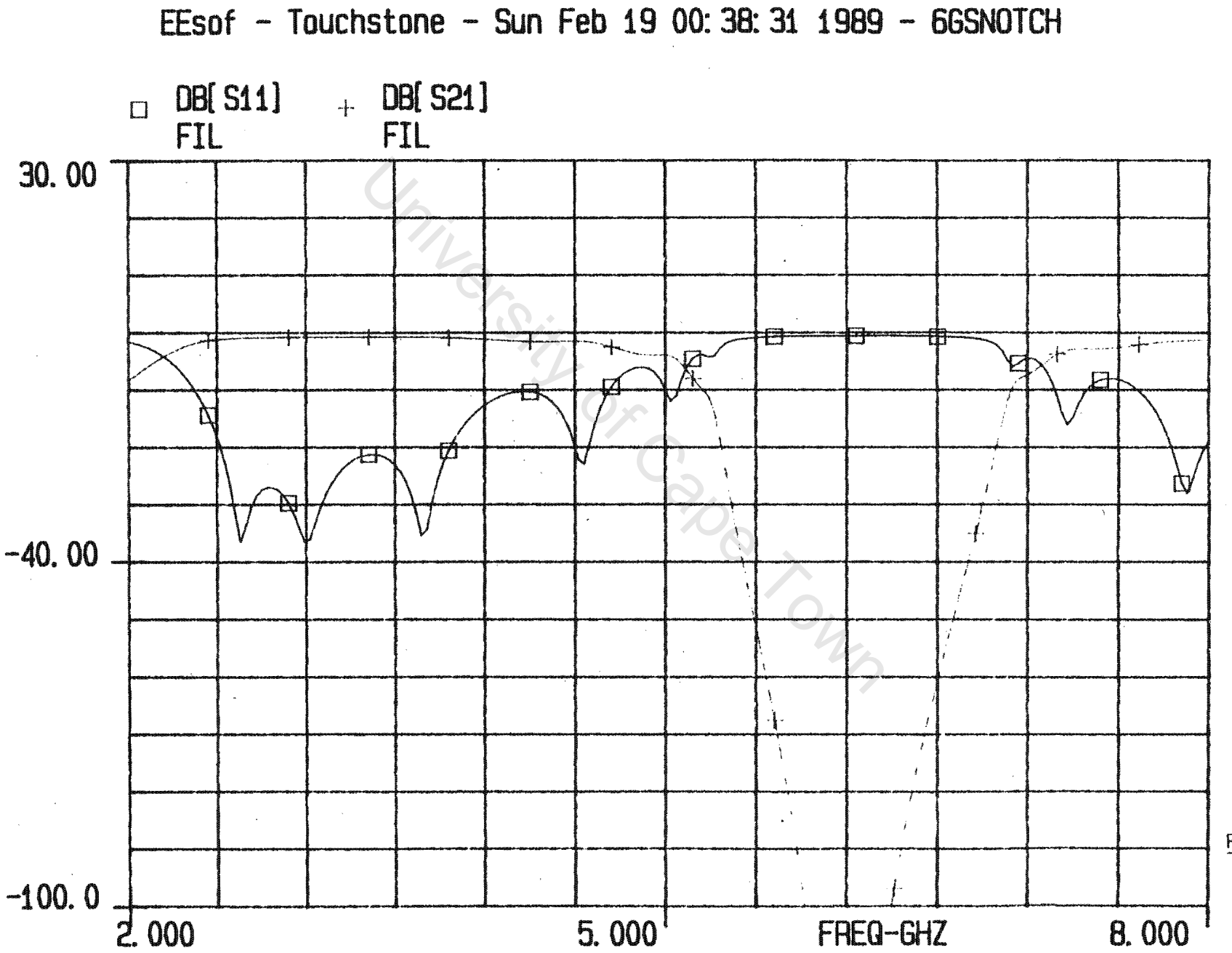

FIGURE 57

Now $Z_{in}(6GHz) \rightarrow 0$ since $Z_1 \rightarrow 0$ (short circuit stub)

Therefore the stub presents a low impedance for signals at 6 GHz. At 3 GHz, however, $\lambda(3) = 2*\lambda(6)$
therefore $\lambda(6)/2 = \lambda(3)/4$
i.e. at 3 GHz, the stub is a quarter wavelength long, therefore:

$$Z_{in}(3GHz) = Z_o^2/Z_1$$
$$= 50^2/0$$

therefore, $Z_{in}(3GHz) \rightarrow \infty$, and hence the 3 GHz signal will tend not to propagate into the stub. The expectation thus is that 6 GHz frequency components will tend to be reflected, while the 3 GHz component is propagated with very little attenuation.

7.3.2 Testing the 6 GHz notch filter

A 6 GHz notch filter was constructed using RT-Duroid 5880 and the dimensions laid down in Appendix G. A positive photo print of the filter is shown in figure 59.

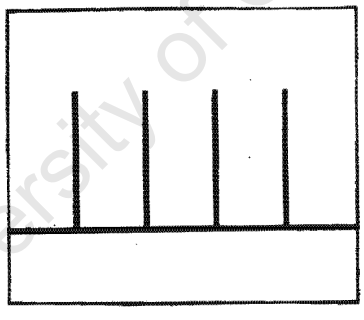

Figure 59. Positive print of 6 GHz notch filter

The return loss and insertion loss for the 6 GHz filter was measured using an HP 8410 B network analyser. Figure 60(a)&(b) show the characteristics of this filter.

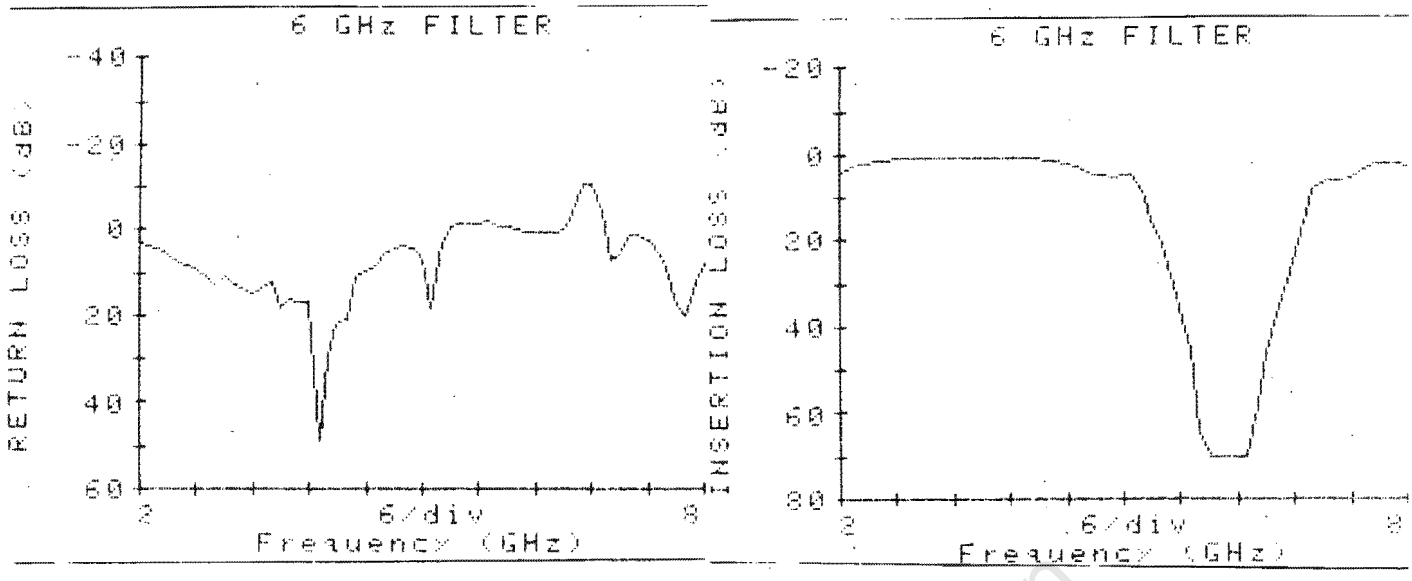

Figure 60(a)&(b). Return and insertion loss of 6 GHz notch filter

Comparing figure 60 and figure 56, it can be noted how accurately the filter conforms to theoretical prediction. Table 7 compares the practical results with theoretical prediction.

	Freq(GHz)	S12(dB)	notch bandwidth (MHz)
predicted	6	>-100	1400
actual	6	-70	1800
predicted	3	+/-0	-
actual	3	-0.4	-

Table 7. Predicted and actual characteristics of 6 GHz filter

The transmission is approximately 0 dB at 3 GHz, as expected. The depth of the null is less than what is expected, but this could be due to losses in the microwave substrates which were not taken into account by the program.

7.3.3 Conclusions

The 6 GHz notch filter compares favourably with that designed on Touchstone. Table 7 indicates that it will work satisfactorily as

a notch filter at 6 GHz, and that there will be negligible attenuation of the 3 GHz signal:

$$\% \text{ attenuation} = 100-100*\text{ALOG}(-0.4/10) \text{ (at 3GHz)}$$
$$= \underline{9\%}$$

CHAPTER 8

DESIGN AND CONSTRUCTION OF 6 GHz POWER SPLITTERS/COMBINERS

8.1 Theory of power splitter operation

8.1.1 Determining the isolation and transmission coefficients of the splitter

From figure 46 in chapter 6, it can be seen that the frequency multiplication system requires a power splitter and a power combiner. Both devices must operate at a center frequency of 6 GHz and have a wide enough bandwidth to ensure frequency drift of the oscillators. The coupling between the input port and the output ports must be as close as possible to 3 dB to ensure maximum power transfer. Thus there must be adequate return loss at the input port and suitable isolation between the two output ports.

A three port hybrid which works well as both a power splitter and power combiner is that described by Wilkinson. This has been described by Cohn [14]. Figure 61 shows a Wilkinson power splitter with quarter wavelength transformers and 100Ω isolation resistor.

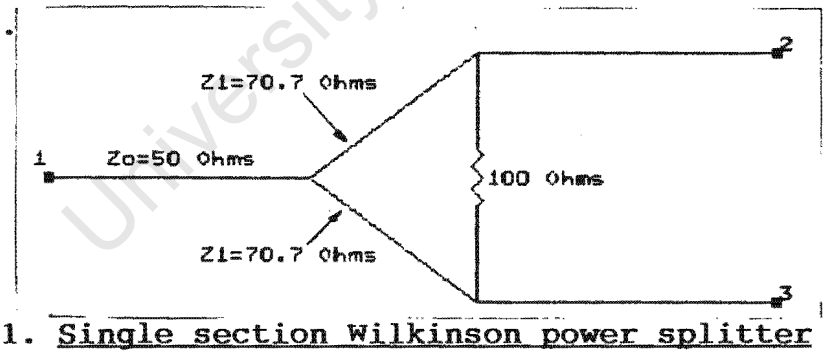

Figure 61. Single section Wilkinson power splitter

As power enters port 1 it is split equally between the two output ports 2 and 3. Theoretically, there is zero phase difference between the ports, with the isolation resistor across the output ports providing output matching and isolation.

The role of the resistor can be analysed by the method of even and odd mode excitation of ports 2 and 3 with a load Z_o connected to port 1.

With even mode excitation, waves of equal amplitude and zero phase difference are applied to ports 2 and 3. The voltage difference between the ports is zero, and no power is dissipated in the resistor. The power output at port 1 is the total power from ports 2 and 3 minus the reflected power.

Since there is no current flow through the resistor, figure 61 can be redrawn as in figure 62. The left hand load is replaced by $2*Z_o$ because of the bisection of the circuit.

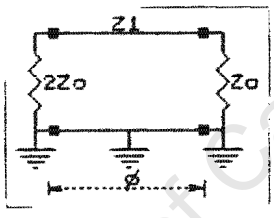

Figure 62. Circuit bisected for even mode analysis

Odd mode excited waves are now applied to ports 2 and 3. These are waves of equal amplitude but opposite phase. The application of these signals to the output ports creates a substantial voltage difference across the resistor.

Because of symmetry,the midpoint of the resistor and the node at port 1 are at ground potential, figure 61 can thus be redrawn as follows in figure 63.

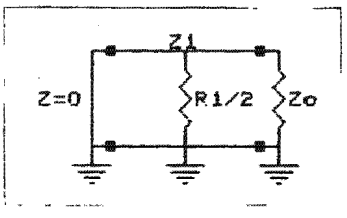

Figure 63. Circuit bisected for odd mode analysis

If the situation is reversed and incident waves approach from the left (port 1), then figures 62 & 63 can be redrawn as in figures 64 & 65.

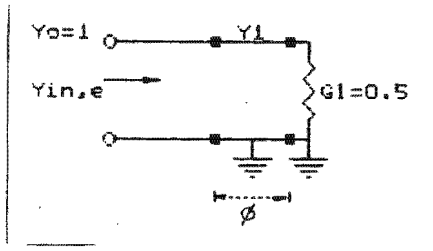

Figure 64. Admittance circuit: even mode

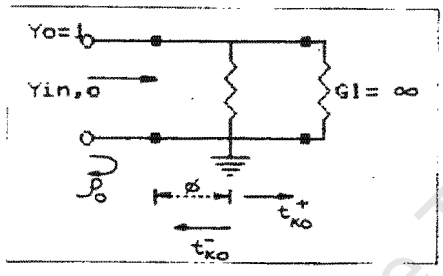

Figure 65. Admittance circuit: odd mode

Admittance representation is simpler to analyse. It has been shown , that the following substitutions can be made.

$$Y_1 = 1/Z_1 \quad , \quad G_1 = 1/R_1 \quad , \quad Y_o = 1/Z_o = 1$$
$$G_1 = 1/(2*Z_o) = 0.5$$

ρ_e and ρ_o are the even and odd mode reflection coefficients, and ρ_1, ρ_2,and ρ_3 are the voltage reflection coefficients at ports 1,2 and 3. t_{12}, t_{13} and t_{23} are the voltage transmission coefficients between the ports.

It has been shown that the following results hold for the symmetrical three port case:

$$|\rho_e| = |\rho_1|$$
$$t_{12} = t_{13} \qquad ..(8.1)$$
$$|t_{12}| = |t_{13}| = 0.5*\sqrt{(1-\rho_e)^2} \qquad ..(8.2)$$

$$\rho_2 = \rho_3 = 0.5*(\rho_e + \rho_o) \quad ..(8.3)$$
$$t_{23} = 0.5*(\rho_e - \rho_o) \quad ..(8.4)$$

The isolation provided by the resistor can be understood in a different way.

Firstly it is assumed that the source impedance is 50Ω . A match at the input is achieved by transforming the 50Ω (characteristic impedance) to 100Ω . This is done by using a quarter wavelength transformer, with a line impedance of 70.7Ω . The resistor R (from figure 61) has a value of 100Ω. Each output port effectively has two loads of 100Ω in parallel with it (which equals 50Ω). The input port is thus matched to the resistor.

Any signal incident at port 2 can reach port 3 via two routes. One is through the resistor, which is assumed to have zero length. The other path is through the two quarter wavelength sections. The two signals thus arrive at port 3 with equal amplitude but 180° out of phase (odd mode). The two waves thus destructively interfere and cancel each other. Therefore the resistor isolates port 2 from port 3.

The magnitude of the isolation is determined by the difference in path length between ports 2 and 3. A major source of error is the resistor length, which is theoretically zero. This is not possible and the consequence is that the two signals will not arrive exactly 180° of phase. This will decrease the isolation between the ports.

8.1.2 Simulating the 6 GHz power splitter

The power splitter/ combiner used in the frequency multiplication system required a reasonably wide bandwidth to accommodate shifts in frequency of the oscillators. The return loss from the input and output ports had to be low, hence the VSWR for the ports had to be as close as possible to unity. The isolation between the

output ports had to be high and the coupling between input and output ports had to be as tight as possible to ensure maximum power transfer.

The standard single section Wilkinson power splitter described before had a usable bandwidth of 1.44:1 for VSWR <1.22 and isolation > 20 dB. The bandwidth could be increased by adding more resistive elements, but a bandwidth ratio of 1.44 :1 was satisfactory for the frequency multiplication system. It was thus decided that a single section Wilkinson power splitter be used for the system.

A program entitled 6GSPLIT.CKT was written for the package Touchstone, to determine how closely it conformed to theoretical prediction. The program can be found in Appendix H. It describes the return loss from port 1, the isolation between ports 2 and 3, and the transmission loss from port 1 to ports 2 and 3. It was designed using widths and lengths for a 6 GHz transmission line (obtained from Appendix A). A plot of the power splitters characteristics can be found in figure 66. These characteristics are summarised in table 8.

FREQ-GHZ	DB[S11] SPLIT	DB[S12] SPLIT	DB[S13] SPLIT	DB[S23] SPLIT
2.00000	-10.714	-3.545	-3.545	-3.169
2.50000	-11.496	-3.502	-3.502	-9.651
3.00000	-12.559	-3.452	-3.452	-11.158
3.50000	-13.839	-3.400	-3.400	-12.806
4.00000	-15.397	-3.351	-3.351	-14.777
4.50000	-17.530	-3.309	-3.309	-17.314
5.00000	-20.377	-3.278	-3.278	-20.356
5.50000	-27.074	-3.263	-3.263	-26.788
6.00000	-43.727	-3.264	-3.264	-55.993
6.50000	-26.699	-3.284	-3.284	-27.056
7.00000	-21.140	-3.321	-3.321	-20.916
7.50000	-17.798	-3.373	-3.373	-17.391
8.00000	-15.442	-3.437	-3.437	-14.923

Table 8. Characteristics of 6 GHz power splitter

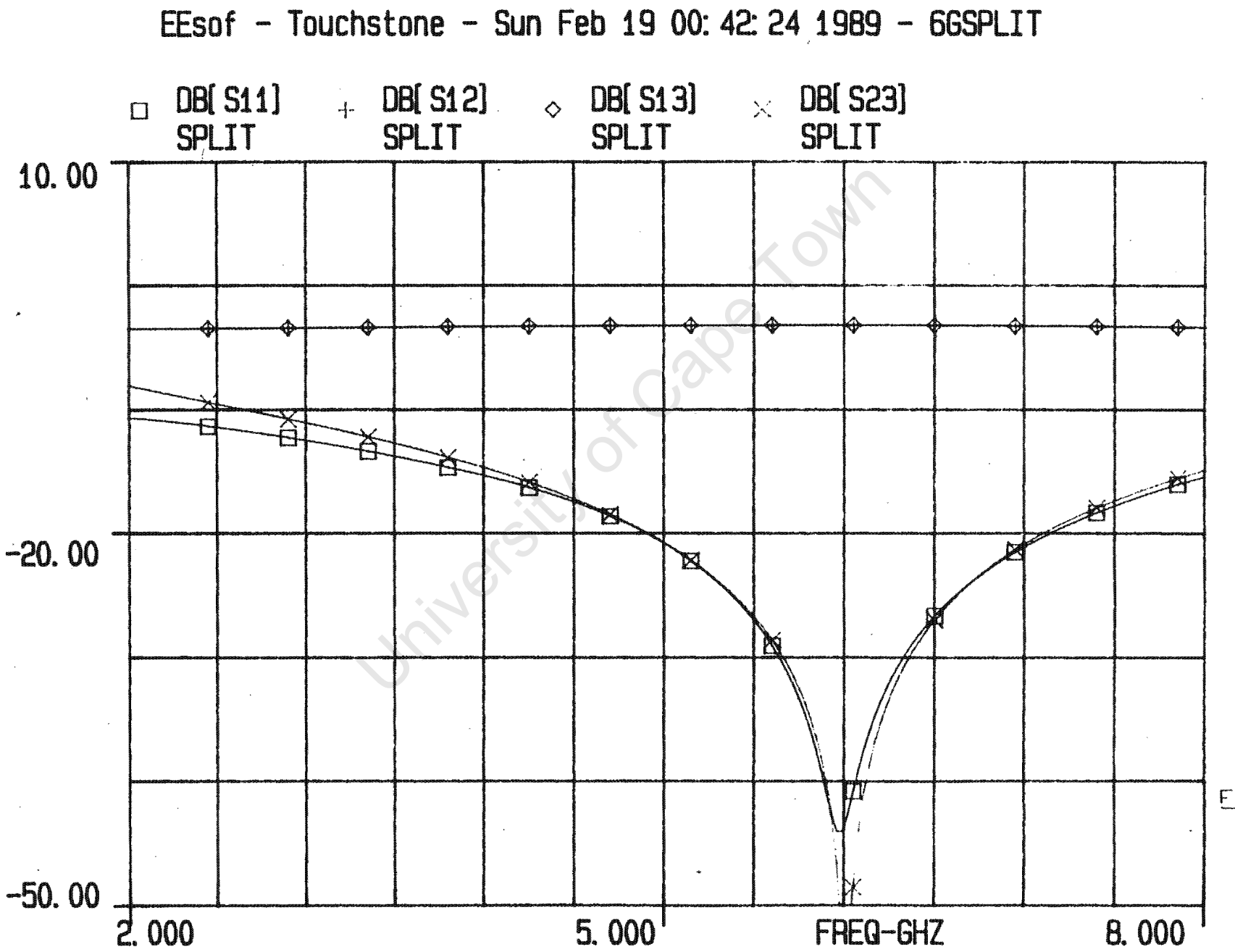

FIGURE 66

It can be seen that the return loss from port 1 is lowest (-43.7 dB) at 6 GHz, the isolation between ports 2 and 3 is greatest (= 55.99 dB) at 6 GHz. The coupling is tightest at 6 GHz with a transmission loss of -3.264 dB.

It can also be seen that the return loss and isolation is below= 20 dB for the 2:1 bandwidth, and the transmission loss is almost linear varying from -3.263 dB to -3.373 dB.

These values indicate that the simulation results conform to those predicted by theory.

The VSWR for each of the ports was determined using the formulas:

$$\text{VSWR(port1)} = \frac{1 + \text{ALOG (S11/20)}}{1 - \text{ALOG (S11/20)}} \qquad ..(8.5)$$

$$\text{VSWR(ports 2\&3)} = \frac{1 + \text{ALOG (S23/20)}}{1 - \text{ALOG (S23/20)}} \qquad ..(8.6)$$

Figure 67 shows the VSWR for the splitter for the input and output ports.

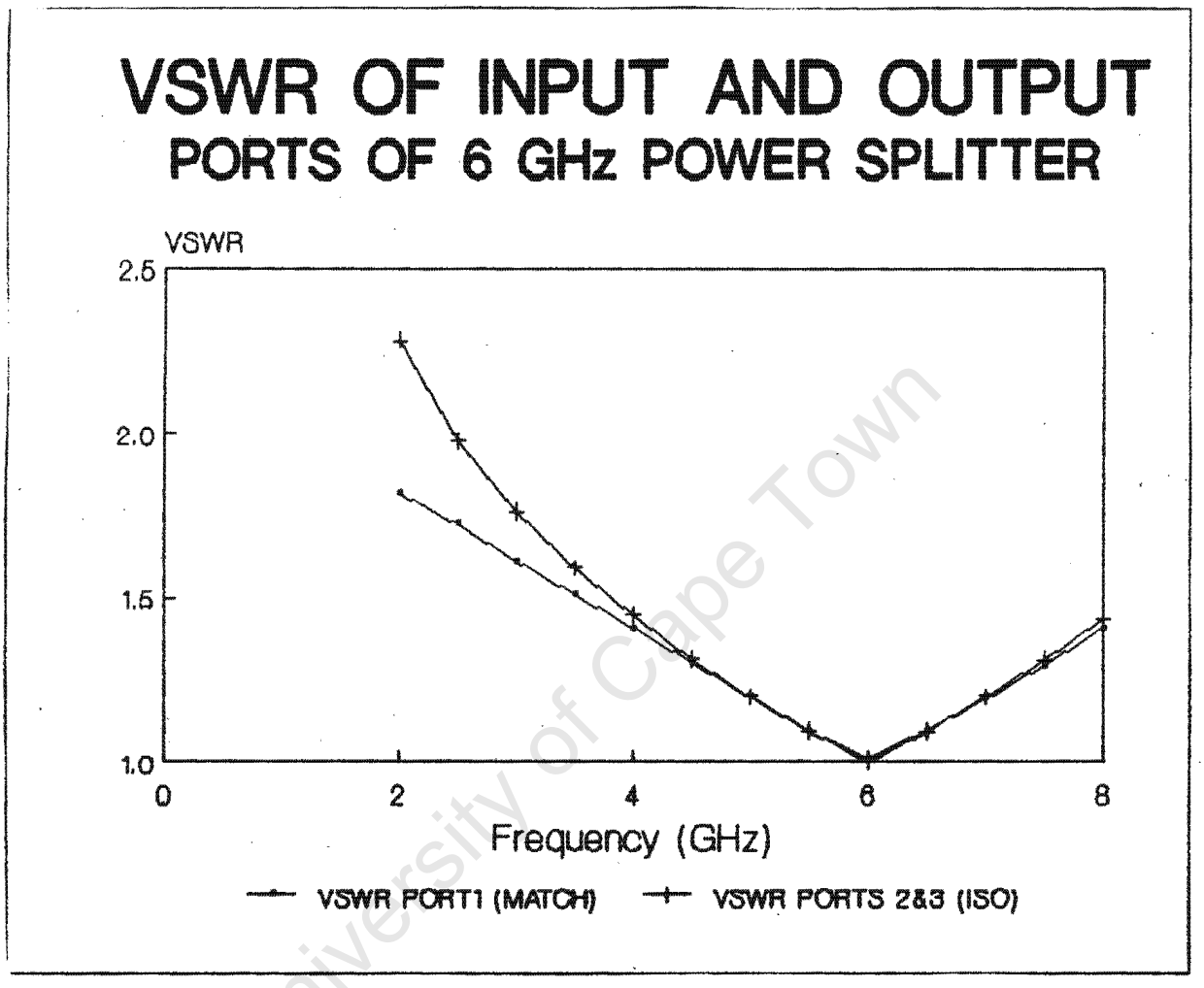

Figure 67. VSWR of the power splitter

From figure 67 it can be seen that the VSWR is approximately <1.22 for the bandwidth ratio of 1.44:1. The VSWR approaches unity at the center frequency of the power splitter. The characteristics of this splitter indicate that it will operate effectively over the bandwidth of the frequency multiplication system.

8.1.3 Simulating the effects of the quarter wavelengths and isolation resistor

The simulation package Touchstone is useful in analysing the effects of resistance, line widths and lengths, and other factors on the losses of the power splitter.

The first step in analysing the effect of each component of the power splitter on its operation was to determine the return loss and isolation for a simple three port circuit. The impedances of the two output ports would then be increased from 50Ω to 70.7Ω , and the effect of this change on the reflection coefficients and isolation, would be noted. Finally, a 100Ω resistor would be placed across the terminals of the output ports. This is the standard power splitter/combiner.

A program entitled 3PORT1.CKT was written for the simulation package Touchstone, and can be found in Appendix H. The aim of the program was to determine the characteristics of a simple three port circuit as in figure 68.

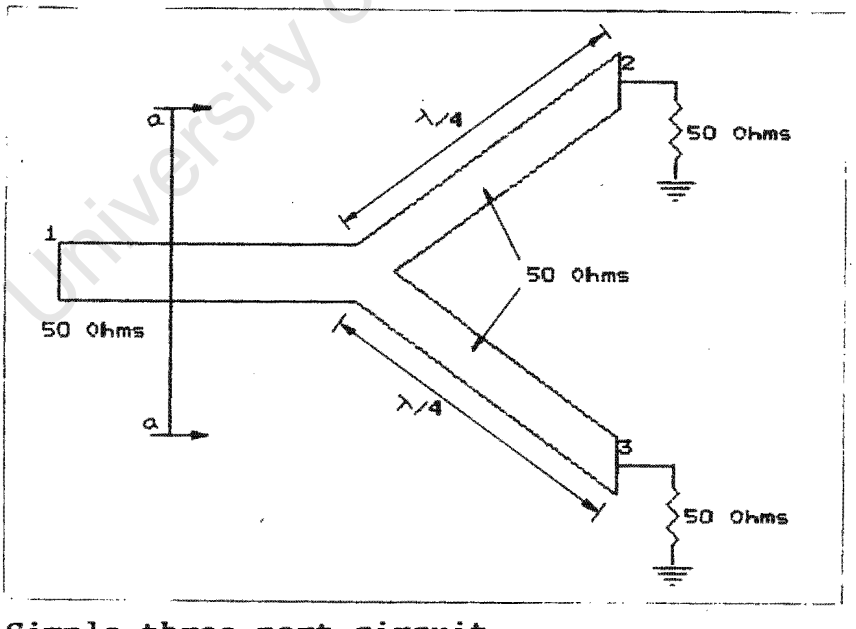

Figure 68. Simple three port circuit

This circuit can be analysed using simple transmission line formulas:

Impedance looking in at a : = 50Ω//50Ω
= 25Ω

Reflection coefficient from a back to source

$$\rho = \left| \frac{Z_1 - Z_o}{Z_1 + Z_o} \right|$$

Power reflected: $P_{ref}(a) = |\rho|^2 * P_{in}$
$= P_{in}/9$

Therefore $S11 = 10*LOG(P_{in}/P_{in}/9)$
$= \underline{9.54\ dB}$

Power transmitted: $= P_{in} - P_{ref}(a)$
$= P_{in}(1 - 1/9)$
$= P_{in}(8/9)$

Power transmitted into each element: $= P_{in}(4/9)$
Therefore transmission loss $= -10*LOG(P_{in}/P_{in}(4/9))$
$= \underline{-3.52\ dB}$

Table 9 shows the return loss and reflections from the output ports for the program 3PORT1.CKT.

FREQ-GHZ	DB[S11] SPLIT	DB[S12] SPLIT	DB[S13] SPLIT	DB[S23] SPLIT
2.00000	-9.687	-3.570	-3.570	-3.554
2.50000	-9.674	-3.573	-3.573	-3.562
3.00000	-9.657	-3.576	-3.576	-3.570
3.50000	-9.640	-3.579	-3.579	-3.576
4.00000	-9.626	-3.584	-3.584	-3.579
4.50000	-9.619	-3.589	-3.589	-3.580
5.00000	-9.619	-3.595	-3.595	-3.579
5.50000	-9.625	-3.601	-3.601	-3.576
6.00000	-9.635	-3.607	-3.607	-3.573
6.50000	-9.647	-3.613	-3.613	-3.571
7.00000	-9.660	-3.617	-3.617	-3.570
7.50000	-9.669	-3.620	-3.620	-3.573
8.00000	-9.676	-3.622	-3.622	-3.577

Table 9. Characteristics of a simple three port device

It can be seen that at 6 GHz the return loss is -9.635 dB close to the predicted value of -9.54 dB. Similarly, it was predicted that the transmission loss would be -3.52 dB. From table 9 a loss of -3.607 dB was obtained. This program thus confirms the results obtained from theory.

A second program 3PORT2.CKT was written and can be found in Appendix H. The circuit model contained quarter wavelength sections with $50*\sqrt{2} = 70.7\Omega$ characteristic impedances. Figure 69 shows the circuit and Table 10 contains the characteristics of the circuit.

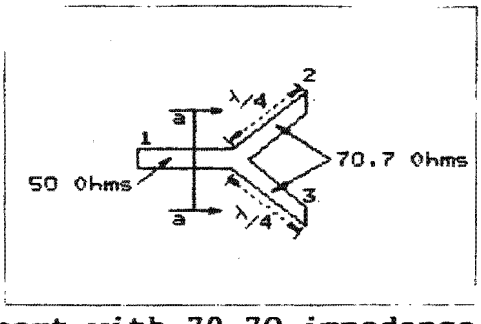

Figure 69. Three port with 70.7Ω impedance transformer lines

FREQ-GHZ	DB[S11] SPLIT	DB[S12] SPLIT	DB[S13] SPLIT	DB[S23] SPLIT
2.00000	-10.807	-3.449	-3.449	-4.431
2.50000	-11.489	-3.392	-3.392	-4.784
3.00000	-12.406	-3.331	-3.331	-5.123
3.50000	-13.635	-3.269	-3.269	-5.427
4.00000	-15.294	-3.213	-3.213	-5.683
4.50000	-17.600	-3.164	-3.164	-5.883
5.00000	-21.035	-3.127	-3.127	-6.023
5.50000	-27.149	-3.104	-3.104	-6.104
6.00000	-46.007	-3.099	-3.099	-6.127
6.50000	-26.468	-3.112	-3.112	-6.095
7.00000	-20.807	-3.142	-3.142	-6.010
7.50000	-17.558	-3.189	-3.189	-5.872
8.00000	-15.349	-3.247	-3.247	-5.680

Table 10. Characteristics for three port with 70.7Ω lines

Comparing table 10 and table 9, it can be seen that the return loss from port 1 has improved from -9.635 dB to -46 dB. The coupling between the input and output ports has tightened slightly from -3.607 dB to -3.099 dB, and the isolation has increased from -3.573 dB to -6.127 dB.

It can be seen that increasing the impedance of the two quarter wavelength transformers, has dramatically improved the return loss from the input port, with minor improvement to the isolation and coupling.

To complete the analysis of the splitter, a 100Ω resistor was added to the output stage. This is thus the standard single section power splitter. The results for the splitter have been shown in table 8. Comparing tables 8 and 10, it can be seen that the primary effect of the resistor is to increase the isolation from -6.127 dB to -55.993 dB. The return loss from port 1 has decreased slightly from -46.009 dB to -43.727 dB, as well as the

transmission loss which has decreased from -3.099 dB to -3.264 dB. These values are still satisfactory for the operation of the power splitter.

8.2 Designing the 6 GHz power splitter/combiner

In designing the power splitter it is important to note the effects of the following physical parameters on the splitters performance.

8.2.1 Physical constraints on power splitter operation

a) Front end T-junction
b) Coupling between conductors
c) Non zero length isolating resistors
d) Curved conductors

a) front end T-junction

It has been shown [15],[16] that the first discontinuity that a signal sees on entering a power splitter is the t-end junction. The signal splits into two even sections at this point. It is also at this point that the transmission line width changes. The front end t-junction effect was modelled on Touchstone. It was found that its main effect was to alter the VSWR of the input port.

b) Coupling between conductors

After separation from the T-end junction, the two quarter wavelength sections must be separated by the length of an resistor. If these lines were parallel to each other, there would be coupling between them. The center frequency at which the splitter operates will also be the frequency at which coupling is greatest. The effect of this coupling was to reduce the input VSWR.

The coupling between the lines can be reduced by making the

spacing between adjacent conductors as great as possible, and to ensure that conductors are not parallel to each other.

d) Non zero length isolating resistors

It has already been indicated that non zero length resistors change the path length difference between ports 2 and 3. Signals travelling from port 2 to 3 via the quarter wavelength sections should be 180° out of phase with the signals flowing through the resistor. However, if the resistor length is non zero, the phase difference will not be 180° and the isolation between the ports will decrease.

It has been shown that the input return loss and the isolation nulls occur at higher frequencies than the center frequency of operation of the power splitter.

A solution is thus to use resistors with the shortest possible lengths.

d) Curved conductors

It is known [17] that parallel transmission lines will couple to each other, and a solution is to curve the conductors. Slow curves offer less radiation loss at high frequencies than the sharp bends. It has been suggested that a minimum radius of 2 or 3 times the line width would be used. A radius of approximately 5 times the line width was used in the final design.

Touchstone did not have an algorithm to model curved conductors, thus no analysis of the effects of curved conductors could be made.

8.2.2 The schematic of the power splitter

Line widths and lengths were obtained from Appendix A, for the 6 GHz power splitter. These dimensions are given below for two impedances.

Z_o (6 GHz)	W (mm)	L(mm)
50	0.76	36.57
70.7	0.43	37.24

The lengths of the quarter wavelength sections were chosen to be $(5/4)\lambda$ instead of the customary $\lambda/4$ lengths. This was done to ease practical problems with the positioning of isolation resistors. A quarter wavelength at 6 GHz was 9.31 mm. The resistor had a length of 1 mm. This was a substantial part of a quarter wavelength. It was decided that if the transformer lengths could be increased, then there would be less constraint on the positioning of the resistor. Thus more gentler curves could be used. This would also have the advantage that the conductors could be placed further apart, thus reducing coupling.

The circuit was tested using Touchstone. The program called 6GSPLIT2.CKT can be found in Appendix H. Various algorithms were used to determine the operation of the splitter more accurately. Losses due to the front end T-junction, the change in line width at the resistor node, and the effects of the resistors length,width and resistivity, could be analysed. The results of this program can be seen in figure 70.

Comparing figures 70 and 66, it can be seen that the depths of the nulls for the isolation and return loss have been reduced. The results can be seen more clearly in Table 11.

FREQ-GHZ	DB[S11] SPLIT	DB[S12] SPLIT	DB[S13] SPLIT	DB[S23] SPLIT
2.00000	-11.057	-3.584	-3.604	-8.930
2.50000	-9.700	-3.771	-3.756	-4.148
3.00000	-12.018	-3.597	-3.574	-10.100
3.50000	-21.975	-3.339	-3.335	-15.867
4.00000	-17.560	-3.402	-3.418	-14.965
4.50000	-10.995	-3.697	-3.750	-8.410
5.00000	-9.799	-3.887	-3.840	-4.888
5.50000	-12.502	-3.666	-3.633	-10.707
6.00000	-24.183	-3.421	-3.420	-16.436
6.50000	-16.514	-3.505	-3.538	-14.368
7.00000	-10.893	-3.780	-3.873	-7.830
7.50000	-10.025	-3.964	-3.887	-5.727
8.00000	-12.918	-3.719	-3.683	-11.191

Table 11. Characteristics of designed splitter

A notch at approximately 3.6 GHz has been created by the $(5/4)\lambda$ length sections. It was found that the reduction in the input match and isolation was predominantly caused by the isolation resistors length and width. The effect of the increased transformer lengths was to decrease the bandwidth of the power splitter, at 6 GHz, and to allow operation at a lower frequency. The bandwidth of the power splitter was still adequate for the needs of the frequency multiplication system.

Thus the reduction in the bandwidth of the system, is overshadowed by the practical advantages of using larger than usual transformer sections.

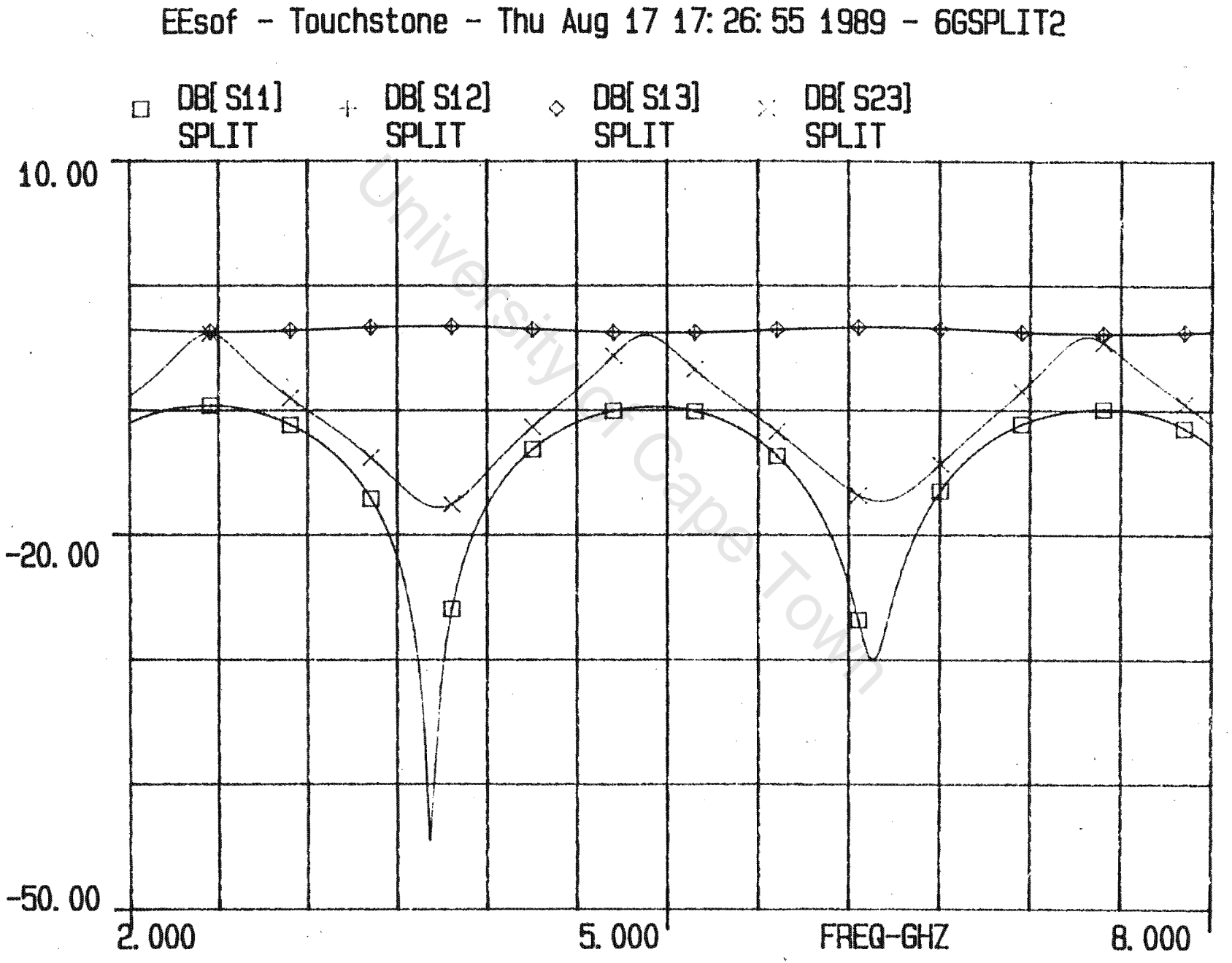

FIGURE 70

8.2.3 Testing the power splitter

A power splitter was designed and constructed using ethic described before. A positive print of the device can be found in figure 71.

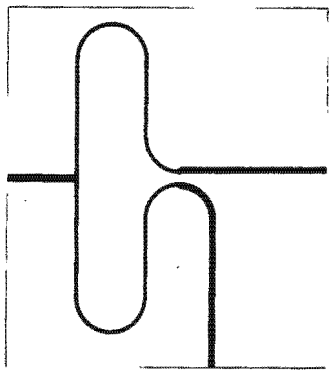

Figure 71. Positive print of power splitter

The characteristics of the power splitter were obtained from analysis with a network analyser. Figures 72(a)..(f) show the return loss, isolation between the output ports and coupling between input and output ports.

From figure 72(d) it can be seen that there is a null at 6.5 GHz (return loss -24 dB). The return loss at 6 GHz was approximately 8 dB. The return loss is best at 6.5 GHz, because of the length and width of the isolation resistor. Even though the return loss is low at 6 GHz, the power splitter will be driven from a good source (6 GHz oscillator) which has an output impedance of 50Ω . The isolation at 6 GHz was found to be 25 dB, with a 1.4 GHz bandwidth null. This value is close to what is defined in the literature as typical power splitter characteristics.

The coupling between the input port and output port 3, is shown in figure 72(f). The coupling at 6 GHz was found to be approximately 3 dB. It was noticed, however, that the coupling tended to vary between 2.6 dB and 4.5 dB over the band from 5 to 6 GHz.

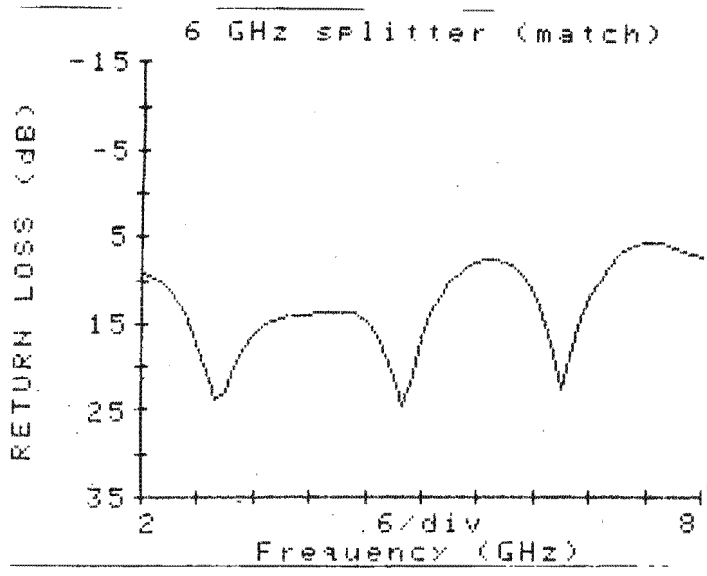

fig. 72(a)

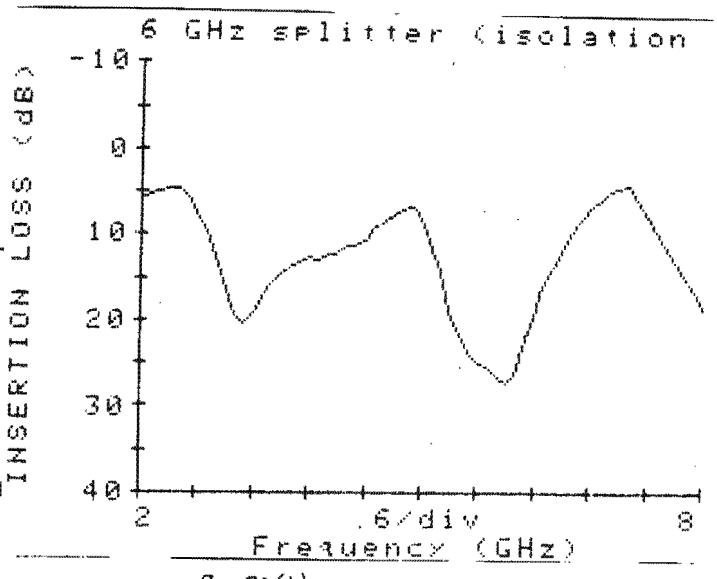

fig 72(b)

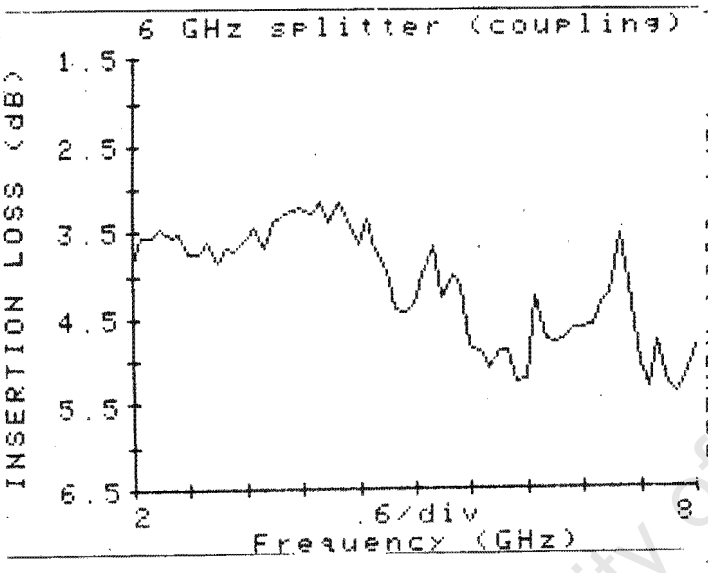

fig 72(c)

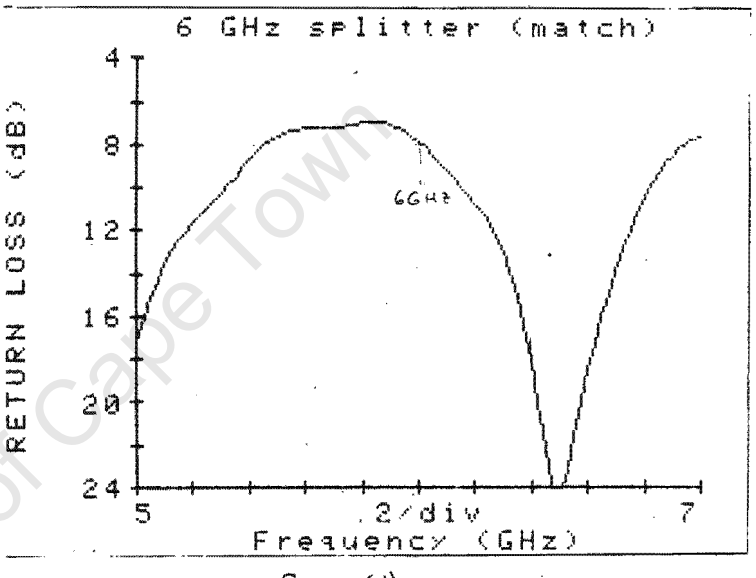

fig 72(d)

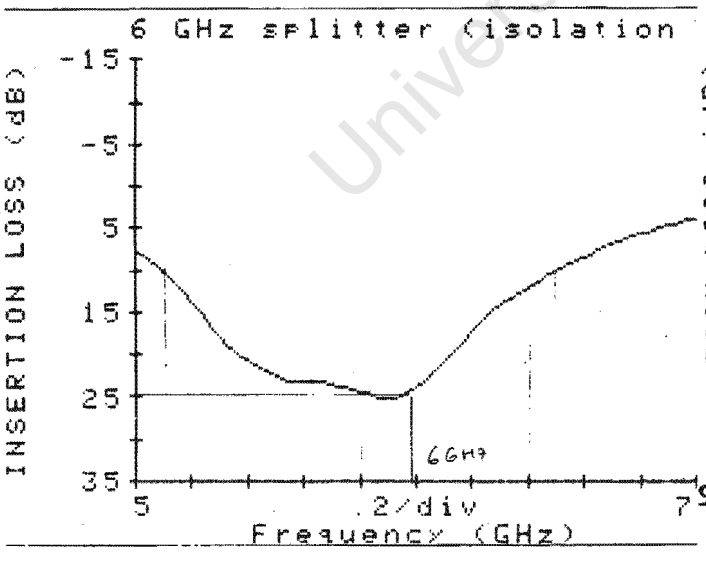

fig 72(e)

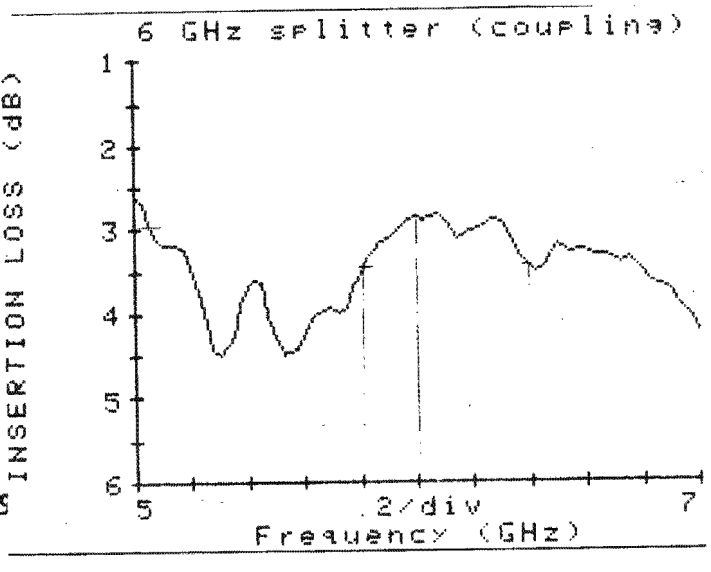

fig 72(f)

This means that the power coupled from the input to the output port varies from between 36 and 55%. The power reaching the single ended mixer might be too low to switch the diode on. The oscillator is not expected to wander in frequency from 5 to 6 GHz, however. A more realistic spread of frequencies would be 5.8 to 6.4 GHz where the power split varies from 3 to 3.5 dB (45 to 50%). It is expected that the single ended mixer could cope with a 45% reduction in oscillator power, as explained in chapter 10.

Further simulation on Touchstone indicated that resistor placement was very critical, and predominantly effected the return loss. A second version of the power splitter was constructed, and the position of the resistor optimized to produce minimum return loss. It was found that a match of -14 dB could be attained with negligible change in the isolation and transmission losses.

8.2.4 Conclusions

The power splitter will operate effectively over the band from 5.8 to 6.4 GHz. The coupling varying from 3 to 3.5 dB, the isolation from 10 dB to 25 dB and the return loss from 8 to 18 dB over this band. It has been indicated that the poor return loss at the center frequency is improved with correct resistor placement.

CHAPTER 9

THE 6 GHz DIRECTIONAL COUPLER

From figure 46 it can be seen that a directional coupler, centered at 6 GHz, is required for the transmitter unit. Power, at 6 GHz, will be reversed coupled to the single ended mixer, while the main component of 3 GHz signal is transmitted directly to the 3 GHz horn antenna. The next section analyses the directional coupler and discusses a computer aided design technique.

9.1 The theory of directional coupler operation

A directional coupler is a four port device consisting of two parallel transmission lines separated by a short distance. The coupling length is usually set at a quarter wavelength corresponding to the center frequency of operation.

It is known [18] that the lowest mode of propagation along parallel lines in a homogeneous media is a TEM mode. Due to the inhomogeneities in microstrip, TEM modes cannot be propagated because of different phase velocities in the different media.

In microstrip the inhomogeneity is caused by the dielectric which has a relative permittivity ϵ_r and a relative permeability μ_r. The relative permeability is generally close to unity, since the dielectric is non magnetic. Figure 73(a) shows a microstrip coupler, while figure 73(b) indicates the electric field distribution for even and odd mode excitation of the coupled lines.

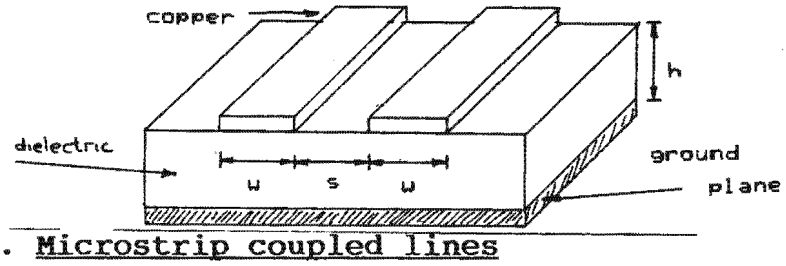

Figure 73(a). Microstrip coupled lines

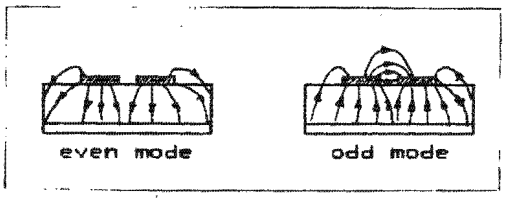

Figure 73(b). Electric fields due to even and odd mode excitation

Even mode propagation results when signals of equal phase and amplitude are transmitted down the coupled lines. Odd mode propagation results when waves of equal amplitude but opposite phase are propagated down the coupled line.

Characteristic impedances and phase velocities in even and odd modes may be found from the even and odd mode inductances and capacitances. The inductance is computed from the capacitance of a medium with dielectric constant of one. Thus the inductive coupling coefficient K_1 is not dependent on the relative permittivity but on the relative permeability.

The coupled transmission lines can be modelled with capacitances and inductances, as in figure 74(a)&(b)

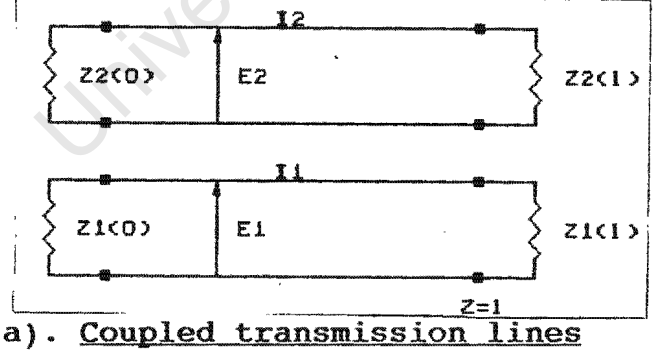

Figure 74(a). Coupled transmission lines

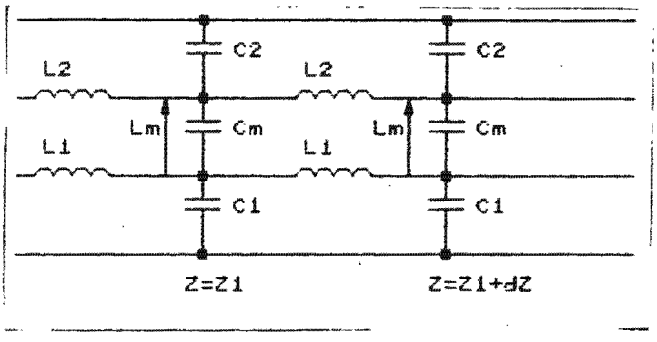

Figure 74(b). Equivalent circuit

Figure 74 indicates the lossless case of two coupled lines where L_j,C_j (j=1,2) are the self inductance and self capacitance per unit length of line j. L_m and C_m are the mutual inductance and mutual capacitance per unit length of line j.

It is known [19],[20] that couplers using microstrip generally have unequal inductive and capacitive coupling coefficients. The exact values of these coefficients are important in the calculation of the coupling coefficients as well as the directivity of the coupler. In the next section the formulas governing these coefficients will be discussed.

9.1.1 Determining the coupled mode formulas

It has been shown [21] that empirical formulas exist for the coupling coefficients, based on the spacing (S) between the lines, the width (W) of the lines and the height (H) of the substrate. These formulas are indicated below.

$$K_c = 0.55*\exp\left[-(A_1*S/H + B_1*W/H)\right] \qquad ..(9.1)$$

$$K_1 = 0.55*\exp\left[-(A_2*S/H + B_2*W/H)\right] \qquad ..(9.2)$$

Where:

$A_1(\epsilon_r) = 1 + (1/4)*Ln(\epsilon_r+1)/2$

$A_2(\mu_r) = 1 + (1/4)*Ln(\mu_r+1)/2$

$$B_1(\epsilon r) = (1/10)*\sqrt{\epsilon_r+1}$$
$$B_2(\mu_r) = (1/10)*\sqrt{\mu_r+1}$$

These formulas indicate that the capacitive coupling coefficient K_c depends on the relative permittivity ϵ_r, while the inductive coefficient K_l varies with the relative permeability μ_r.

The directional coupler can be modelled in terms of wave dynamics, as shown in figure 75.

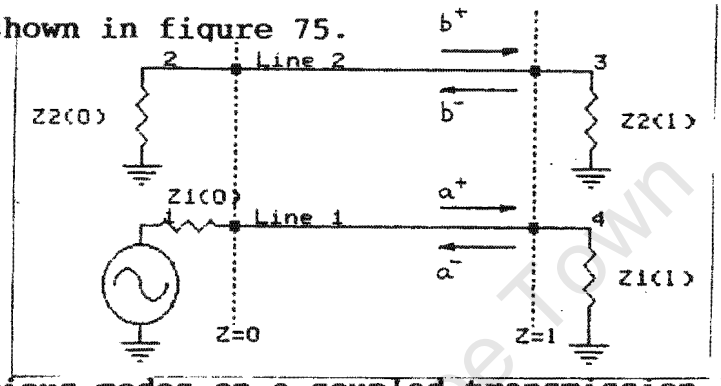

Figure 75. Various modes on a coupled transmission line

The arrows in figure 75 indicate the direction of flow of the various waves:

$a_+(z)$ and $b_+(z)$ are the complex amplitudes of the forward travelling waves on line 1 and 2 respectively. $a_-(z)$ and $b_-(z)$ are the complex amplitudes of the backward travelling waves. The power flowing at any point z along line 1 is given by $a_+(z)^2/2$ (power in forward direction). The power flow in the backward direction is given by $a_-(z)^2/2$. The average power on line 1 at any point z is then given by $[a_+(z)^2 - a_-(z)^2]/2$. Similar relationships hold for line 2 and the b_{+-} modes.

It has been shown [22] that the coupling coefficients and directivity are defined as follows:

$$C = \sqrt{\frac{|b_-(0)|^2*[1-|\rho_2(0)|^2]}{|a_+(0)|^2}}$$

$$C(dB) = -20*\text{Log } C$$

$$D = \sqrt{\frac{|b_+(1)|^2*[1 - |\rho_2(1)|^2]}{|b_-(0)|^2*[1 - |\rho_2(0)|^2]}}$$

$$D(dB) = -20*\text{Log } D$$

where $\rho_i(z)$ is the voltage reflection coefficient of line i at position z.

These are the definitive cases for the coupling coefficients and directivity, however it has been shown that there are approximations for various special cases. A case of particular interest is that of where $K_1 \neq K_c$, $\beta_1 = \beta_2$ (The case for microstrip). This case holds for a medium where the inductive and capacitive coupling coefficients are not equal, but the phase constants for the lines are equal.

The following definitions are used:

$$\phi_1 = \sqrt{(1 + K_1)*(1 - K_c)} \qquad ..(9.3)$$

$$\phi_2 = \sqrt{(1 - K_1)*(1 + K_c)} \qquad ..(9.4)$$

$$\theta_1 = \beta_1 *\phi_1*l \qquad ..(9.5)$$

$$\theta_2 = \beta_2 *\phi_2*l \qquad ..(9.6)$$

$$\Delta = K_1 - K_c \qquad ..(9.7)$$

$$l = \frac{\lambda_o}{4*\sqrt{\epsilon_{reff}}} \frac{\sqrt{1 - K_1^2}}{\sqrt{1 - K_1*K_c}} \qquad ..(9.8)$$

and $$\beta_o = \frac{w\sqrt{\epsilon_{reff}}}{c} \frac{\sqrt{1 - K_1*K_c}}{\sqrt{1 - K_1^2}}$$

where β_1, β_2 = line phase constants

Generally, $\beta_o * l = \pi/4$ for the transmission line directional coupler.

Using the formulas above, the mode amplitudes can be obtained. The mode amplitudes formulas can be found in Appendix I.

For this case, it is assumed that the coupler is matched at all ports. When $K_1 \neq K_c$, coupling is introduced between b_+ and the a_+ and b_- modes. Similarly, the a_- mode couples to b_+ and b_-.

9.2 Designing the 6 GHz directional coupler

In the design of the directional coupler, the spacing between the lines is important because it determines the tightness of the coupling. This value is important since the amplitude of the signal coupled from the transmitter will be used as an RF signal for a single ended mixer. This signal may at worst be 30 dB below the magnitude of the local oscillator (in this case 4mW).

It must also be noted that the minimum spacing between the lines that could be etched, was 0.4 mm. This was due to constraints of the etching and cartographic equipment.

The first step in designing the coupler was to determine the inductive and capacitive coupling coefficients. A program called COUPLER.TRU (which can be found in Appendix I) was written. The aim of the program was to calculate inductive and capacitive coefficients for various microstrip characteristics. The following values were chosen to describe the microstrip and the parallel coupling lines.

$\epsilon_r = 9.6$

$\mu r = 1$

height of dielectric h = 0.635 mm
characteristic impedance = 50Ω
length of line l = 4.8 mm
spacing between lines s = 0.4 mm
width of line = 0.56 mm
center frequency = $6*10^9$ Hz

The program produced the following results.

$K_c = 0.1691$ and $K_1 = 0.2586$

Inserting these values in equations (9.3) .. (9.7), the following results were obtained.

$$\phi_1 = \sqrt{(1 + K_1)*(1 - K_c)}$$
$$= \underline{1.0226}$$
$$\phi_2 = \sqrt{(1 - K_1)*(1 + K_c)}$$
$$= \underline{0.9310}$$
$$\theta_1 = \beta_1*\phi_1*l$$
$$= \underline{1.6063}$$
$$\theta_2 = \beta_2*\phi_2*l$$
$$= \underline{1.4624}$$
$$\Delta = K_1 - K_c$$
$$= \underline{0.0895}$$

These values are then inserted into eq's (9.9) .. (9.13), giving:

$$\frac{|b_-(0)|}{|a_+(0)|} = \underline{0.2136} \quad ..(9.18)$$

$$\frac{|b_+(1)|}{|b_-(0)|} = \underline{0.3216} \quad ..(9.19)$$

$$\frac{|a_-(0)|}{|a_+(0)|} = \underline{0.0174} \quad ..(9.20)$$

$$\frac{|a_+(1)|}{|a_+(0)|} = \underline{0.9769} \quad ..(9.21)$$

$$\frac{|b_+(1)|}{|a_+(0)|} = \underline{0.0689} \qquad ..(9.22)$$

$$C(dB) = S_{12} = -20 * \log (0.2136)$$
$$= \underline{13.4076\ dB} \qquad ..(9.23)$$

$$D(dB) = -20*\log (0.3216)$$
$$= \underline{9.8526\ dB} \qquad ..(9.24)$$

$$S_{11} = -20*\log (0.0174)$$
$$= \underline{35.21\ dB} \qquad ..(9.25)$$

$$S_{13} = -20*\log (0.0689)$$
$$= \underline{23.24\ dB} \qquad ..(9.26)$$

$$S_{14} = -20*\log (0.9769)$$
$$= \underline{0.2027\ dB} \qquad ..(9.27)$$

Inserting eq's (9.20) into (9.16), the following VSWR was obtained.

$$VSWR = \frac{1 + 0.0174}{1 - 0.0174} = \underline{1.035}$$

9.2.1 Simulating the 6 GHz directional coupler

It was decided to model the coupler on Touchstone to determine if the coupling coefficients determined earlier were correct. The simulation would also give an indication of the couplers performance over a wide band from 5 to 7 GHz. A program called 6GCOUP2.CKT was written and can be found in Appendix I. The program analyses the directional coupler described in the previous section. A plot of its characteristics can be seen in figure 76, and a summary of the coefficients can be found in Table 12.

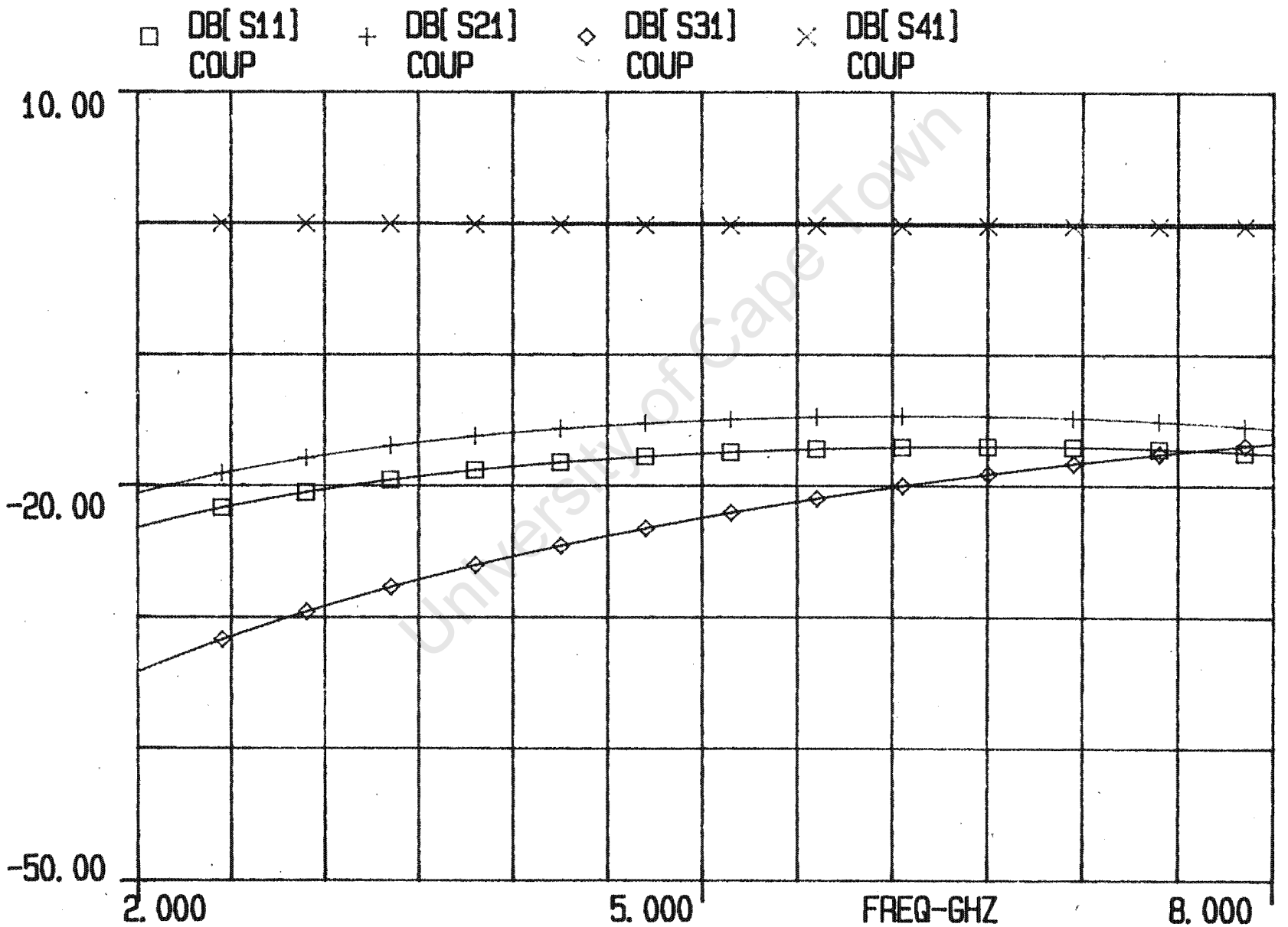

FIGURE 76

FREQ-GHZ	DB[S11] COUP	DB[S21] COUP	DB[S31] COUP	DB[S41] COUP
2.00000	-35.558	-19.844	-30.498	-0.061
2.50000	-33.932	-18.146	-28.580	-0.087
3.00000	-32.736	-16.859	-27.029	-0.115
3.50000	-31.862	-15.873	-25.731	-0.143
4.00000	-31.246	-15.123	-24.612	-0.170
4.50000	-30.849	-14.571	-23.625	-0.194
5.00000	-30.646	-14.190	-22.734	-0.214
5.50000	-30.620	-13.966	-21.913	-0.229
6.00000	-30.764	-13.889	-21.141	-0.239
6.50000	-31.068	-13.958	-20.404	-0.243
7.00000	-31.524	-14.178	-19.692	-0.242
7.50000	-32.103	-14.556	-18.998	-0.236
8.00000	-32.744	-15.113	-18.320	-0.227

Table 12. Coupling and reflection coefficients for coupler

Comparing the results of Table 12 with those of eqs (9.23) .. (9.27), it is found that they agree within a few percent of each other.

9.2.2 Construction and testing of the directional coupler

A 6 GHz directional coupler was designed using the dimensions from the previous section. The active coupling lengths were set at 4.8 mm. The positive print of the coupler can be seen in figure 77.

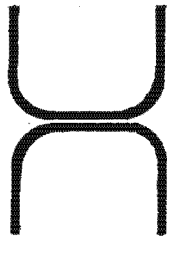

Figure 77. Positive print of 6 GHz directional coupler

The coupler was attached to a network analyser and the coupling and reflection losses determined. The results of the test are shown in figures 78(a) .. (d). These results are summarised in table 13.

S_{11}(dB)	S_{12}(dB)	S_{13}(dB)	S_{14}(dB)
16	16.3	16.7	0.6

Table 13. Measured coupling coefficients for coupler

The results from table 13 can be combined with those from table 12 and those from eq's (9.23) .. (9.27), as below in table 14.

Description	S_{11}(dB)	S_{12}(dB)	S_{13}(dB)	S_{14}(dB)
theory(T'stone)	-30.76	-13.889	-21.141	-0.239
theory(eq's)	-35.21	-13.408	-23.24	-0.203
actual	-16	-16.3	-16.7	-0.6

Table 14. Comparing actual with predicted coupling values

As can be seen from table 14, the values obtained from the actual measurements of the coupler differed from what was expected. Only the coupling from ports 1 to 2 (S12) and S14 were close to their predicted values.

It was discovered, however, that during the etching of the directional coupler, the line widths were reduced to below their initially designed values. This was due to the effect of parasitic etching under the template. Figure 79 indicates this phenomenon.

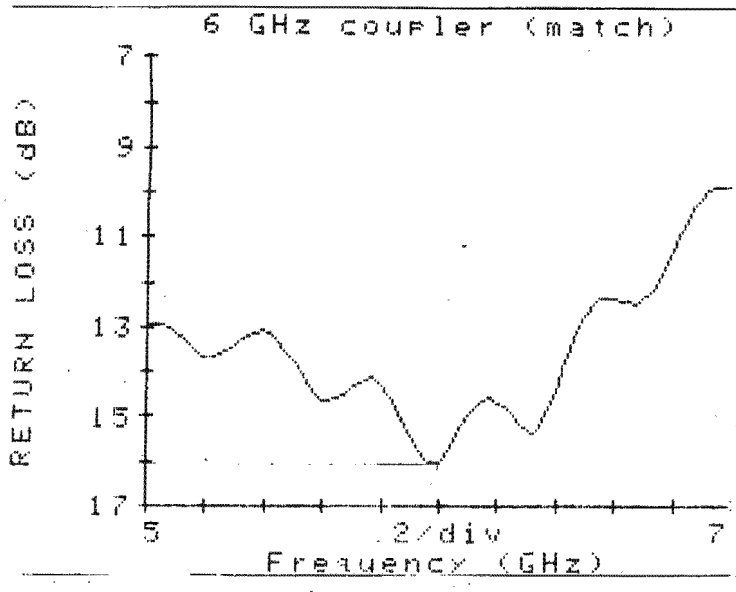

fig 78(a)

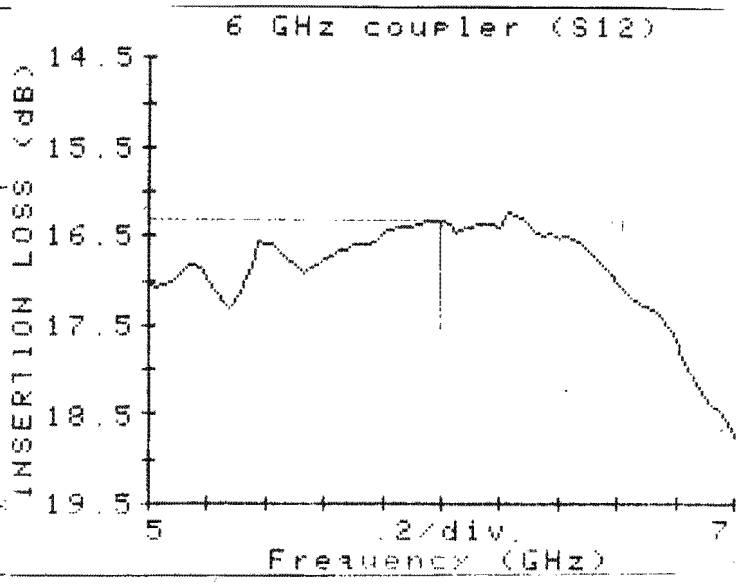

fig 78(b)

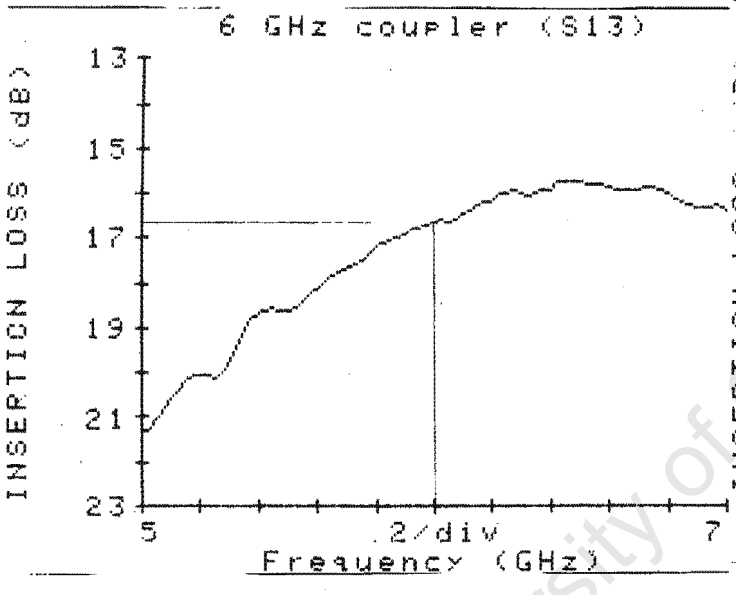

fig 78(c)

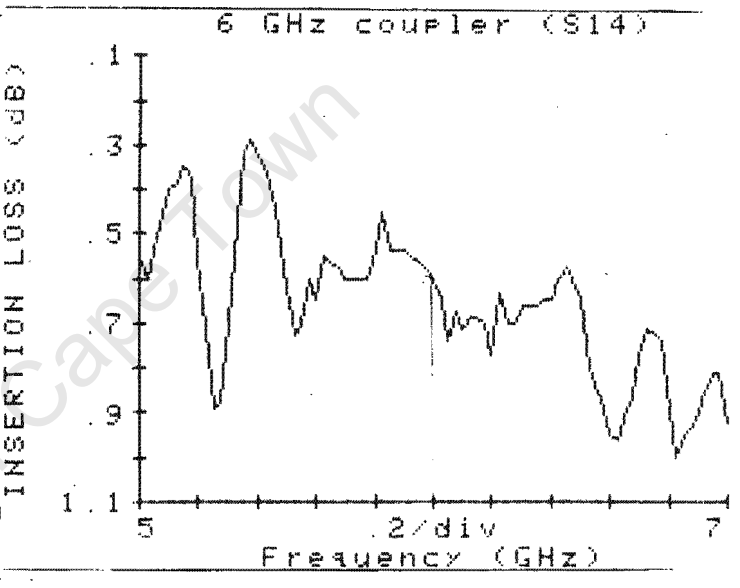

fig 78(d)

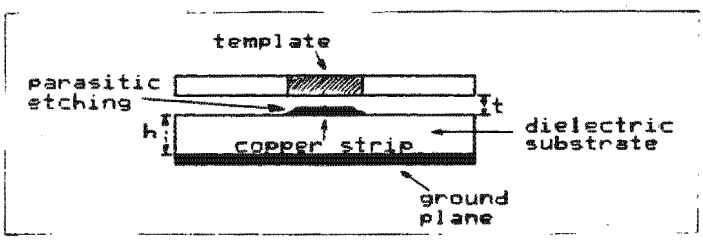

Figure 79. Parasitic etching of copper below template

This parasitic etching reduces the width of the coupling lines. The reduction in width is proportional to the thickness of the copper. The problem in couplers is compounded by the fact that as the widths of the lines is reduced, so the gap between them increases (by twice the thickness of the copper strip). A program called 6GCOUP3.CKT (in Appendix I) was written which would simulate the effect of this reduction in line width and corresponding increase in gap spacing. The results of this program can be found in table 15.

FREQ-GHZ	DB[S11] COUP	DB[S21] COUP	DB[S31] COUP	DB[S41] COUP
2.00000	-26.362	-20.554	-29.438	-0.065
2.50000	-24.724	-18.870	-27.641	-0.091
3.00000	-23.508	-17.599	-26.232	-0.120
3.50000	-22.603	-16.630	-25.094	-0.148
4.00000	-21.945	-15.898	-24.152	-0.175
4.50000	-21.494	-15.364	-23.353	-0.197
5.00000	-21.226	-15.001	-22.659	-0.215
5.50000	-21.126	-14.796	-22.034	-0.228
6.00000	-21.192	-14.739	-21.453	-0.234
6.50000	-21.426	-14.831	-20.890	-0.235
7.00000	-21.845	-15.077	-20.328	-0.229
7.50000	-22.473	-15.489	-19.751	-0.219
8.00000	-23.355	-16.089	-19.152	-0.206

Table 15. Effects of parasitic etching on coupling coefficients

Comparing table 15 to table 14 it can be seen that the return loss now more accurately reflects what was actually measured (S_{11} reduced from -30.76 dB to -21.19 dB). The coupling coefficients (S_{12} and S_{13}) in table 14 are now more closely simulated. S_{12} has been reduced from -13.889 dB to -14.739 dB closer to the -16.3 dB actually measured. S_{13} and S_{14} remained almost unaffected.

9.2.3 Conclusions

It has been shown that the directional coupler would couple to a backward travelling wave with a coefficient of 16.3 dB. This reduced value of coupling was shown to be due to parasitic etching of the parallel transmission lines. Parasitic etching reduces the coupling line widths, and consequently increases the gap between lines. In the next section it will be shown that this value of coupling is sufficient to allow 6 GHz second harmonic signals to couple from the transmitter to the single ended mixer shown in figure 46.

CHAPTER 10

DEVELOPING THE 3 GHz AND 6 GHz OSCILLATOR UNITS

In chapter 6 it was shown that the frequency would require a 3 GHz transmit oscillator and a 6 GHz local oscillator. The specifications for the units were as follows:

a) At least 10 mW output at center frequency
b) Varactor tuned over a band of at least 500 MHz (half the bandwidth of the power splitters)
c) Fast tuning over this band, to ensure synchronisation of 6 GHz local oscillator with the 3 GHz transmit oscillator
d) For the 3 GHz oscillator, a second harmonic available at approximately 20 dB below the fundamental

Suitable oscillators in both the 3 GHz and 6 GHz frequency range, were obtained. Both belonged to the Avantek VTO-8100 series of varactor tuned oscillators. A description of the oscillators can be found in Appendix J. A summary of the oscillators' characteristics can be found in table 16.

Model no.	freq. range (GHz)	power output (dBm)	voltage (VDC)	harmonics (dBc)
8240	2.4-3.7	+10	+15	-18
8520	5.2-6.1	+10	+15	-25

Table 16. Characteristics of varactor tuned oscillators

The oscillators produce exactly the power output required. They operate over bandwidths in excess of 500 MHz, and according to the specification sheet, these oscillators can sweep across their frequency band in less than one microsecond. They thus satisfy the specifications shown previously. The 3 GHz oscillator has a second harmonic available at -18 dBc from the fundamental.

In the next section, power supply designs will be described. However, since both units require the same DC voltages, only the 3 GHz oscillator power supply will be described.

10.1 Designing the 3 GHz oscillator power supply

Figure 80 shows two views of the oscillator package. The 3 GHz and 6 GHz oscillator have the same package dimensions.

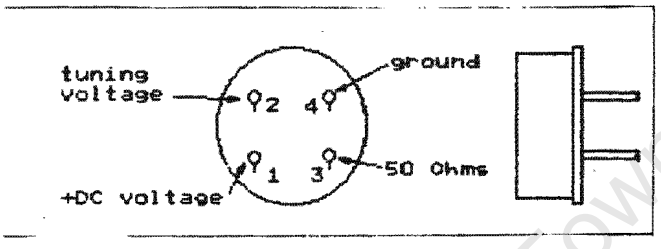

Figure 80. Schematic of VTO-8100 series oscillators

From this figure it can be seen that the oscillator requires a 15 VDC power supply, a ground rail, a tuning voltage unit and a section of 50Ω transmission line, which was connected to the output pin.

The oscillator had to be mounted onto microstrip so as to provide a 50Ω line for the output pin. It was decided that the power supply (without transformer) would be mounted onto the microstrip board so that the power supply and oscillator would be effected by the same thermal transients.

Figure 81 shows the power supply which would provide a stable +15 VDC supply (within +/- 5%).

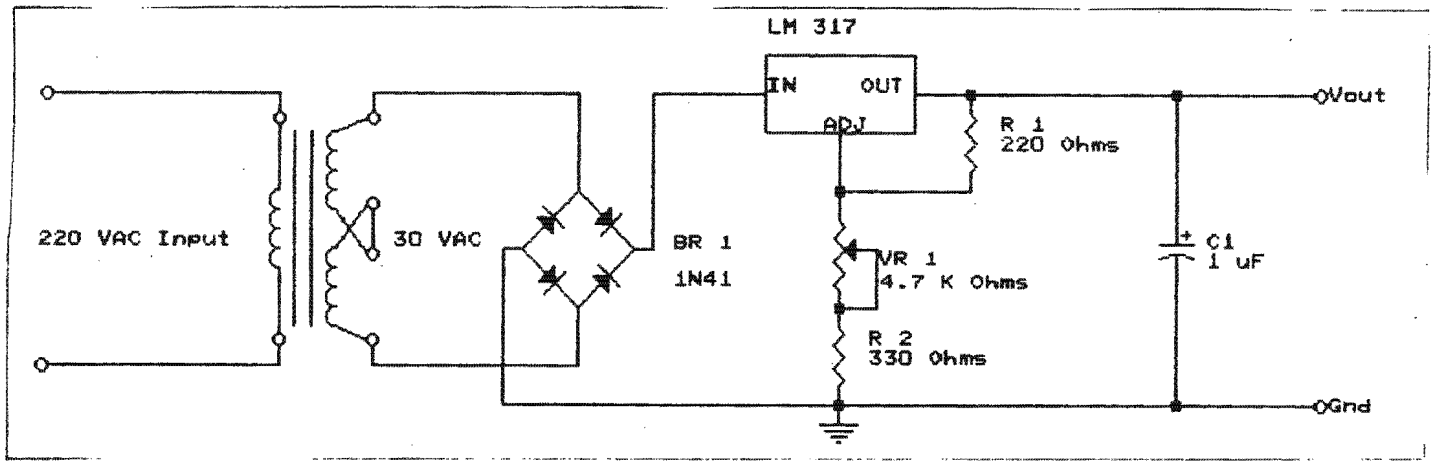

Figure 81. Oscillator power supply and ground rail

The transformer and bridge rectifier were connected together on a separate section of PCB. The voltage regulator and the assorted resistors and capacitors were attached to the microstrip board shown in figure 82.

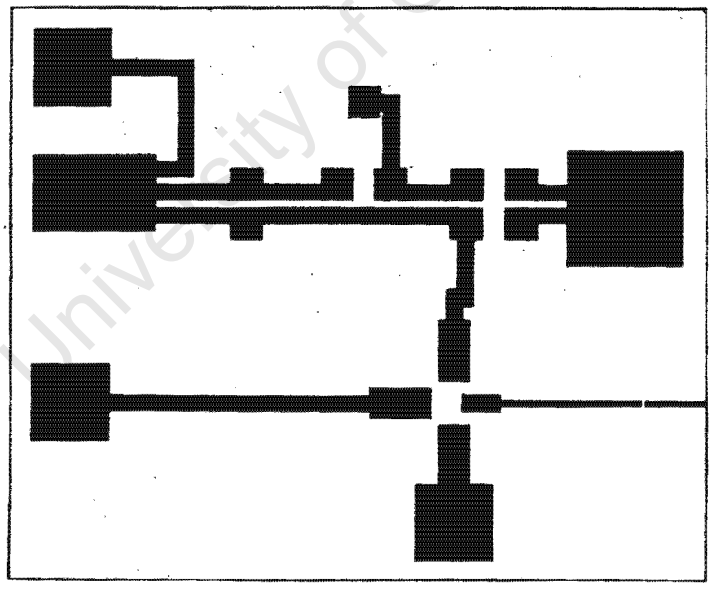

Figure 82. Positive print of oscillator power supply

A DC blocking capacitor was added to the 50Ω output transmission line. A value of 220 pF was chosen for the chip capacitor. The reactance of the capacitor was found to be:

$$X_C = 1/w*c$$
$$= 1/(3*10^9*2*\pi*220*10^{-12})$$
$$= \underline{0.24}$$

Thus at 3 GHz the capacitor has a small reactance, and will thus have a very small effect on the fundamental frequency.

The phase lag produced by the capacitor is correspondingly small.

$$\text{phase lag} = \tan^{-1}(0.24/50)$$
$$= \underline{0.3^o}$$

The oscillator and power supply unit were connected together. A variable power supply was attached to the tuning line. In the next section the oscillators' output power will be measured and the tuning voltage will be determined.

10.2 Measuring the output power and tuning voltage of the oscillator

Figure 83 shows the test rig used to measure the output power of the oscillator and its tuning voltage.

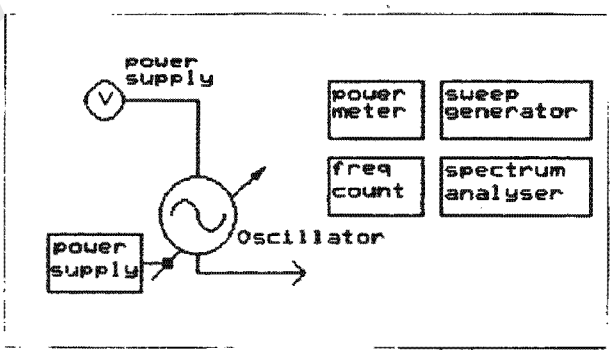

Figure 83. Test rig to measure oscillators output power and tuning voltage

The first step was to check that the oscillators power supply was set to +15 V. The oscillator was then connected to the spectrum analyser via SMA - coaxial connectors. By alternately attaching the oscillator from the spectrum analyser to the freq. counter, it was determined that the oscillator produced a maximum amplitude 3 GHz signal with the tuning voltage set at 10.03 volts.

A sweep generator was then attached to the spectrum analyser. It was set to a center frequency of 3 GHz. The power of this signal was varied until it had the same amplitude on the spectrum analyser at the 3 GHz oscillator signal. The sweep generator was then attached to the power meter, where the output power was found to be 17.5 mW at 3.002 GHz.

Using this same technique the second harmonic was found to have an amplitude of 0.8 mW.

Thus the second harmonic is:

$$-10*\text{Log}\ (0.8/17.5) = \underline{-13.4\ \text{dBc}}$$

below the fundamental frequency. This value is better than anticipated by the oscillator specifications.

10.3 Designing the tuning unit of the oscillator

It was shown in the previous section that the oscillator required the tuning voltage to be set at 10.03 volts to produce the 3 GHz signal at maximum power. The tuning unit was thus deigned to tune between 9.5 - 10.5 volts. A schematic of the tuning unit is shown below in figure 84.

The tuning unit was constructed on PCB and mounted on top of the microstrip board used by the power supply. This was done to ensure thermal uniformity with the oscillator and the power supply. The input pins of the tuning unit were attached to the output of the voltage regulator used by the power supply, while the output of the tuning unit was attached to the tuning pin of the oscillator power supply.

The complete 3 GHz oscillator unit was tested and it was found to produce a 3 GHz signal at 17.5 mW with a signal at 6 GHz of 0.8 mW. The 6 GHz oscillator was constructed using the same techniques as the 3 GHz oscillator. It was found to produce a fundamental frequency signal (at 6 GHz) with an amplitude of 15 mW.

10.4 The 3 GHz power amplifier

From figure 46 it can be seen that the frequency multiplication system requires a 3 GHz power amplifier. This amplifier is used to boost the 3 GHz signal from 10 mW to 1 W. Reception of the reflected 6 GHz harmonic from the density tracer, is improved if the transmit power is increased.

A power amplifier suitable for this application of increasing the transmit power from 10 mW to 1W, is the minicircuits ZHL-42 broadband linear amplifier. Details of the amplifier are given below in table 17, with a full description in Appendix J.

Freq (GHz)	Gain (dB) min	Maximum power (dBm) output	input
0.7 - 4.2	30 +/- 1.0	+29	+10

Table 17. Characteristics of 3 GHz amplifier

As can be seen, this amplifier requires a maximum input power of +10 dBm, and will produce a maximum output power of 1 W.

In the next chapter, the single ended mixer and sweep and lock circuit will be discussed.

CHAPTER 11

THE 6 GHz SINGLE ENDED MIXER

Figure 85 indicates the two single ended mixers required for the frequency multiplication system.

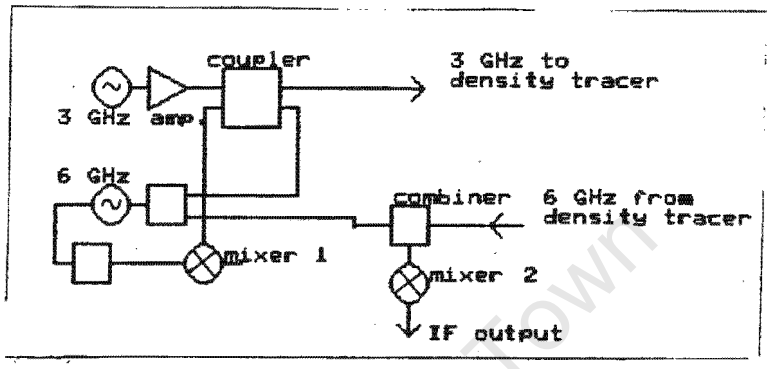

Figure 85. Single ended mixers in the frequency multiplication system

The single ended mixer/power combiner unit in the receiver (mixer 2) section could have been replaced by a balanced mixer. This device would have ensured local oscillator AM noise reduction as well as cancellation of the third order intermodulation products. However, the double beam lead diodes needed for this mixer were not available and were considered too expensive and delivery time too long (12 weeks), to warrant their purchase. However, since local oscillator noise is not a problem with this system, there was no need to use balanced mixers. Thus single ended mixers were used, as single mixer diodes were available.

The other advantage was that both the single ended mixer and the power combiner were duplicates of units used in the local oscillator feedback loop (mixer 1). This meant that only one design had to be made for each unit. A theoretical description of a single ended mixers operation, will be given in the following section.

11.1 Theory of single ended mixer operation

A [23] single ended mixer is a single input, single output device. It is designed to convert radio frequencies (RF) to an intermediate frequency (IF) as efficiently as possible. The reason for this is that amplication and detection is simplified at IF frequencies. The frequency conversion is produced by a mixer diode with a fast response and high cutoff frequency. The diode is turned on and off by the local oscillator signal.

Both the RF and LO signals enter the mixer via the input port. As can be seen from figure 85, the 6 GHz second harmonic from the transmit oscillator is coupled to the RF local oscillator signal (nominally 6 GHz + 10.7 MHz IF). These two signals then enter the single ended mixer where they are mixed and the difference component (IF), is sent via the output (IF) port to the sweep and lock circuit.

The second single ended mixer produces the difference between the local oscillator (6 GHz + 10.7 MHz) with the received signal (nominally 6 GHz). The two signals are initially combined with a power combiner ,described in chapter 8, and then fed into the mixers input port.

11.1.1 The operation of the mixer diode

Central to the operation of the single ended mixer is the mixer diode, which is a nonlinear device (there is a nonlinear relationship between the current induced in the diode and the voltage across it). This is indicated in figure 86.

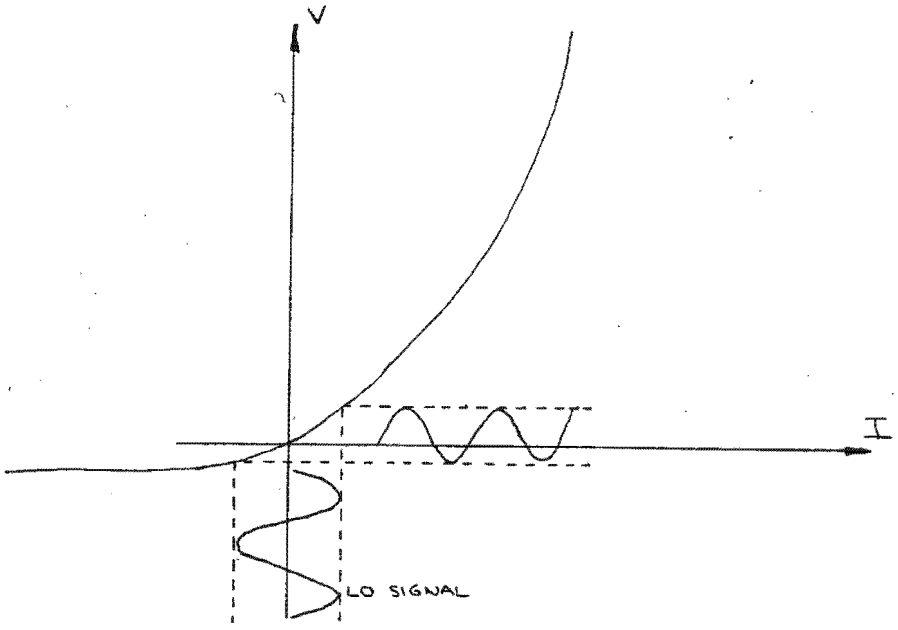

Figure 86. V-I characteristic of diode

When an alternating voltage is applied to the diode, the current takes the form as indicated in figure 86 along the positive current (I) axis. It can be seen that there is less current flowing during the negative half cycles than during the positive half cycles. There is thus a net positive current which has a magnitude related to that of the applied voltage. The current through the diode can be expressed in terms of voltage via a Taylor series (because of its nonlinear nature). Generally the current is related accurately by the square of the applied voltage.

Analysed in terms of transmission line theory, the local oscillator drives the diode into heavy forward conduction for nearly half a cycle and into reverse bias for the other half cycle. This causes the reflection coefficient on the line to vary periodically, as a function of time, as shown in figure 87.

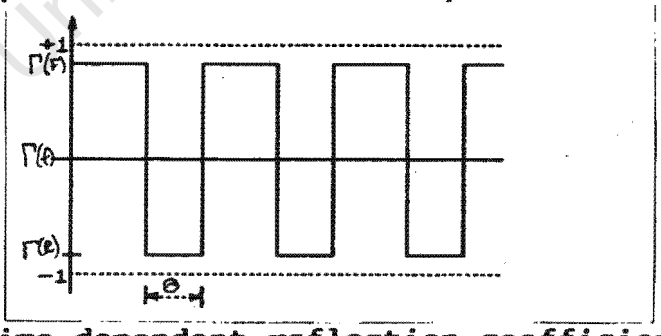

Figure 87. Time dependent reflection coefficient

With the forward and reverse reflection coefficients given by:

$$\Gamma_F = -1 + 2*(R_B + R_S)/Z_o \qquad ..(11.1)$$

$$\Gamma_R = 1 - 2*Z_o*w^2*C_j{}^2*R_S \qquad ..(11.2)$$

and the conduction angle Θ given by:

$$\Theta = 2*\arccos(V_F/\ (8*Z_o*P_L)$$

where R_B = Barrier resistance
R_S = Epitaxy layer resistance
C_j = Junction capacitance
Z_o = line impedance
V_F = Forward voltage
P_L = local oscillator power

The time periodic reflection coefficient is a square and can be expressed as a square wave, however if the RF signal voltage is applied, the voltage of the reflected signal can be calculated and will be given by:

$$V_R(t) = \Gamma(t)*V_s*\cos(w*t)$$
$$= \Gamma_0*V_s*\cos(w*t) + (1/2)*\Gamma_1*V_s*[\cos(w_L - w_s)t + \cos(w_L + w_s)t] + .. \qquad ..(11.3)$$

The important term is that involving $w_L - w_s$, this is the difference frequency (IF). The ratio of reflected power at this frequency to the incident power at w_s is the conversion efficiency.

$$\eta = P_{IF}/P_S$$
$$= (0.5*\Gamma_1*V_s)^2/V_s{}^2$$
$$= \Gamma_1{}^2/4 \qquad ..(11.4)$$

For the ideal case the conversion angle is approximately 180^o,

and the conversion loss becomes 3.9 dB. This value is usually worse since most mixer diodes do not have such large conduction angles. They vary between 120° and 170°. The smaller the conduction angle, the worse the conversion loss.

Since the maximum gain of a diode is unity, and it is a square law device, as the signal strength decreases so its gain decreases. This gain factor is important in determining how efficiently a mixer diode is operating and is hence related to the conversion efficiency which is the ratio of the power of the IF signal to that of the local oscillator.

Generally a problem exists whereby not only will a RF signal of frequency $f_{LO} + f_{IF}$ produce an intermediate frequency of f_{IF}, but also that with a frequency of $f_{LO} - f_{IF}$. This is known as the image rejection problem. For the frequency multiplication system, where the local oscillator and the transmit oscillator are free running, the system would lose information if one of the signals were rejected. Thus image rejection filtering would not be suitable in this context.

11.2 <u>The basic mixer circuit</u>

Figure 88(a) shows [24],[25] in equivalent circuit of a basic mixer system.

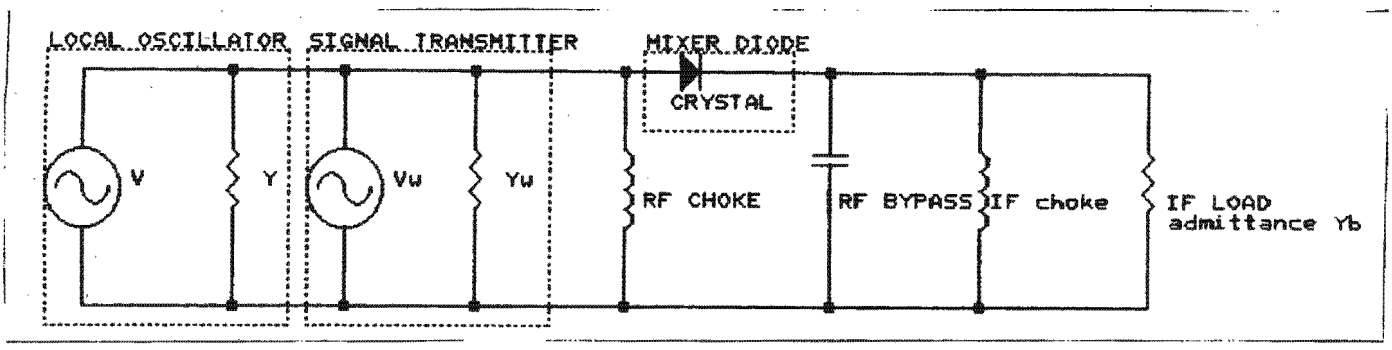

Figure 88(a). Equivalent circuit of a basic mixer (ref 23)

Each unit described in figure 88(a) can be compared to a similar unit in the frequency multiplication system. The signal transmitter is comparable to the transmitter/coupler unit in figure 46. The local oscillator in figure 88(a) has an equivalent unit in the receiver feedback loop. The RF choke, RF bypass and the crystal are all contained in the single ended mixer. Figure 88(b) shows the frequency multiplication equivalent of the basic mixer circuit.

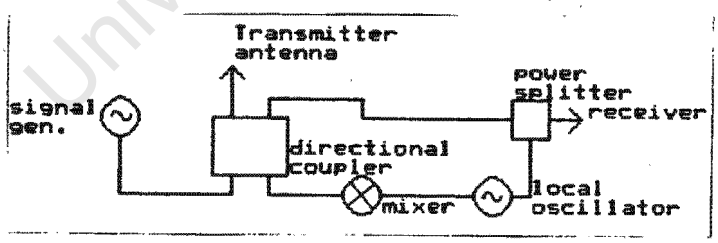

FIgure 88(b). Basic mixer circuit

From figure 88(a) it can be seen that the signal generator is represented by a current generator i_{sc} and an internal admittance Y_{sc} while the local oscillator by a current generator i_{oc} and an internal admittance Y_{oc} . These two current generators are connected in parallel to the mixer diode, and hence to the output terminals of the IF output port which is connected to the IF amplifier.

The RF and IF chokes on either side of the diode provide a low resistance path to the rectified current. There is thus no appreciable current flowing through the diode. It is thus not biased by the local oscillator. Hence Schottky mixer diodes (such as the DMK 5068) would be suitable in this context. These diodes have been shown earlier to operate adequately at this frequency.

The microstrip biasing circuit for the single ended mixer is shown in figure 89.

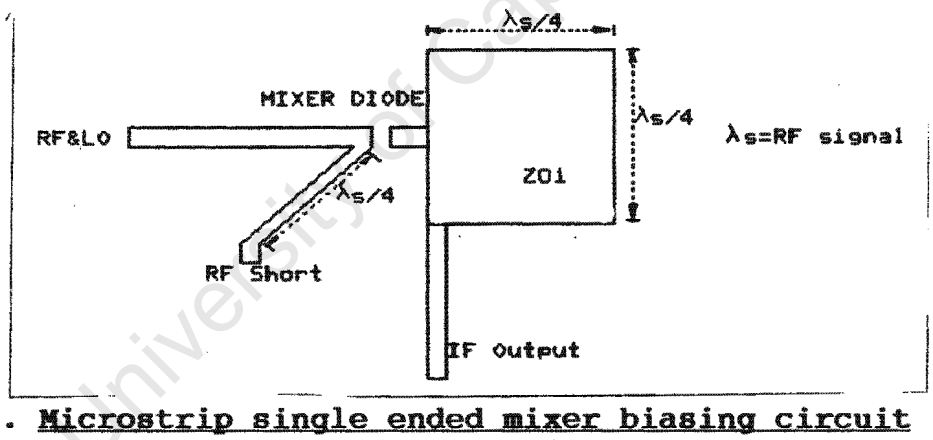

Figure 89. Microstrip single ended mixer biasing circuit

Comparing figures 88(a) and 89 it can be seen that the short circuited quarter wavelength in figure 89 is equivalent to the RF choke. Both units provide a low resistance for the RF rectified current.

The open circuited patch ensures that the RF and LO signals are not applied across the terminals of the IF output. This has the

same operation as the RF bypass capacitor, which ensures that the RF voltages of both the signal and local oscillators are applied across the diode. There is thus a high impedance to RF and LO signals but a lower resistance for IF signals.

In Appendix K it has been proved that the short circuit line acts as an RF choke and that the low impedance open circuited stub is a high impedance at RF/LO frequencies.

Figure 90 summarises the operation of the biasing circuit.

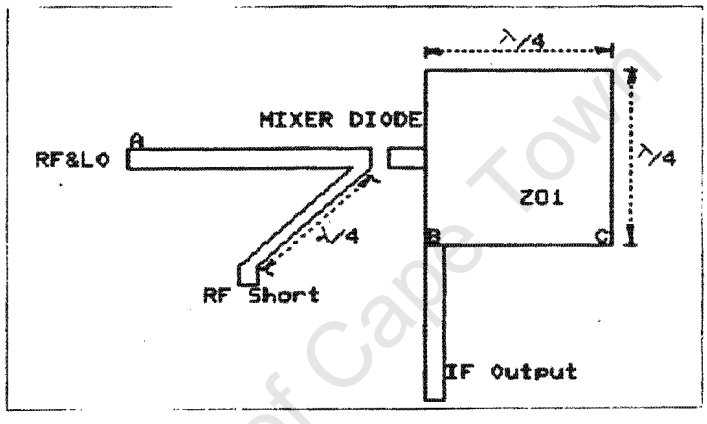

Figure 90. Biasing circuit

At 6 GHz point A is a very high impedance while point B is at ground potential. This means that the RF bypass and RF choke ensure that RF&LO signals are applied across the diode.

At 10.7 MHz point A is at ground potential while point B is a very high potential. Thus the diode is reverse biased at IF frequencies, ensuring that the IF signals flow through the IF output line.

It might seem that the diode should be matched to the transmission line for all the harmonics of the fundamental frequency, but this is not necessary. The fundamental frequency will have the highest amplitude, thus the diode need only be

matched to the transmission line using a quarter wavelength stub, the RF stub. Similarly the diode IF impedance should be matched to the IF amplifier. However, the impedance at IF frequencies is of the order of 100-200Ω, this is close enough to the characteristic impedance of 50Ω to not warrant additional I.F. matching.

11.3 Designing the 6 GHz single ended mixer

A DMK 5068 mixer diode was used in the single ended mixer. From appendix C, it can be seen that the diode has a high cutoff frequency of 500 GHz. It could thus be expected that the mixer would have a low conversion loss.

It was assumed that the single ended mixer would be operating with an RF signal of approximately 6 GHz, and a local oscillator at 6 GHz + 10.7 MHz. From Appendix A the lengths and widths for the mixer were obtained as follows:

w = 0.76 mm l = 36.57 mm

The single ended mixer was designed according to figure 89. A positive print of the completed mixer can be seen in figure 91.

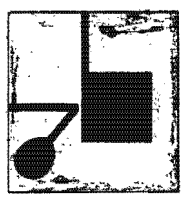

Figure 91. Positive print of single ended mixer

11.4 Testing the mixer

It is possible to determine how efficiently a mixer diode is matched to the transmission line by measuring the reflected signal from the diode at a particular RF frequency, generally the local oscillator frequency. The lower the amplitude of the reflected signal, the greater the match at that particular frequency. It is assumed that the LO signal strength is much greater than that of the RF signal.

It would seem that measuring the match of the mixer on an ordinary automatic network analyser (such as the HP 8410 B) would be the solution. However, network analysers such as the 8410 produce very low power (in order of microwatts) test port frequencies. This is far too low. The match of the mixer must be determined while the diode is hard on, and is rectifying. The minimum local oscillator power necessary to turn the diode is generally about 1 mW. For this reason a scalar network analyser was used to measure the match. Scalar network analysers use an external source of power, in the experiment a sweep oscillator was used. Figure 92 shows a test rig to measure the reflected power from the single ended mixer.

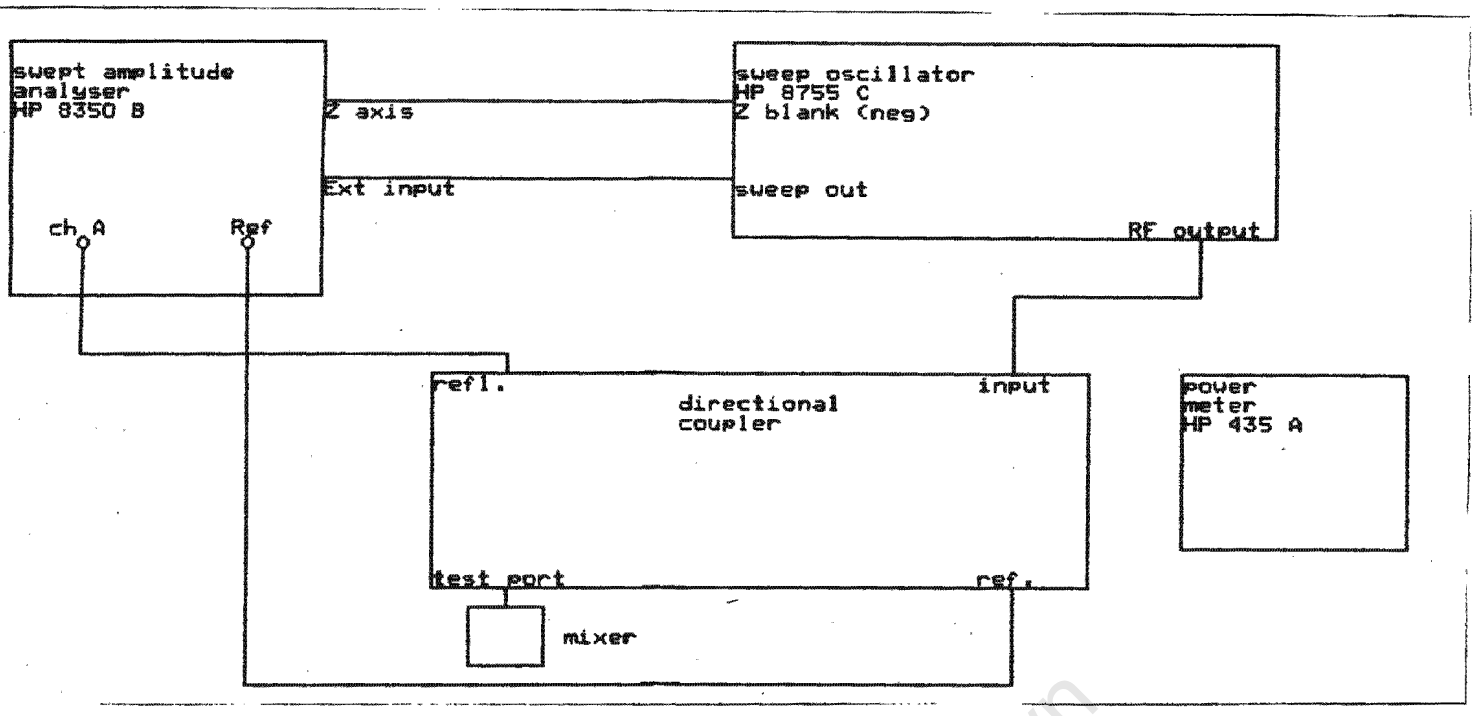

Figure 92. Test rig to measure the match of the mixer

11.5 Results

The mixer was attached at the test port of the directional coupler and the reflected power over a frequency band from 5.2 GHz to 6.5 GHz was determined and can be seen in figure 93.

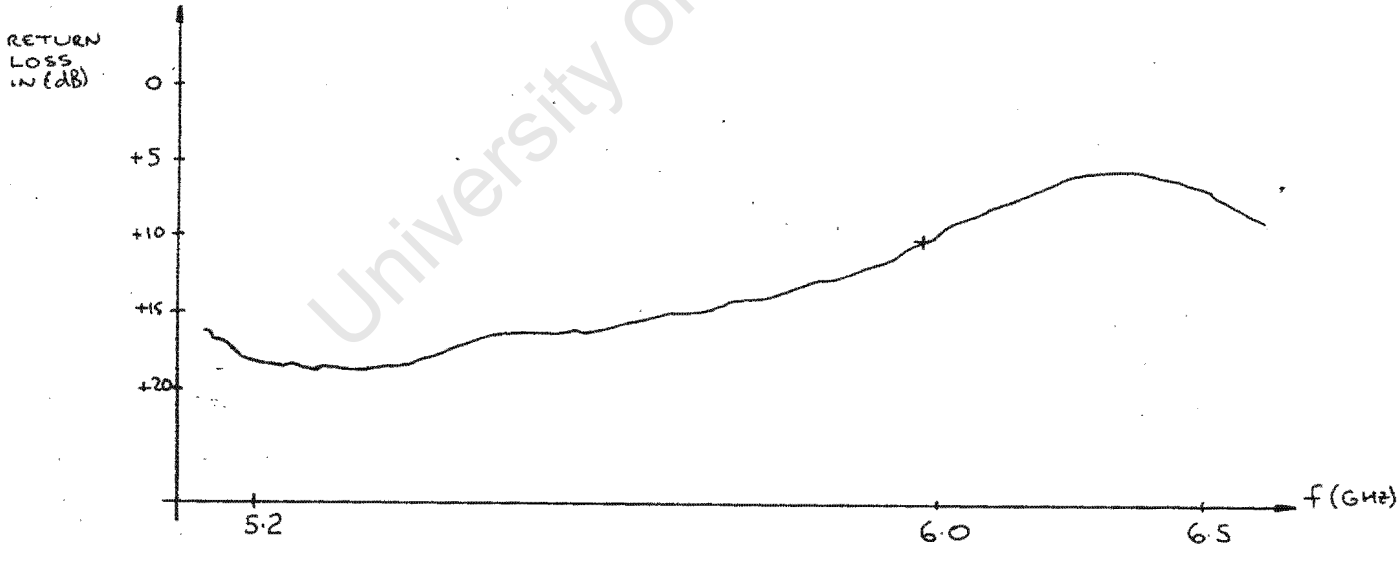

Figure 93. Match of single ended mixer

From figure 93 it can be seen that the match is best at 5.3 GHz (-18 dB), while the match at 6 GHz is found to be -10 dB. It was found that the local oscillator had a power of 6.8 mW at 6 GHz. Even though the mixer is best matched at 5.3 GHz, the mixer can still operate adequately with a match of 10 dB.

The isolation of the mixer to local oscillator signals was determined as follows. A sweep oscillator was connected to the mixer LO port and set to 10 dBm at 6 GHz. The amount of LO power leaking through the IF port was then measured. It was found that the mixer had an isolation of 31 dB, which was more than adequate.

The conversion loss was measured by coupling an RF signal at 6.0107 GHz of -10 dBm, onto the transmission line. The IF power was measured in the same way as for the isolation test. The IF power was found to be -29 dBm. The conversion loss is thus -29 dBm + 10 dBm = -19 dBm. This is quite low as conversion losses of -8 dB are typical. It has been proved that the diode is matched correctly to both the RF and IF ports, as indicated by the return losses and the isolation. The poor efficiency was caused by the softening of the mixer diodes V-I characteristics. This was most likely caused by electrostatic damage to the diode, during handling.

The second single ended mixer was constructed and was also found to have as poor a conversion efficiency. The results for the tests were:

Return loss = -9.5 dB
Isolation = 30 dB
Conversion loss = -19.5 dB

As only two diodes were available, this version of the single ended mixer would have to be used for the system. Futher, the system should still perform adequately but with a reduced range

performance with these mixers.

11.6 Conclusions

The single ended mixer operates effectively at the center frequency of 6 GHz. It has a satisfactory match of 10 dB, and an isolation of 31 dB. The mixers conversion loss is poor, between-19 dB and -19.5 dB, but due to lack of mixer diodes, these will be used for the system.

11.7 Sweep and lock circuit

It has been shown in Chapter 6 how the local oscillator will track the second harmonic of the transmit oscillator using a sweep and lock circuit. The sweep and lock circuit used was from a Plessey S.A. MRA-7 distance measuring device.

A circuit diagram for the sweep and lock circuit can be found elsewhere [25]. A detailed description of the circuits operation will not be given here, save to indicate that it requires a 10.7 MHz tone at its input.Its output will drive the tuning voltage pin of the local oscillator until the difference between its output (nominally 6GHz + 10.7 MHz) and the second harmonic of the transmit oscillator (nominally 6 GHz) is 10.7 MHz.

In the next section, the final integration of the frequency multiplication system will be performed, and the full system will be tested.

CHAPTER 12

FINAL INTEGRATION AND TESTING OF FREQUENCY MULTIPLICATION SYSTEM

12.1 Determining the transmitter unit power

It was decided that it was best to determine the operation of each sub unit before integrating the complete frequency multiplication system. The first unit to be tested was the transmitter unit including transmit oscillator, RF amplifier, directional coupler, 6 GHz notch filter and 3 GHz horn antenna. The test was to determine the power at point A in figure 94.

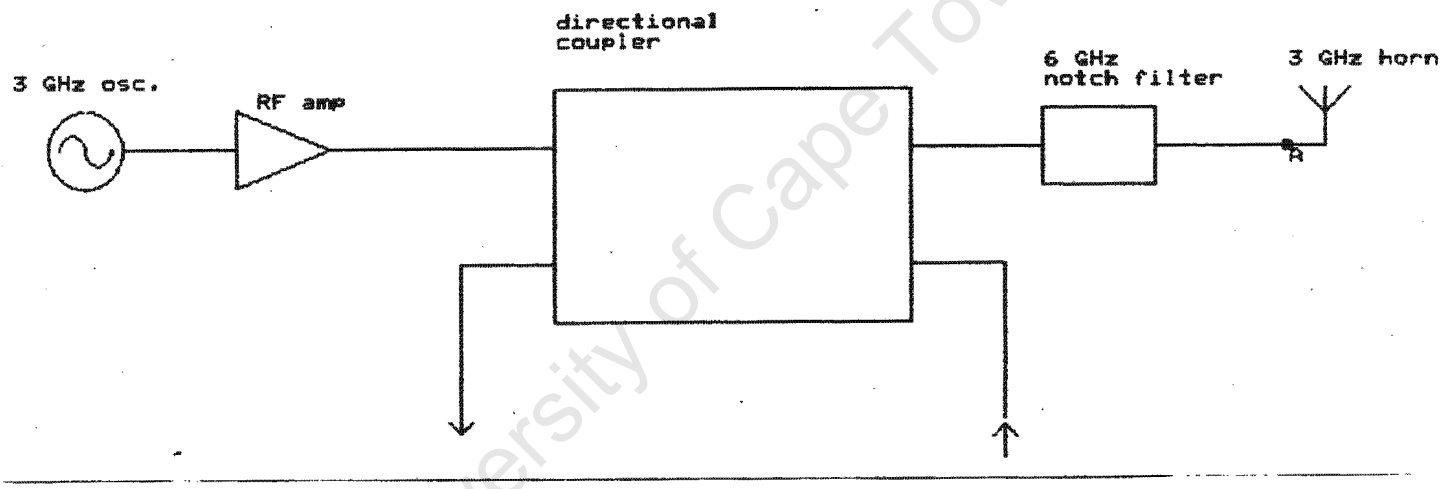

Figure 94. Test rig to measure transmitter unit power

The transmitter unit was connected together as in figure 94. The transmit oscillator was powered up and its output connected to a HP 5351B frequency counter. It was found to be producing a fundamental frequency of 3.03 GHz. The oscillator was then connected to a spectrum analyser and the amplitude of the signal noted. Another signal was connected via a sweep analyser and its amplitude adjusted until it had the same magnitude as the output of the oscillator. The sweep generator was then attached to a

power meter, where its output power was found to be 11.3 dBm.

The power amplifier stipulates that the input should not exceed +10 dBm, for this reason a 3 dB attenuator was between the amplifier and the transmit oscillator. The power at point A in figure 94, was then measured. Using a similar measurement technique, the power was found to be +28 dBm or 631 mW. This was considered an adequate value.

This amplitude was lower than the 30 dBm expected, because of the losses in the coupler and the 6 GHz notch filter. The power out of the amplifier was measured to be 30.4 dBm at 3 GHz.

12.2 Measuring the receiver unit IF output power

Figure 95 shows the receiver unit with power splitter and power combiner, single ended mixer and 3 GHz notch filter, and receive signal and local oscillator signal provided by sweep generators.

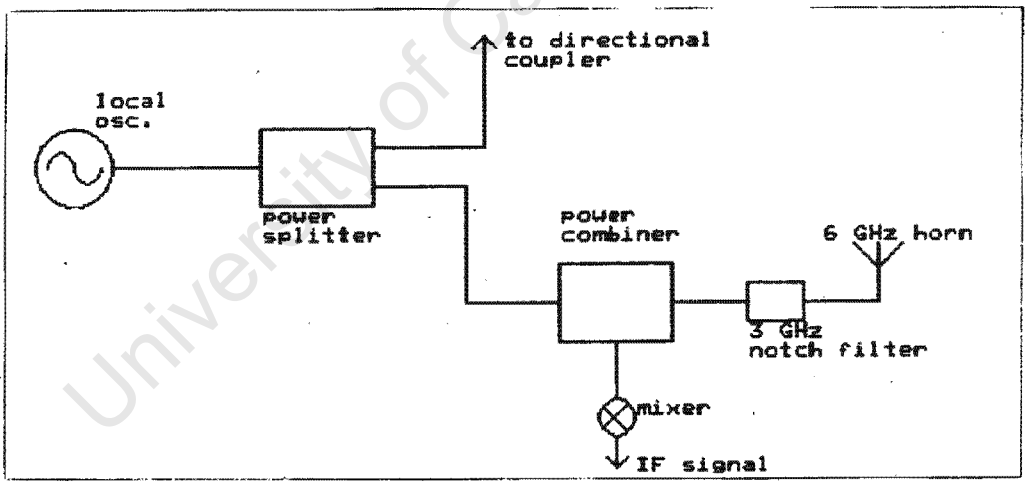

Figure 95. IF power measurement test rig

The output of the single ended mixer was attached to a low frequency spectrum analyser (HP 8590A). The sweep generator was attached to a frequency counter, and its frequency altered by

The system was powered up and the output of the receivers single ended mixer was connected to an HP 8590A spectrum analyser. An IF signal at 10.7 MHz was recovered with an amplitude of between -61 and -63 dBm. The cross dipole antenna was positioned 30 cm from the transmit and receive antennas.

This is adequate for detection of the cross dipole antenna.

12.4 Improving system performance

It has been shown that the single ended mixer designed previously has a low conversion efficiency. The effect of this is to reduce the magnitude of the IF signal in the receiver unit. After investigation, it was found that the mixer diodes V-I characteristic had softened, and that this was the cause of the poor conversion efficiency. It was decided that a commercial balanced mixer should replace the power combiner and single ended mixer in the receiver unit. The balanced mixer had an improved conversion loss and would reduce local oscillator noise and third order intermodulation products.

An ANZAC MD-162 balanced mixer was chosen. It operated over a band from 3 to 10 GHz, with a conversion efficiency of better than - 7.5 dB over this range (-6 dB at 6 GHz). Details of the balanced mixer can be found in Appendix L.

The balanced mixer was placed in the receiver unit as shown in figure 96.

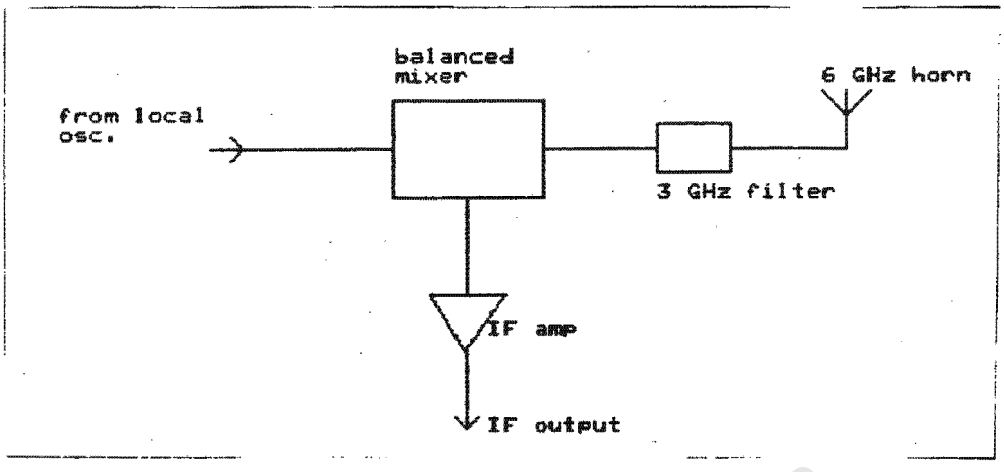

Figure 96. Balanced mixer position in receive unit

The IF output power was measured and found to be -48 dBm with the density tracer placed 30 cm from the receive antenna. The system performance has thus improved by 61-48 = 13 dBm. The system could thus detect the density tracer to a greater distance, as shown below:

$$P_T = P_R/r^4$$

since the received power has increased by 13 dBm or 19.95 .
The increase in range is thus given by:

$$(19.65)^{0.25} * 30 \text{ cm} = 63 \text{ cm}$$

This is in excess of the original 20 cm specification.
As can be seen the increase in system performance is 13 dBm, which is the same as the increase in conversion efficiency:

19 dBm - 6 dBm = 13 dBm.

The increase in received power at IF, is thus due to the increased conversion efficiency of the balanced mixer.

12.5 Counting the density tracers

The counter unit follows the IF amplifier in the receiver as shown in figure 97.

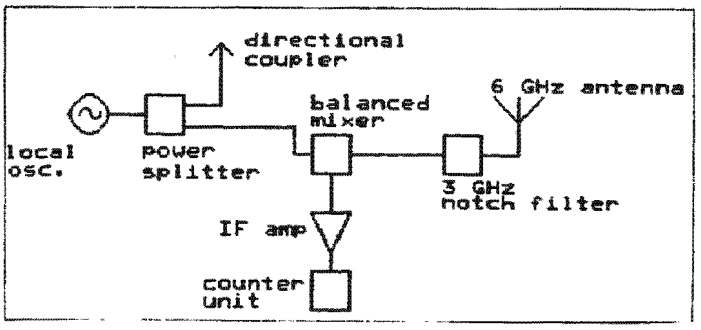

Figure 97. Counter unit position in the receiver unit

The output of the IF amplifier is passed through a FM demodulator where the IF is detected and a pulse of DC is produced. The IF amplifier and FM demodulator are included with the sweep and lock circuit but will not be discussed here [26]. The DC pulse is then sent to a hysteretic comparator which changes the slowly changing pulse into a square pulse. This pulse is then sent to MC 14553 B three digit counter which counts the pulses and sends the number to a seven segment display. The counter circuitry used here can be found in Appendix L.

12.6 Conclusions

It has been shown that the frequency multiplication system can detect a 32 mm density tracer with adequate sensitivity at the specified distance of 20 cm. Techniques for improving the sensitivity of detection have been discussed. A circuit to count the IF pulses and hence the number of density tracers, has been described.

CHAPTER 13

CONCLUSIONS AND FUTURE WORK

13.1 Conclusions

The thesis begins by introducing the user to dense medium separation and the techniques used to measure the separation efficiency of cyclones. It was shown that the separation efficiency is the efficiency whereby the cyclone separates desired product from undesirable reject material from the mine.

The problems associated with measuring this separation were discussed and the indicator used, the density tracer, was described. The disadvantage of standard means of density tracer counting was discussed, and techniques using active and passive means of detection was discussed. Passive detection techniques were considered suitable. Metal detection, microwave corner reflectors and frequency mixing and multiplication were attempted.

It was found that there were discrimination problems with both metal detection and microwave corner reflectors. Frequency multiplication and frequency mixing were then attempted. Frequency mixing was found to be expensive, needing two transmitters and horn antennas. Fast detection was necassary hence the frequency mixing system required either crystal locked oscillators or fast sweep and lock circuits. Both these solutions are complex and expensive.

For these reasons frequency multiplication was investigated. This technique utilised a mixer diode characteristic of producing a second harmonic of an input signal if driven hard enough. The diode was mounted inside a density tracer on a dual frequency antenna. The density tracer received a transmitted signal and transmitted the second harmonic. This signal was detected by a

receiver and indicated the passage of a density tracer.

A cross dipole antenna was designed. This antenna was mounted inside the density tracer with the diode across its feedpoints. A prototype system was designed and constructed. It utilized a 500 MHz transmitter unit and a 1 GHz receiver. The test proved succesful and for this reason a higher frequency system was constructed. The density tracer was reduced in size to that of the specified 32 mm. This resulted in a system with a 3 GHz transmitter and 6 GHz receiver.

A unique frequency multiplication system was devised which utilized a sweep and lock circuit in the receiver feedback loop which kept the receivers local oscillator locked onto the transmit oscillators second harmonic.

This technique made it possible to use free running oscillators in both the transmitter and the reciver, a considerable saving had crystal locked oscillators been used. It also made it possible to reduce the frequency of detection to 10.7 MHz (FM IF).

The bulk of this thesis was concerned with the construction of the components of the frequency multiplication system. Each of these components, shown below, were constructed and after testing proved adequate for their task.

a) 3/6 GHz cross dipole antenna
b) 3 and 6 GHz horn antennas
c) 3 and 6 GHz notch filters
d) 6 GHz power splitter/combiner
e) 6 GHz directional coupler
f) 3 and 6 GHz oscillator power supplies
g) 6 GHz single ended mixers

The diodes for the 6 GHz single ended mixers were found to have softened V-I characteristics, possibly due to electrostatic discharge during handling. However, it was decided to use them in any event, since no other diodes were available. The system was intergrated and it was found to operate adequately. The IF output power was found to be -61 dBm with the single ended mixers. The power combiner and single ended mixer in the receiver output stage were replaced with a balanced mixer, and the IF output amplitude rose to -48 dBm. This increase was found to be related to the improvement in conversion efficiency.

13.2 Recommendations

The cross dipole antenna is polarisation sensitive, it would thus be advisable to use circularly polarised antennas for the transmitter and receiver. A future project could consist of the design and construction of these antennas, as well as arrays of these antennas, to ensure the detection of the density tracer in any orientation. There is a 3 dB loss in antenna gain when using circular polarisation, but the advantage of being able to detect the density tracer irrespective of orientation overshadows the minor loss in IF signal strength.

Another field of research could be into the plastic radomes needed to protect the diode/cross dipole antenna. A material will need to be found which is durable to the rigours of the mining environment and also reasonably pervious to microwaves.

The use of this system in other industrial applications could be investigated.

REFERENCES

1. Allan, F.F. 1985. Heavy media Separators. SME mineral processing handbook. Society of mining engineers. New York. pp 4.3-4.19.

2. Davis, J.J. 1986. Density tracers give option to floating sink tests. Coal Age, Vol 91 no. 5, pp 60-62.

3. Wills, B.A. Heavy medium separation. Mineral processing technology. Pergammon press. New York, Vol 29, pp 256-275.

4. Napier-Munn, T.J. March 1985. Use of density tracers for determination of the Tromp curve for gravity separation processes. Trans. Inst. Min. Metall. pp c47-c53.

5. Scott, I.A. and Lyman, G.J. 1987. Metallurgical evaluation of iron ore drum separators using density tracers. Bull. Proc. Australas. Inst. Min. Metall., Vol 202 no.1, pp 49-56.

6. Hall, J.S. 1947. Radar aids to navigation. MIT Radiation laboratory series. McGraw-Hill, New York, 389p.

7. Dubost, G. 1981. Flat radiating dipoles and application to arrays. Research studies press, John Wiley & sons, London, 103p.

8. James, J.R. et al. 1981. Microstrip antenna theory. IEE electromagnetic waves series 12. Peter Peregrinus Ltd, London, 290p.

9. Compton, R.T. 1981. On the performance of a polarization Sensitive Adaptive Array. IEEE-AP, Vol AP-29, no.5, pp 718-725

10. Alberts, P.A. 1988. Development of an automatic system to monitor the performance of a Dense Medium (mineral) Separation process. Second joint symposium on Antennas & Propagation and Microwave Theory & Techniques, pp 13.1-13.5

11. Gandhi, O.P. 1984. Microwave Engineering & applications. Pergammon press, New York, 260p.

12. Kraus, J.D. 1985. Electromagnetics. Third edition. Singapore, McGraw-Hill, 775p.

13. Silver, S. 1949. Microwave antenna theory and design. MIT Radiation laboratory series. New York, McGraw-Hill, 623p.

14. Cohn, S.B. 1968. A class of broadband three port TEM Mode hybrids. IEEE-MTT, Vol MTT-16, no.2, pp 110-116.

15. Easter, B. 1975. The equivalent circuit of some microstrip discontinuities. IEEE-MTT, Vol MTT-23, no.8, pp 655-660.

16. Rachman, D.M. 1988. Computer aided design of broad-band microstrip power dividers. Second joint symposium on Antennas & Propagation and Microwave Theory & Techniques, pp 8.1-8.15.

17. Rachman, D.M. 1988. Computer aided design of broad-band microstrip power dividers. Second joint symposium on Antennas & Propagation and Microwave Theory & Techniques, pp 8.1-8.15.

18. Krage, M.K. and Haddad, G.I. 1970. Characteristics of coupled microstrip transmission. IEEE-MTT, Vol MTT-18, no.4, pp 217-228.

19. Krage, M.K. and Haddad, G.I. 1970. Characteristics of coupled microstrip transmission. IEEE-MTT, Vol MTT-18, no.4, pp 217-228.

20. Akhtarzad, s. et al. 1975. The design of Coupled Microstrip lines. IEEE-MTT, Vol MTT-23, no.6, pp 486-492.

21. Kal, S. et al. 1981. Empirical relations for capacitive and inductive coupling coefficients of coupled microstrip lines. IEEE-MTT, Vol MTT-29, no.4, pp 386-388.

22. Krage, M.K. and Haddad, G.I. 1970. Characteristics of coupled microstrip transmission. IEEE-MTT, Vol MTT-18, no.4, pp 217-228.

23. Pound, R.V. 1948. Microwave mixers. MIT Radiation laboratory

series. New York, McGraw-Hill, pp 19-28.

24. Pound, R.V. 1948. Microwave mixers. MIT Radiation laboratory series. New York, McGraw-Hill, pp 120-122.

25. Katoh, M. and Akaiwa, Y. 4-GHz Intergrated circuit mixer. IEEE-MTT, Vol MTT-19, no.7, pp 634-637.

26. MRA-7 Operators manual, Plessey SA.

APPENDIX A

LINE WIDTHS AND LENGTHS FOR VARIOUS FREQUENCIES

```
LineCalc (TM) - Configuration( 400 1200 100 16517 1968 1000 1 )
                Synthesis     Tue Sep 26 01:06:14 1989

 MSUB   ER=4.8   H=1.6   T=0.017   RHO=0.84   RGH=0

 TAND   TAND=9e-4

 FREQ   F=1

 DIM    FREQ gHz          LNG mm           ANG deg
-------------------------------------------------------------------------------

 MLIN . .  W=2.83   L=158.43
-------------------------------------------------------------------------------

      ZO=50                                  Keff=3.58          A,dB=0.08

  E(eff)=360
```

```
LineCalc (TM) - Configuration( 400 1200 100 16517 1968 1000 1 )
                Synthesis     Tue Sep 26 01:06:51 1989

 MSUB   ER=4.8   H=1.6   T=0.017   RHO=0.84   RGH=0

 TAND   TAND=9e-4

 FREQ   F=2

 DIM    FREQ gHz          LNG mm          ANG deg
-------------------------------------------------------------------------------

 MLIN . .  W=2.81   L=78.92
-------------------------------------------------------------------------------

      Z0=50                                  Keff=3.61          A, dB=0.06

  E(eff)=360
```

LineCalc (TM) - Configuration(400 1200 100 16517 1968 1000 1)
Synthesis Tue Sep 26 01:02:35 1989

MSUB ER=10 H=.635 T=0.01778 RHO=0.84 RGH=0

TAND TAND=9e-4

FREQ F=6

DIM FREQ gHz LNG mm ANG deg

MLIN . . W=0.57 L=4.83

Z0=50 Keff=6.70 A,dB=0.02

E(eff)=90.00

LineCalc (TM) - Configuration(400 1200 100 16517 1968 1000 1)
Synthesis Tue Sep 26 01:04:07 1989

MSUB ER=2.2 H=0.2548 T=0.01778 RHO=0.84 RGH=0

TAND TAND=9e-4

FREQ F=3

DIM	FREQ gHz	LNG mm	ANG deg
MLIN . .	W=0.76	L=18.29	

Z0=50 Keff=1.87 A,dB=0.04

E(eff)=90.00

LineCalc (TM) - Configuration(400 1200 100 16517 1968 1000 1)
Synthesis Tue Sep 26 01:04:45 1989

MSUB ER=2.2 H=0.2548 T=0.01778 RHO=0.84 RGH=0

TAND TAND=9e-4

FREQ F=6

DIM FREQ gHz LNG mm ANG deg

MLIN . . W=0.76 L=9.14

Z0=50 Keff=1.87 A,dB=0.03

E(eff)=90.00

LineCalc (TM) - Configuration(400 1200 100 16517 1968 1000 1)
Synthesis Tue Sep 26 01:05:21 1989

MSUB ER=2.2 H=0.2548 T=0.01778 RHO=0.84 RGH=0

TAND TAND=9e-4

FREQ F=6

DIM FREQ gHz LNG mm ANG deg

MLIN . . W=0.43 L=9.31

Z0=70.7 Keff=1.80 A,dB=0.04

E(eff)=90.00

APPENDIX B

E AND H PLANE PLOTS FOR CROSS DIPOLE ANTENNA

DATE:	FREQUENCY:	COMMENTS:
15.3.89	Freq = 2.86 GHz	
TESTED BY:	ANTENNA UNDER TEST: Crossed Dipoles	
TRANSMITTING ANTENNA:	PLANE OF CUT: 'E'	

NIST NIAST

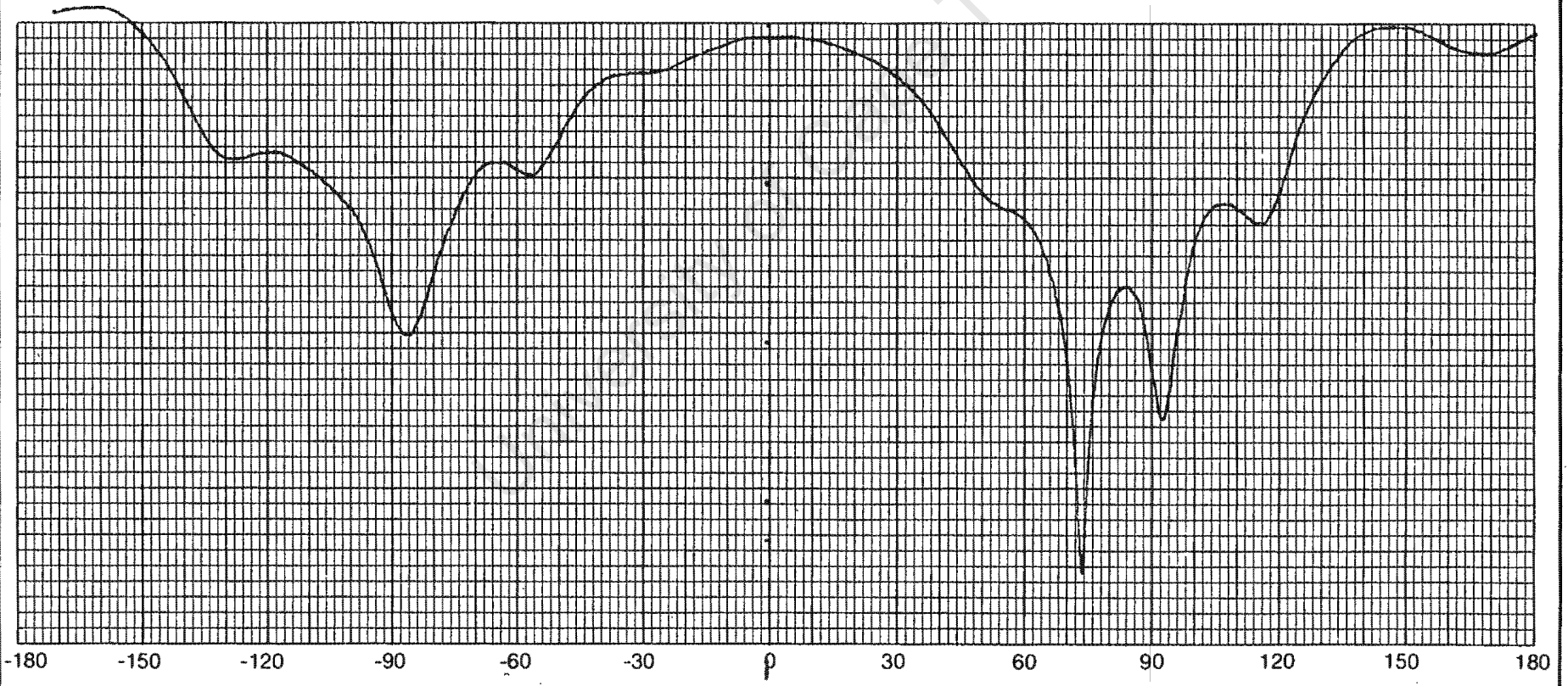

DATE:	FREQUENCY:	COMMENTS:
15.3.89	2.86 GHz	
TESTED BY:	ANTENNA UNDER TEST: Crossed Dipoles	
TRANSMITTING ANTENNA:	PLANE OF CUT: 'H'	

NIST NIAST

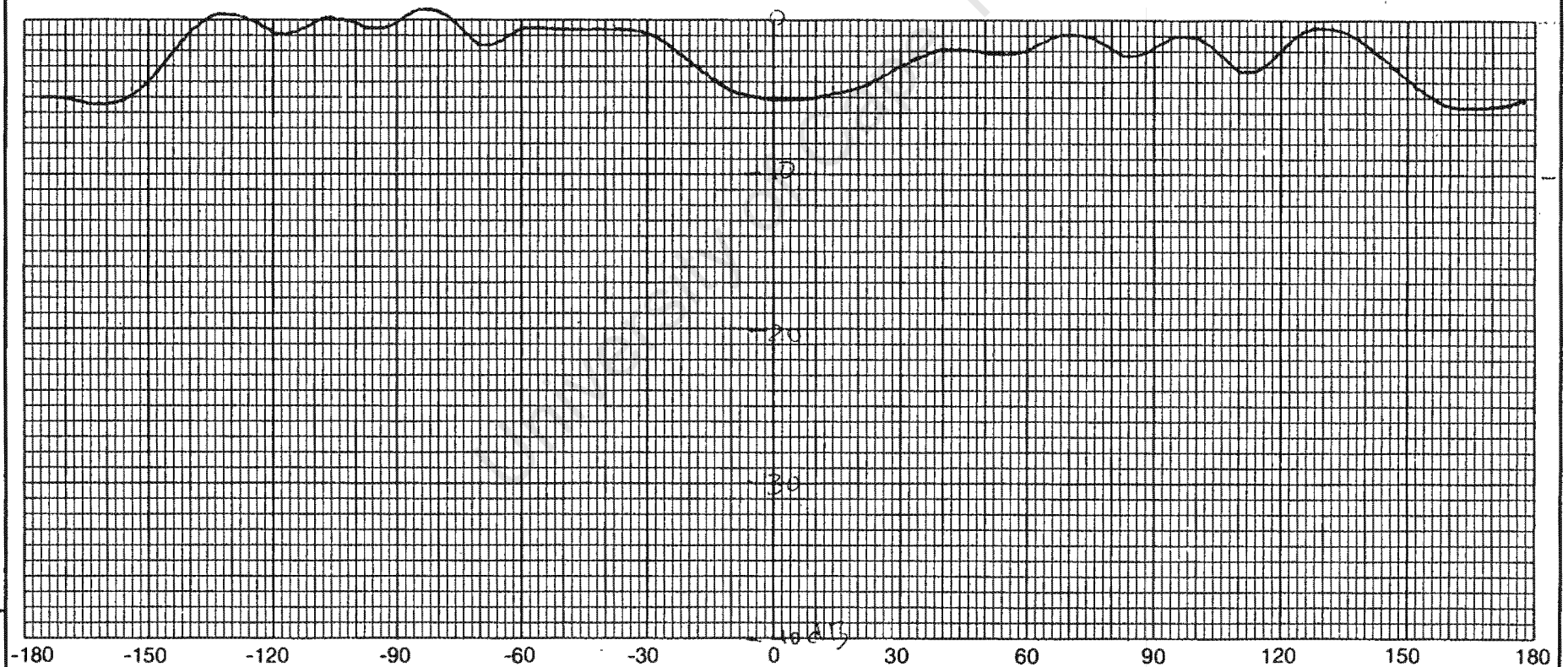

10 dB

159

GAcsir 74HL2134*1173

DATE:	FREQUENCY: 1.439GHz	COMMENTS:
TESTED BY:	ANTENNA UNDER TEST: Crossed Dipole	
TRANSMITTING ANTENNA:	PLANE OF CUT: 'E'	

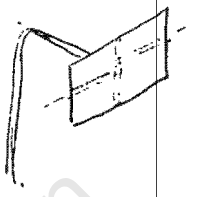

NIST
NIAST

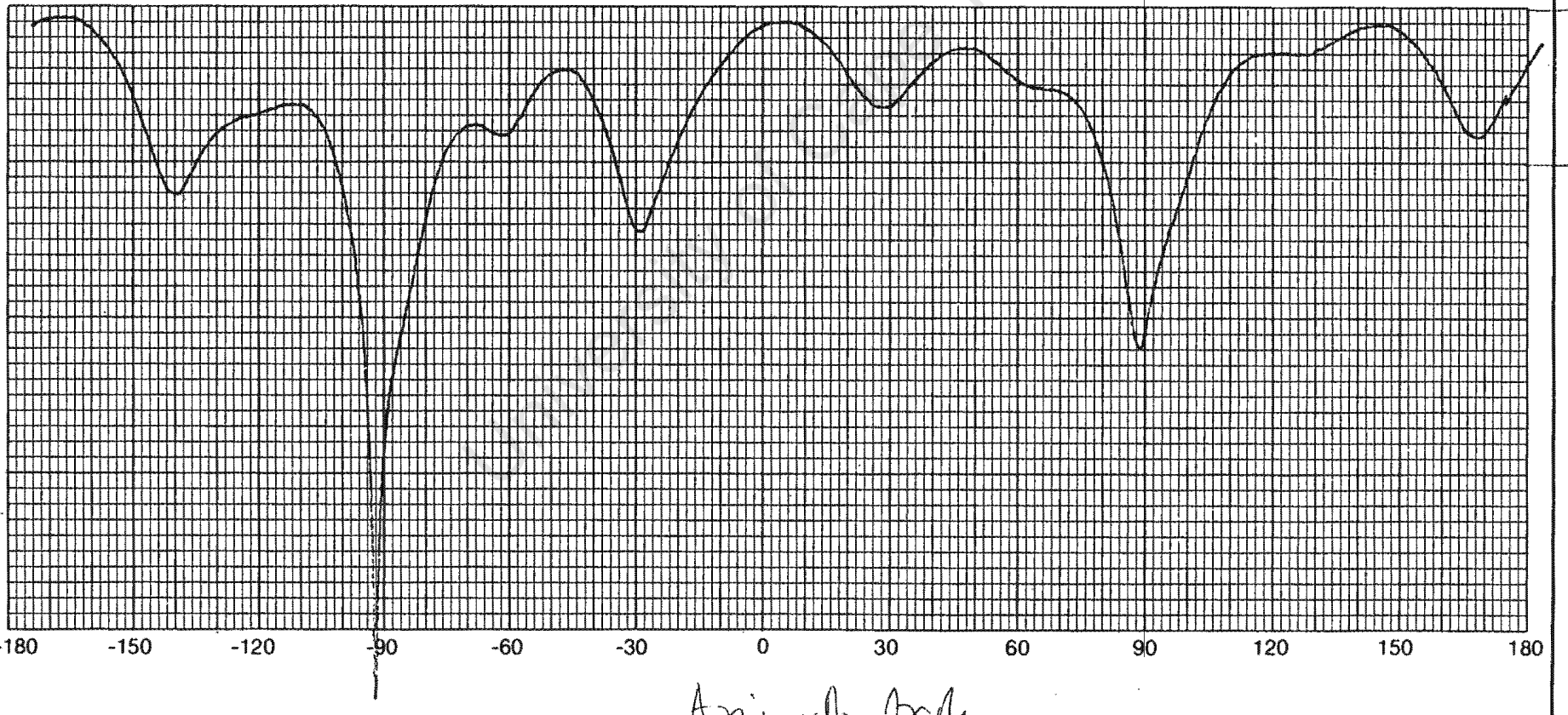

159

GAcsir 74HL2134'1173

DATE:	FREQUENCY: 1,439 MHz	COMMENTS:
TESTED BY:	ANTENNA UNDER TEST: Crossed Dipole	
TRANSMITTING ANTENNA:	PLANE OF CUT: 'H'	

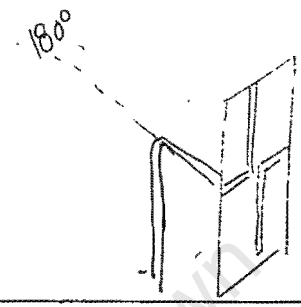

NIST NIAST

-90°

-180 -150 -120 -90 -60 -30 0 30° 60 90 120 150 180

← Azimuth →
(degrees)

NO.

GAcsir 74HL2134 1173

APPENDIX C

CHARACTERISTICS OF DMK 5068 SCHOTTKY MIXER DIODE

Schottky Diodes

REFERENCE NUMBER: 10100

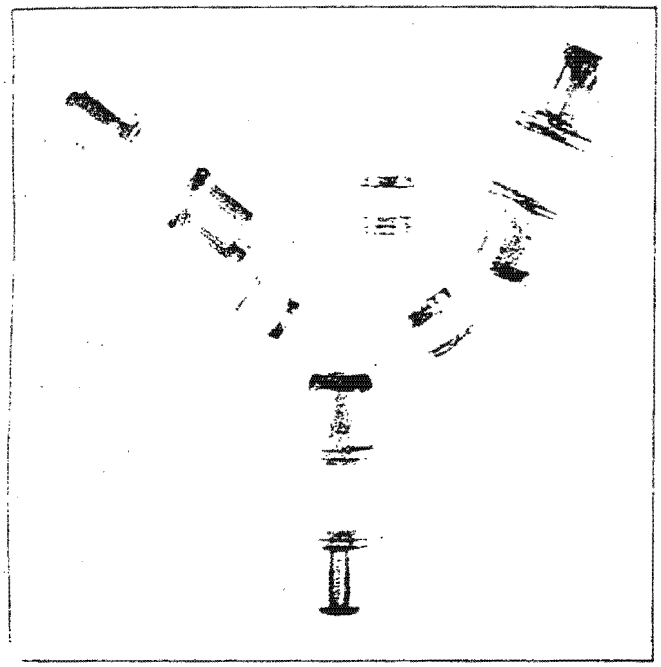

Gallium Arsenide Schottky Barrier Mixer Diodes

Features

- Low Noise Figure
- Excellent Cutoff
- Ideal for Image Enhancement Mixers
- Passivated Planar Construction for Reliability

Description

Alpha's series of gallium arsenide Schottky barrier diodes are available in beam lead, chip and packaged forms for mixer applications through 90 GHz. They are designed for low junction capacitance as well as low series resistance and exhibit calculated cutoff frequencies in excess of 900 GHz.

The packaged diodes are hermetically sealed and may be used in waveguide, stripline or coaxial configurations.

Beam lead diodes are particularly well suited for MIC work. The beam lead design eliminates the problems associated with bonding to the junction, as is the case with a chip diode. A line of chip diodes is available for those who prefer to use chip and wire techniques for their MIC work. Capacitance ranges and series resistances on the beam lead and chip diodes are comparable to those of their packaged counterparts.

Beam lead and chip diodes may be mounted on a variety of standard or special substrates; if desired, Alpha will also bond them directly into a customer circuit.

Outline Drawings

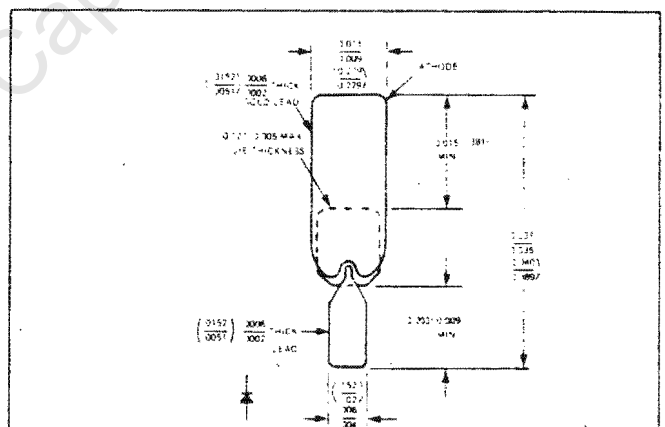

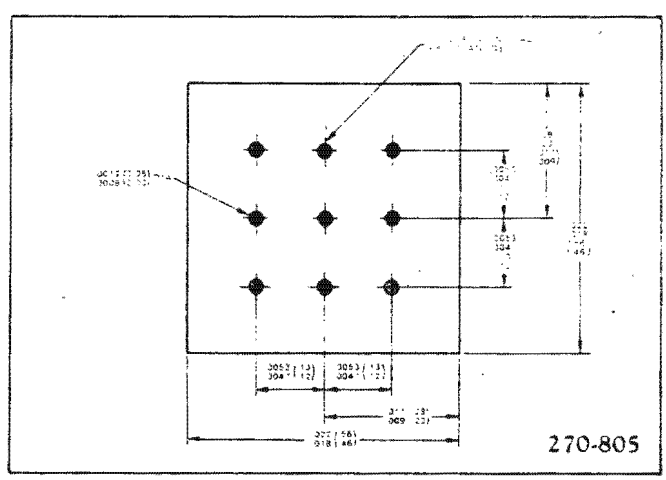

Note: Millimeters in parentheses.

Alpha

Printed in U.S.A.
Specifications subject to change without notice.

These diodes are categorized by noise figure for mixer applications in three frequency ranges: X, Ku, and Ka-bands. Chips are available for use up to 90 GHz. Gallium arsenide diodes are particularly well suited for image enhancement mixer circuits due to their high cutoff frequency. Conversion loss for these diodes approaches the theoretical minimum of 3.0 dB (single sideband) in X-band and is significantly lower than silicon Schottky diodes at frequencies above 12 GHz.

Matched pairs of mixer diodes are used in conjunction with a hybrid or magic-tee primarily for suppressing noise originating in the local oscillator. They are also used to isolate the local oscillator arm from the signal arm, thus minimizing radiation and absorption of signal power. Other uses are for specific reflection of signals through the hybrid and for balanced modulators and discriminators.

The matching criteria for packaged mixer diodes are as follows:

a) Conversion loss (within 0.3 dB of each other)
b) IF impedance (within 25 ohms of each other)
c) The VSWR of individual diodes, when not otherwise restricted (such as 1.3 on premium units), is limited to 1.6 max.

These specifications allow the noise figure of the receiver to deteriorate no greater than 0.1 dB due to local oscillator noise. The VSWR limit allows a maximum of 5% leakage; in practice, this leakage is generally less than 2%.

A typical V_f vs I_f curve is plotted in Figure 1. Figure 2 shows a typical plot of capacitance vs bias voltage.

Noise Figure and IF Impedance as a function of Local Oscillator drive level with DC bias is shown in Figure 3.

Diodes may also be especially tailored to meet your particular electrical specifications or package configuration needs.

See Catalog Section VIII for Application Notes:

80800 Mixer and Detector Diodes
80000 Bonding Methods
80850 Handling Precautions for Schottky Barrier and Point Contact Mixer and Detector Diodes

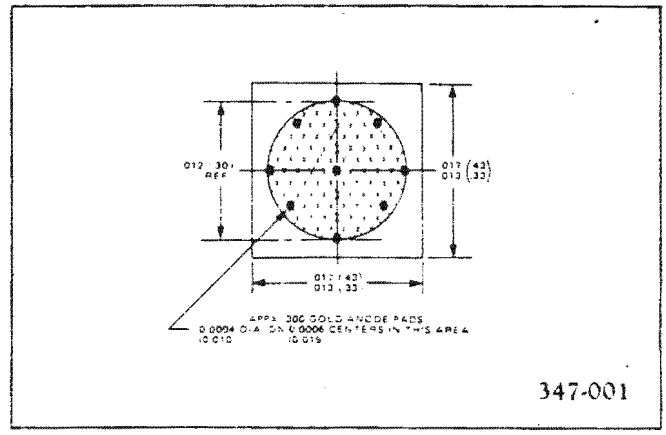

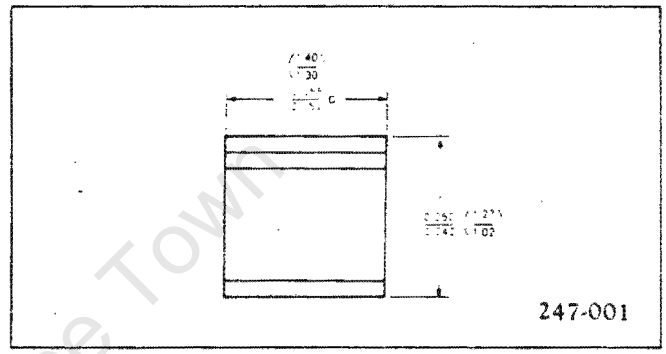

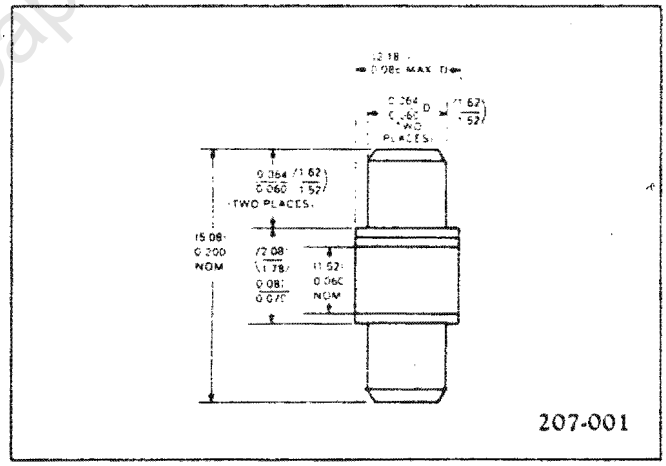

Note: Millimeters in parentheses.

Typical Ku-Band Mixer Diodes

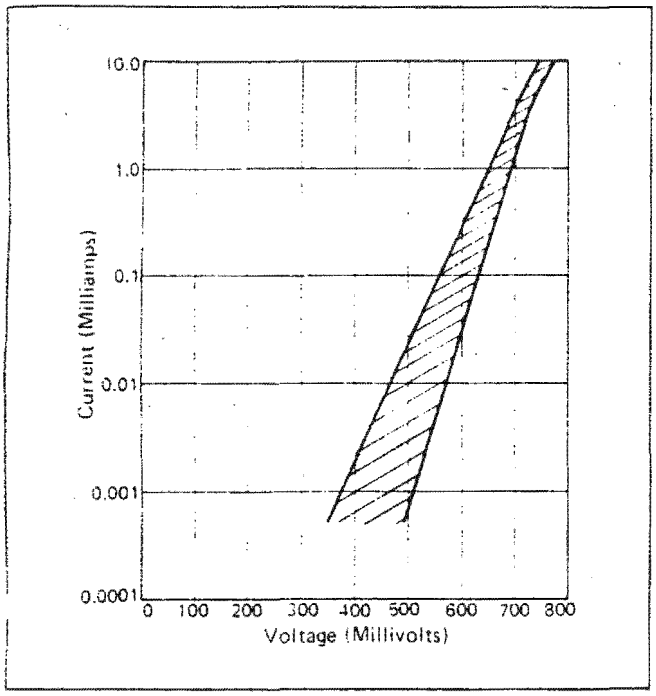

Figure 1. Forward DC Characteristic Curve Range—Voltage vs Current

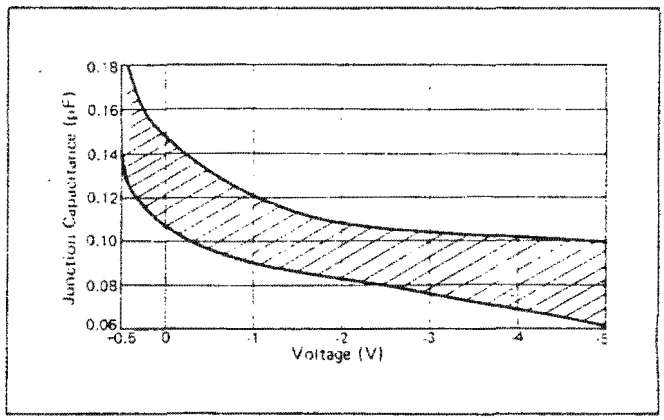

Figure 2. Junction Capacitance Range vs Voltage

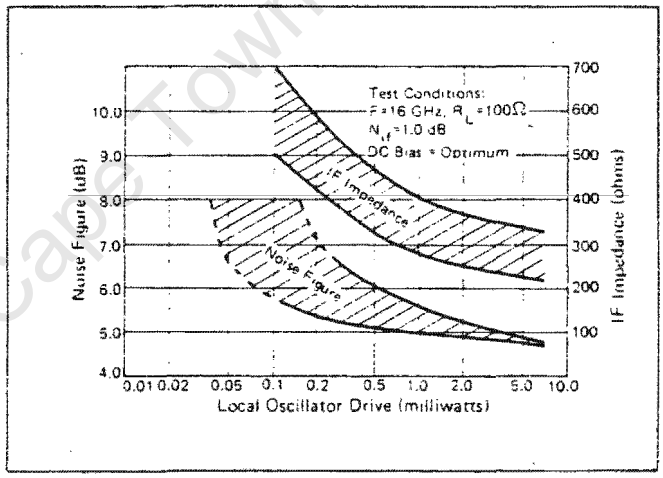

Figure 3. RF Parameters vs Local Oscillator Drive Level

Frequency Band	Type Number: Polarity Reversible	Electrical Characteristics: NF[1] dB Max.	F_{co}[2] (GHz) Min.	Cj@0V pf Min.	Cj@0V pf Max.	Package Outline
Packaged:						
X	DMK6600A	4.5	750	0.10	0.20	207-001
X	DMK6601A	4.5	750	0.10	0.20	247-001
X	DMK6600	5.0	500	0.10	0.20	207-001
X	DMK6601	5.0	500	0.10	0.20	247-001
Ku	DMK6602A	4.8	750	0.05	0.15	207-001
Ku	DMK5068A	4.8	750	0.05	0.15	247-001
Ku	DMK6602	5.3	500	0.05	0.15	207-001
Ku	DMK5068	5.3	500	0.05	0.15	247-001
Ka	DMK6603A	5.5	600	—	0.08	207-001
Ka	DMK4058A	5.5	600	—	0.08	247-001
Ka	DMK6603	6.0	350	—	0.08	207-001
Ka	DMK4058	6.0	350	—	0.08	247-001
Beam Lead Singles:						
X	DMK6604A	5.0[3]	500	0.10	0.20	174-001
X	DMK6604	5.5[3]	350	0.10	0.20	174-001
Ku	DMK6605A	5.3[3]	500	0.05	0.15	174-001
Ku	DMK6605	5.8[3]	350	0.05	0.15	174-001
Ka	DMK6606A	6.0[3]	350	—	0.10	174-001
Ka	DMK6606	6.5[3]	300	—	0.10	174-001
mm	DMK4791	—	900	—	0.07	174-001
mm	DMK4784[5]	—	1000	—	0.04	366-001
Beam Lead Pairs:						
Ku	DMK6591	—	500	0.05	0.15	378-012
Beam Lead Quads:						
Ku	DMK6592	—	500	0.05	0.15	294-003
Chips:						
X	CMK7703A	4.5[3]	750	0.10	0.20	270-801
X	CMK7703	5.0[3]	500	0.10	0.20	270-801
Ku	CMK7704A	4.8[3]	750	0.05	0.15	270-801
Ku	CMK7704	5.3[3]	500	0.05	0.15	270-801
Ka	CMK7705A	5.0[3]	600	—	0.08	270-801
Ka	CMK7705	5.5[3]	350	—	0.08	270-801
Ka	CMK7701	5.5[3]	600	—	0.06	347-001
mm	CMK7702	6.9[3]	1200	—	0.04	347-001

All types:
Forward voltage, V_f = 600-800 mV@1 mA
Breakdown voltage, V_B = 4.0V Min.@10 μA

Notes:
Maximum operating temperature = 150°C
Note 1. Single sideband noise figure measured with L.O. = 7 mW and including N_i = 1.0 dB.
Note 2. $F_{co} = \frac{1}{2\pi R_S C_{j0}}$ where $R_S = R_T$ (@ 10 mA) − R_B; $R_B = \frac{28}{0.01}$ (for 10 mA).
Note 3. Noise figure is determined by lot sampling.
Note 4. Electrical characteristics are specified for each diode in a pair or quad configuration.
Note 5. To be supplied bonded by Alpha on customer substrate.

Frequency Table

Band	Freq. (GHz)
X	8.2-12.4
Ku	12.4-18.0
Ka	26.5-40.0
mm	40.0-100.0

APPENDIX D

FLANGE DIMENSIONS FOR HORN ANTENNAS

Circular flanges

S Band

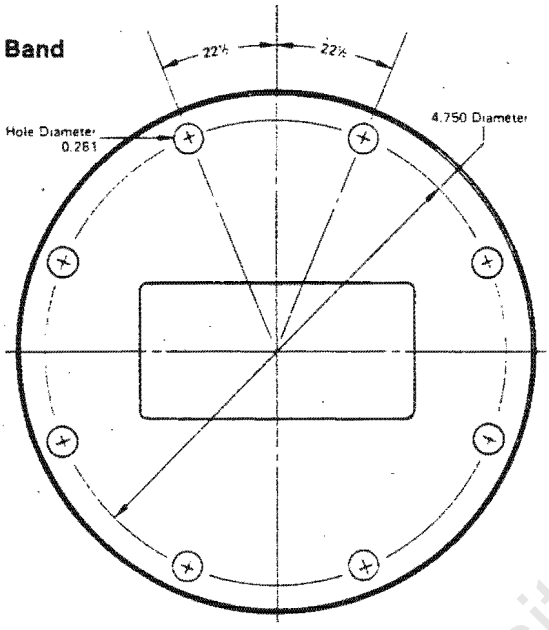

G Band

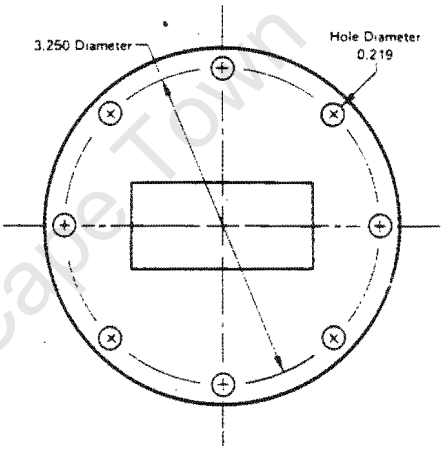

J Band

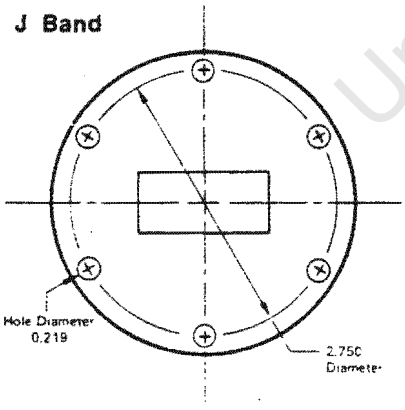

Band Designations		Frequency Range (GHz)	Material B=Brass A=Alum.	Cover Flange UG–	Hole Dia. (In.)
HP	EIA WR–				
S	284	2.60 - 3.95	B A	53 584	0.281
G	187	3.95 - 5.85	B A	149A 407	0.219
J	137	5.85 - 8.20	B A	344 441	0.219

GENERAL INFORMATION
Waveguide
Standard data chart

HP Band Designation	Frequency Range TE$_{10}$ Mode GHz)	Band Designations IEC R-	EIA WR-	British WG-	JAN[1] RG-	Other Common Usage	Material B-Brass A-Alum. S-Silver	JAN[2] Flange Designation Choke UG-	Cover UG-	Waveguide Dimensions Inside Width cm (in.)	Inside Height cm (in.)	Inside Tol ±m (mils)	Outside Width cm (in.)	Outside Height cm (in.)	Outside Tol ±m (mils)	Nom. Wall Thickness mm (in.)	Cutoff Frequency (GHz)	Theoretical Attenuation Low to High Frequency[3] Brass/Alum/Silver dB/100 ft	Theoretical Attenuation Low to High Frequency[3] Brass/Alum/Silver dB/100 Meters	Theoretical[4] CW Power Low to High Frequency Megawatts Kilowatts)
	1.12 - 1.70	14	650	6	69 103	L	B A		417B 418B	16.510 (6.50)	8.255 (3.25)	±12.7 ±5	16.916 (6.66)	8.661 (3.41)	±12.7 (±5)	2.03 (0.080)	0.908	0.412 - 0.272 0.269 - 0.178	1.353 - 0.894 0.883 - 0.584	11.8 - 17.1
	1.45 - 2.20	18	510	7			B A			12.954 (5.10)	6.477 (2.55)	±12.7 ±5	13.360 (5.26)	6.883 (2.71)	±12.7 (±5)	2.03 (0.080)	1.16	0.574 - 0.390 0.374 - 0.255	1.883 - 1.280 1.229 - 0.836	7.5 - 10.6
	1.70 - 2.60	22	430	8	104 105	1S,R	B A		435B 437B	10.922 (4.3)	5.461 (2.15)	±12.7 ±5	11.328 (4.46)	5.867 (2.31)	±12.7 (±5)	2.03 (0.080)	1.375	0.759 - 0.504 0.496 - 0.329	2.492 - 1.655 1.626 - 1.080	5.2 - 7.5
	2.20 - 3.30	26	340	9A	112 113		B A		553A 554A	8.636 (3.40)	4.318 (1.70)	±12.7 ±5	9.042 (3.56)	4.724 (1.86)	±12.7 (±5)	2.03 (0.080)	1.735	1.030 - 0.716 0.673 - 0.468	3.382 - 2.352 2.207 - 1.535	3.4 - 4.71
S	2.60 - 3.95	32	284	10	48 75		B A	54 585A	53 584	7.214 (2.84)	3.404 (1.34)	±12.7 ±5	7.620 (3.00)	3.810 (1.50)	±12.7 (±5)	2.03 (0.080)	2.080	1.435 - 0.982 0.937 - 0.642	4.711 - 3.225 3.074 - 2.105	2.18 - 3.1
	3.30 - 4.90	40	229	11A	— —		B A		CMR229 —	5.817 2.29)	2.908 1.145)	±12.7 ±5	6.142 2.418)	3.233 (1.273)	±12.7 (±5)	1.63 0.064)	2.59	1.828 - 1.296 1.184 - 0.846	6.002 - 4.255 3.917 - 2.777	1.56 - 2.14
G	3.95 - 5.85	48	187	12	49 95	C,H	B A	148C 406B	149A 407	4.755 (1.872)	2.215 (0.872)	±12.7 ±5	5.080 (2.00)	2.540 (1.00)	±12.7 (±5)	1.63 (0.064)	3.16	2.595 - 1.869 1.760 - 1.220	8.849 - 6.134 5.774 - 4.003	(941 - 1317)
C	4.90 - 7.05	58	159	13	— —	C	B A		CMR159 —	4.039 (1.59)	2.019 0.759)	±10.2 ±4	4.364 1.718)	2.344 (0.923)	±10.2 (±4)	1.63 0.064)	3.71	3.091 - 2.324 2.019 - 1.518	10.15 - 7.630 6.622 - 4.980	(754 - 983)
J	5.85 - 8.20	70	137	14	50 106	XN,C,G	B A	343B 440B	344 441	3.484 (1.372)	1.580 (0.622)	±10.2 ±4	3.810 (1.50)	1.905 (0.750)	±10.2 (±4)	1.63 (0.064)	4.29	3.821 - 3.018 2.496 - 1.971	12.54 - 9.907 8.187 - 6.465	(554 - 696)
H	7.05 - 10.00	84	112	15	51 68	XB,W	B A	52B 137B	51 138	2.850 (1.122)	1.262 (0.497)	±10.2 ±4	3.175 (1.25)	1.588 (0.625)	±10.2 (±4)	1.63 (0.064)	5.26	5.355 - 4.161 3.497 - 2.717	17.58 - 13.66 11.47 - 8.913	(355 - 454)
	7.00 - 11.00	—	102	—	— —		B A			2.591 (1.02)	1.295 (0.510)	±7.6 ±3	2.845 (1.12)	1.549 0.610)	±7.6 (±3)	1.27 0.050)	6.50	6.939 - 4.360 4.532 - 2.848	22.78 - 14.31 14.87 - 9.34	(280 - 424)
X	8.20 - 12.40	100	90	16	52 67		B A	40B 136B	39 135	2.286 0.90)	1.016 (0.40)	±7.6 ±3	2.540 (1.00)	1.270 (0.50)	±7.6 (±3)	1.27 (0.050)	6.56	8.362 - 5.784 5.461 - 3.778	27.45 - 18.99 17.91 - 12.39	(206 - 293)
M	10.00 - 15.00	120	75	17	— —		B A			1.905 (0.75)	0.953 (0.375)	±7.6 ±3	2.159 (0.850)	1.207 (0,475)	±7.6 (±3)	1.27 (0.050)	7.88	9.893 - 6.909 6.461 - 4.512	32.48 - 22.68 21.19 - 14.80	(166 - 229)
P	12.40 - 18.00	140	62	18	91 — 107	KU,Y,U	B A S	541A — —	419 — —	1.580 (0.622)	0.790 (0.311)	±6.4 ±2.5	1.783 (0.702)	0.993 (0.391)	±7.6 (±3)	1.02 (0.040)	9.49	12.46 - 0.162 8.141 - 5.984 6.165 - 4.531	40.92 - 30.08 26.71 - 19.63 20.22 - 14.87	(119 - 157)
N	15.00 - 22.00	180	51	19	— —		B A S			1.295 (0.510)	0.648 (0.255)	±6.4 ±2.5	1.499 (0.590)	0.851 (0.335)	±7.6 (±3)	1.02 (0.040)	11.6	17.02 - 12.33 11.12 - 8.054 8.418 - 6.099	55.88 - 40.49 36.47 - 26.42 27.62 - 20.01	(79 - 106)
K	18.00 - 26.50	220	42	20	53 121 66		B A S	596A 598A —	595 (425)[5] 597 —	1.087 (0.420)	0.432 (0.170)	±5.1 ±2	1.270 (0.500)	0.635 (0.250)	±7.6 (±3)	1.02 (0.040)	14.1	26.66 - 19.58 17.41 - 12.79 13.18 - 9.684	87.51 - 64.28 57.11 - 41.95 43.25 - 31.77	(43 - 58)
	22.00 - 33.00	260	34	21	— — —		B A S		1530	0.864 (0.340)	0.432 (0.170)	±5.1 ±2	1.067 (0.420)	0.635 (0.250)	±7.6 (±3)	1.02 0.040)	17.3	32.58 - 22.66 21.27 - 14.80 16.11 - 11.20	106.94 - 74.37 69.79 - 48.54 52.86 - 36.76	(34 - 47)
R	26.50 - 40.00	320	28	22	— — 98	V,KA,U	B A S	600A	599 (381)[5] — —	0.711 (0.280)	0.356 (0.140)	±3.8 ±1.5	0.914 (0.360)	0.559 (0.220)	±5.1 (±2)	1.02 (0.040)	21.1	44.29 - 30.33 28.92 - 19.81 21.9 - 15.00	145.4 - 99.57 94.88 - 64.98 71.85 - 49.21	(23 - 32)
	33.00 - 50.00	400	22	23	— 97	Q	B S		383 —	0.569 (0.224)	0.284 (0.112)	±2.5 ±1	0.772 (0.304)	0.488 (0.192)	±5.1 (±2)	1.02 .0.040)	26.35	30.84 - 20.96	101.2 - 67.78	(14 - 20)
	40.00 - 60.00	500	19	24	— —		B S			0.478 (0.188)	0.2388 (0.094)	±2.5 ±1	0.681 (0.268)	0.442 (0.174)	±5.1 (±2)	1.02 (0.040)	31.4	38.79 - 27.21	127.3 - 89.25	(10 - 14)
V	50.00 - 75.00	620	15	25	— 98	M	B S		385 —	0.3759 (0.148)	0.1879 (0.074)	±2.5 ±1	0.579 (0.228)	0.391 (0.154)	±5.1 (±2)	1.02 .0.040)	39.9	57.30 - 39.15	188.0 - 128.4	(6 - 9)
	60.00 - 90.00	740	12	26	— 99	E	B S		387 —	0.3099 (0.122)	0.1549 (0.061)	±1.3 ±0.5	0.5130 (0.202)	0.3581 (0.141)	±5.1 (±2)	1.02 (0.040)	48.4	78.33 - 52.51	256.9 - 172.3	(4 - 6)
	75.00 - 110.00	900	10	27	— —					0.2540 (0.100)	0.1270 (0.050)	±1.3 ±0.5	0.4572 (0.180)	0.3302 (0.130)	±5.1 (±2)	1.02 (0.040)	59.0	100.5 - 70.71	329.7 - 231.9	(3 - 4)

Abbreviations:
IEC—International Electrotechnical Commission
JAN—Joint Army Navy
EIA—Electronic Industry Association

[1] For more information refer to U.S. Military Specification, MIL-W-85, Waveguide, Rigid, Rectangular.
[2] For more information refer to U.S. Military Specification, MIL-F-3922, Flanges, Waveguide Cover.
[3] Attenuation computations: Rectangular guide, TE_{10} mode; Resistivities, Brass, (65-35) 6.63 x 10^{-6} Ω/cm; Aluminum, 2.83 x 10^{-6} Ω/cm; Silver, 1.62 x 10^{-6} Ω/cm.
[4] CW Power computations: Breakdown strength of air taken at 15,000 volts per centimeter. Safety factor of approximately 2 at sea level is assumed.
[5] HP instrumentation flanges mate with rectangular cover flanges noted. Flange adapters are available to mate with UG-425/U and UG-381/U. Specify 11515A (K-Band, 18.0 - 26.5 GHz) or 11516A (R Band, 26.5 - 40.0 GHz).

APPENDIX E

3 GHz NOTCH FILTER SIMULATION PROGRAMS

```
Touchstone (TM) - Configuration( 100 1600 102 16517 1968 1000 1 3294
              OPENIM.CKT    Sat Dec 10 08:28:31 1988

!IMPEDANCE OF AN OPEN CIRCUIT STUB ON RT-DUROID 5880
!OPERATING RANGE 2-8 GHz
!19 JANUARY 1989

DIM
  FREQ GHZ
  RES OH
  IND NH
  CAP PF
  LNG MM
  TIME PS
  COND /OH
  ANG DEG

CKT
          MSUB ER=2.2  H=0.254  T=0.01778  RHO=0.34  RGH=0
          MLIN 1  2  W=0.76  L=18.29
          MLOC 2     W=0.76  L=18.29              !OCSTUB AT 3 GHz
          MLIN 2  3  W=0.76  L=18.29
          DEF2P  1  3  FIL

FREQ
  SWEEP  2  8  0.05

OUT
  FIL  DB[S11] GR1
  FIL  DB[S12] GR1

GRID
  RANGE  2  8  0.5
  GR1    -70 10 10
```

Touchstone (TM) - Configuration(100 1600 102 16517 19[illegible]
OPENIM.OUT Sat Dec 10 10:21:57 1988

FREQ-GHZ	DB[S11] FIL	DB[S12] FIL
2.00000	-3.803	-2.547
2.50000	-1.251	-6.656
3.00000	-0.157	-41.027
3.50000	-1.233	-6.654
4.00000	-3.808	-2.560
4.50000	-7.116	-1.100
5.00000	-11.266	-0.482
5.50000	-17.674	-0.213
6.00000	-49.833	-0.139
6.50000	-17.582	-0.223
7.00000	-11.223	-0.509
7.50000	-7.110	-1.160
8.00000	-3.846	-2.675

```
Touchstone (TM) - Configuration( 100 1600 102 16517 1968 1000 1 3294 )
             3GNOTCH.CKT     Tue Sep 26 00:51:20 1989

! THIS PROGRAM IS USED TO DETERMINE THE TRANSMISSION AND REFLECTION
! COEFFICIENTS FOR A 3 GHz NOTCH FILTER / 6 GHz PASS FILTER
! 29 JULY 1988

DIM
  FREQ GHZ
  RES OH
  IND NH
  CAP PF
  LNG MM
  TIME PS
  COND /OH
  ANG DEG


CKT

  MSUB   ER=2.2  H=0.2548  T=0.01778  RHO=0.84  RGH=0  !RT 5880
  MLIN   1  2  W=0.76  L=72.79                        !INPUT SECTION
  MLOC   2  W=0.76  L=18.29                           !1ST OC STUB
  MLIN   2  3  W=0.76  L=18.29                        !QW AT 3 GHz
  MLOC   3  W=0.76  L=18.29                           !2ND OC STUB
  MLIN   3  4  W=0.76  L=18.29                        !QW AT 3 GHz
  MLOC   4  W=0.76  L=18.29                           !3RD OC STUB
  MLIN   4  5  W=0.76  L=18.29                        !QW AT 3 GHz
  MLOC   5  W=0.76  L=18.29                           !4TH OC STUB
  MLIN   5  6  W=0.76  L=72.79                        !OUTPUT SECTION
  DEF2P  1  6  FIL


OUT

  FIL DB[S11]  GR1
  FIL DB[S21]  GR1

FREQ
  SWEEP  2  8  .03

GRID
  RANGE  2  8  .5
  GR1    -100 30 10
```

APPENDIX F

A NOTCH FILTER ANALYSIS TECHNIQUE USING PIN DIODES

An important analysis technique in describing the stub filter is to compare its operation to that of isolation PIN diodes used to protect mixer diodes.

PIN diodes are often used to protect mixer diodes, by absorbing any excess energy which might damage the mixer diodes. The degree of protection (i.e the amount of attenuation of the input signal) is determined by the number of PIN diodes connected in parallel with the mixer diode, as well as the spacing (in fractions of wavelengths) between the PIN diodes.

A mathematical technique will be used to show how the protection technique works and then to analyse the operation of filter.

To simplify the explanation and make it more applicable to the stub filter, only forward biased PIN diodes will be used. The reason for this is that PIN diodes provide most of their isolation in this bias position.

The assumption is made that the impedance of a forward biased PIN diode is 1Ω , and that of the mixer diode is 50Ω .

Single PIN diode protection

A simple circuit realisation is:

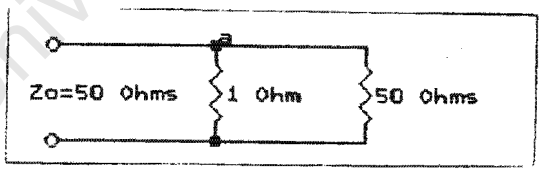

The two resistances are taken in parallel and hence provide an input impedance of:

$$Z(a) = 1//50$$
$$= \underline{0.98\Omega}$$

The reflection coefficient at (a) is:

$$\rho = \frac{Z(a)-Z_o}{Z(a)+Z_o}$$

$$= \frac{0.98-50}{0.98+50}$$

$$= \underline{-0.9616}$$

The amount of power reflected from (a) is:

$$P_{ref}(a) = |\rho|^2 * P_{in}$$

$$= \underline{0.925\ P_{in}}$$

The amount of power transmitted is:

$$P_{tr}(a) = P_{in} - 0.925 * P_{in}$$

$$= \underline{0.075\ P_{in}}$$

Of this ratio the amount of power absorbed by the PIN diode is:

$$P_{pin} = 0.075 * P_{in} * \frac{50}{51}$$

$$= \underline{7.35*10^{-2}*P_{in}}$$

The amount absorbed by the mixer diode:

$$P_{mix} = 0.075 * P_{in} * \frac{1}{51}$$

$$= \underline{1.47*10^{-3}*P_{in}}$$

The isolation provided by the forwarded biased PIN diode:

$$= 10 * \mathrm{Log}_{10} * \frac{1.47*10^{-3}*P_{in}}{P_{in}}$$

$$= \underline{-28.3\ dB} \qquad \ldots(1)$$

Double PIN diode protection

A second PIN diode is connected in parallel with the first PIN diode. It is assumed initially that the two PIN diodes are half a wavelength apart, and that both are forward biased. The isolation provided is calculated as follows:

As before, a parallel branch of models the protection scheme.

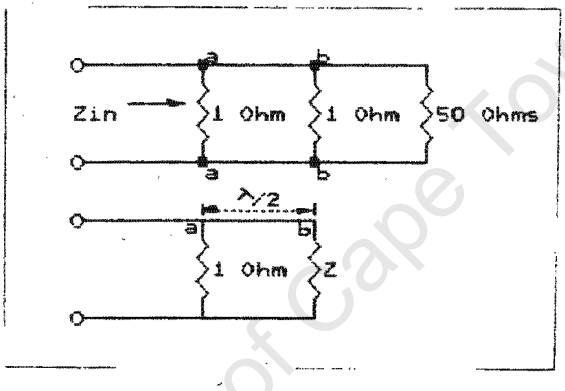

at (b) $Z_{in}(b) = 1//50$

$= \underline{0.98\Omega}$

Since the impedance at (b) is $\lambda/2$ away from (a), the resistances are effectively on top of each other.

Hence the impedance at (a) can be calculated as follows:

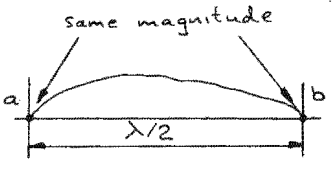

$Z(a) = 1//0.98$

$= \underline{0.495\Omega}$

Reflection coefficient: $\rho = \dfrac{Z(a)-Z_o}{Z(a)+Z_o}$

$= \dfrac{0.495-50}{0.495+50}$

$$= \underline{-0.9804}$$

Power reflected at (a): $P_{ref}(a) = |\rho|^2 * P_{in}$

$$= \underline{0.9612 * P_{in}}$$

Power transmitted at (a): $P_{tr}(a) = P_{in} - P_{in} * |\rho|^2$

$$= \underline{0.0388 * P_{in}}$$

Power at (b): $= 0.0388 * P_{in} * \frac{1}{1.98}$

$$= \underline{0.0196 * P_{in}}$$

Power absorbed by mixer diode: $= 0.01996 * P_{in} * \frac{1}{51}$

$$= \underline{3.843 * 10^{-4} * P_{in}}$$

Isolation: $= 10 * \text{Log}_{10} * \frac{3.843 * 10^{-4} * P_{in}}{P_{in}}$

$$= \underline{-34.15 \text{ dB}} \quad ..(2)$$

This is $\underline{34.15 - 28.3} = \underline{5.85 \text{ dB}}$

If the second PIN diode is placed $\lambda/4$ away from the first PIN diode, the isolation is determined as follows:

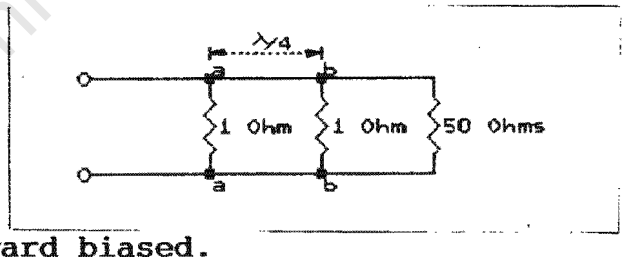

Both PIN's forward biased.

$$Z_{in}(b) = 1//50$$

$$= \underline{0.98\Omega}$$

Since the two diodes are $\lambda/4$ apart the impedance at (b) can be transformed to (a):

$$Z(a) = Z_o^2/Z(b)$$
$$= 50^2/0.98$$
$$= \underline{2551\Omega}$$

The impedance at (a) is then: $Z_{in} = 1//2551$
$$= \underline{0.9996\,\Omega}$$

Reflection coefficient at (a): $\rho = \frac{Z_{in}-Z_o}{Z_{in}+Z_o}$

$$= \frac{0.9996-50}{0.9996+50}$$

$$= \underline{-0.9608}$$

Power reflected at (a): $P_{ref}(a) = |\rho|^2 * P_{in}$
$$= 0.9608^2 * P_{in}$$
$$= \underline{0.9231 * P_{in}}$$

Power transmitted $P_{tx}(a) = \underline{0.0768 * P_{in}}$

Power transmitted to (b): $P_{tx}(b) = 0.0768 * P_{in} * \frac{1}{1+2551}$

$$= \underline{3*10^{-5} * P_{in}}$$

Power absorbed by mixer: $= 3*10^{-5} * P_{in} * \frac{1}{51}$

$$= \underline{5.88*10^{-7} * P_{in}}$$

Therefore the isolation provided by this combination is:

$$10 * \mathrm{Log}_{10} * \frac{5.88*10^{-7} * P_{in}}{P_{in}}$$

$$= \underline{-62.3\ dB} \qquad \ldots(3)$$

Comparing (1),(2) and (3), it can be seen that two forward biased PIN diodes placed $\lambda/4$ apart provide the greatest protection for a mixer diode. It can also be seen that placing the PIN diodes at $\lambda/4$ rather than $\lambda/2$ spacings provides the mixer diode with almost 30 dB more protection.

Analysing the stub filter

Looking at the operation of the stub filter, it can be seen that the stub spacing fulfills the same isolation effect as the spacing between the PIN diodes. Looking at the 3 GHz notch filter we find the following:

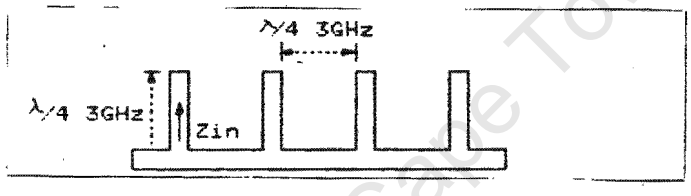

It can be seen that at 3 GHz, the spacing is $\lambda/4$ i.e. greatest isolation. This means that most of the power will be absorbed in the open circuit stub (enfused by the fact that the stub offers little impedance to a 3 GHz signal).

For any 6 GHz component, the spacing between the stubs is $\lambda/2$, and as we have seen this configuration provides the least isolation. Hence since the $\lambda(3)/4$ open circuit stubs offer a high impedance to the 6 GHz signal, and there is little isolation between the stubs, there is little attenuation to a 6 GHz component in this filter.

The 6 GHz notch filter can be similarly described but the explanation would be superfluous and will not be attempted here.

APPENDIX G

6 GHz NOTCH FILTER SIMULATION PROGRAMS

```
Touchstone (TM) - Configuration( 100 1600 102 16517 1968 1000 1 3
              6GNOTCH.CKT     Tue Sep 26 00:52:55 1989

! THIS PROGRAM DETERMINES THE REFLECTION AND TRANSMISSION
! COEFFICIENTS FOR A 6 GHz NOTCH FILTER / 3 ghZ PASS FILTER
! 13 JULY 1988

DIM
  FREQ GHZ
  RES OH
  IND NH
  CAP PF
  LNG MM
  TIME PS
  COND /OH
  ANG DEG


CKT

  MSUB    ER=2.2  H=0.2548  T=0.01778  RHO=0.84  RGH=0  !RT 5880
  MLIN    1  2  W=0.76  L=36.19                        !INPUT SECTION
  MLSC    2  W=0.76  L=18.29                           !1ST SC STUB
  MLIN    2  3  W=0.76  L=8.3825                       !QW AT 3 GHz
  MLSC    3  W=0.76  L=18.29                           !2ND SC STUB
  MLIN    3  4  W=0.76  L=8.3825                       !QW AT 3 GHz
  MLSC    4  W=0.76  L=18.29                           !3RD SC STUB
  MLIN    4  5  W=0.76  L=8.3825                       !QW AT 3 GHz
  MLSC    5  W=0.76  L=18.29                           !4TH SC STUB
  MLIN    5  6  W=0.76  L=36.19                        !OUTPUT SECTION
  DEF2P   1  6  FIL


OUT

  FIL DB[S11]  GR1
  FIL DB[S21]  GR1

FREQ
  SWEEP  2  8  .03

GRID
  RANGE  2  8  .5
  GR1    -100 30 10
```

```
Touchstone (TM) - Configuration( 100 1600 102 16517 1968 1000 1 3294 )
             6GSNOTCH.CKT     Tue Sep 26 00:54:27 1989

! EDIT THIS FILE TO CREATE NEW CIRCUIT FILES.
! DESIGN FOR 6 GHz NOTCH FILTER / 3 GHz PASS FILTER
! INCORPORATING THE SCREW RESISTANCE TO GROUND (SC SECTIONS)
! 13 JULY 1988

DIM
  FREQ GHZ
  RES OH
  IND NH
  CAP PF
  LNG MM
  TIME PS
  COND /OH
  ANG DEG


CKT

  MSUB    ER=2.2  H=0.2548  T=0.01778  RHO=0.84  RGH=0  !RT 5880
  MLIN    1  2  W=0.76  L=36.19                        !INPUT SECTION
  MLIN    2  3  W=0.76  L=18.29                        !1ST SC STUB
  RES     3  0  R=1                                    !RES TO GROUND
  MLIN    2  4  W=0.76  L=8.3825                       !QW AT 3 GHz
  MLIN    4  5  W=0.76  L=18.29                        !2ND SC STUB
  RES     5  0  R=1                                    !RES TO GROUND
  MLIN    4  6  W=0.76  L=8.3825                       !QW AT 3 GHz
  MLIN    6  7  W=0.76  L=18.29                        !3RD SC STUB
  RES     7  0  R=1                                    !RES TO GROUND
  MLIN    6  8  W=0.76  L=8.3825                       !QW AT 3 GHz
  MLIN    8  9  W=0.76  L=18.29                        !4TH SC STUB
  RES     9  0  R=1                                    !RES TO GROUND
  MLIN    8  10 W=0.76  L=8.3825
  MLIN    10  11 W=0.76  L=18.29
  RES     11  0  R=1
  MLIN    10  12  W=0.76  L=8.3825
  MLIN    12  13  W=0.76  L=18.29
  RES    13  0  R=1
  MLIN    12 14  W=0.76  L=36.19                       !OUTPUT SECTION
  DEF2P   1  14  FIL


OUT

  FIL DB(S11)  GR1
  FIL DB(S21)  GR1

FREQ
  SWEEP  2  8  .03

GRID
  RANGE  2  8  .5
  GR1    -100 30 10
```

APPENDIX H

THREE PORT AND POWER SPLITTER SIMULATION PROGRAMS

```
Touchstone (TM) - Configuration( 100 1600 102 16517 1968 1000 1 3294 )
              3PORT.CKT     Tue Sep 26 00:31:03 1989

!CALCULATING THE ISOLATION BETWEEN PORTS FOR A SIMPLE SPLITTER
!OPERATING RANGE 2-8 GHz
!23 JANUARY 1989

DIM
  FREQ GHZ
  RES OH
  IND NH
  CAP PF
  LNG MM
  TIME PS
  COND /OH
  ANG DEG

CKT
          MSUB ER=2.2  H=0.254  T=0.01778  RHO=0.84  RGH=0
          MLIN 1  2  W=0.76  L=18.29
          MLIN 2  3  W=0.76  L=18.29
          MLIN 2  4  W=0.76  L=18.29
          DEF3P  1  3  4  SPLIT

FREQ
  SWEEP  2  8  0.5

OUT
  SPLIT  DB[S11]  GR1
  SPLIT  DB[S12]  GR1
  SPLIT  DB[S13]  GR1
  SPLIT  DB[S23]  GR1

GRID
  RANGE  2  8  0.5
  GR1    -70 10 10
```

Touchstone (TM) - Configuration(100 1600 102 16517 1968 1000 1 3294)
3PORT.OUT Tue Sep 26 00:32:29 1989

FREQ-GHZ	DB[S11] SPLIT	DB[S12] SPLIT	DB[S13] SPLIT	DB[S23] SPLIT
2.00000	-9.686	-3.586	-3.586	-3.586
2.50000	-9.655	-3.593	-3.593	-3.593
3.00000	-9.621	-3.600	-3.600	-3.600
3.50000	-9.593	-3.607	-3.607	-3.607
4.00000	-9.577	-3.612	-3.612	-3.612
4.50000	-9.578	-3.618	-3.618	-3.618
5.00000	-9.594	-3.623	-3.623	-3.623
5.50000	-9.621	-3.628	-3.628	-3.628
6.00000	-9.653	-3.633	-3.633	-3.633
6.50000	-9.683	-3.637	-3.637	-3.637
7.00000	-9.705	-3.642	-3.642	-3.642
7.50000	-9.714	-3.646	-3.646	-3.646
8.00000	-9.710	-3.650	-3.650	-3.650

```
Touchstone (TM) - Configuration( 100 1600 102 16517 1968 1000 1 3294 )
              3PORT2.CKT     Tue Sep 26 00:33:58 1989

!CALCULATING THE ISOLATION BETWEEN PORTS FOR A SIMPLE SPLITTER
!OPERATING RANGE 2-8 GHz
!23 JANUARY 1989

DIM
  FREQ GHZ
  RES OH
  IND NH
  CAP PF
  LNG MM
  TIME PS
  COND /OH
  ANG DEG

CKT
          MSUB ER=2.2   H=0.254   T=0.01778   RHO=0.84   RGH=0
          MLIN 1   2   W=0.76   L=18.29
          MLIN 2   3   W=0.42   L=9.31
          MLIN 2   4   W=0.42   L=9.31
          DEF3P   1   3   4   SPLIT

FREQ
  SWEEP   2   8   0.5

OUT
  SPLIT   DB(S11)  GR1
  SPLIT   DB(S12)  GR1
  SPLIT   DB(S13)  GR1
  SPLIT   DB(S23)  GR1

GRID
  RANGE   2   8   0.5
  GR1     -70 10 10
```

```
Touchstone (TM) - Configuration( 100 1600 102 16517 1968 1000 1 3294 )
              6GSPLIT.CKT     Tue Sep 26 00:40:37 1989

! EDIT THIS FILE TO CREATE NEW CIRCUIT FILES.
!6GHz POWER SPLITTER

DIM
  FREQ GHZ
  RES OH
  IND NH
  CAP PF
  LNG MM
  TIME PS
  COND /OH
  ANG DEG

CKT
   MSUB  ER=2.2  H=0.2548  T=0.01778  RHO=0.84  RGH=0.00
   MLIN  1  2    W=0.76  L=36.57                !50 OHM INPUT
   MLIN  2  3    W=0.43  L=9.31                 !1ST QW SPLIT ELEMENT
   MLIN  2  4    W=0.43  L=9.31                 !2ND QW SPLIT ELEMENT
   RES   3  4    R=100                          !RES. ACROSS PORTS 2 & 3
   MLIN  3  5    W=0.76  L=36.57                !50 OHM OUTPUT SECTION
   MLIN  4  6    W=0.76  L=36.57                !50 OHM OUTPUT SECTION
   DEF3P  1  5  6  SPLIT

OUT
  SPLIT  DB(S11)  GR1
  SPLIT  DB(S12)  GR1
  SPLIT  DB(S13)  GR1
  SPLIT  DB(S23)  GR1
FREQ
  SWEEP  2  8  .03

GRID
  RANGE  2  8  .5
  GR1    -50 10 10
```

```
Touchstone (TM) - Configuration( 100 1600 102 16517 1968 1000 1 3294 )
              6GSPLIT2.CKT     Tue Sep 26 00:36:42 1989

! EDIT THIS FILE TO CREATE NEW CIRCUIT FILES.
!6GHz POWER SPLITTER

DIM
  FREQ GHZ
  RES OH
  IND NH
  CAP PF
  LNG MM
  TIME PS
  COND /OH
  ANG DEG

CKT
   MSUB  ER=2.2  H=0.2548  T=0.01778  RHO=0.84  RGH=0.00
   MLIN  1  2   W=0.7244  L=36.57                !50 OHM INPUT
   MTEE  2  3  4  W1=0.7244  W2=0.3944  W3=0.3944   !APPROX. TEE JUNCTION
   MLIN  3  5   W=0.3944  L=45.88                !1ST QW SPLIT ELEMENT
   MLIN  4  6   W=0.3944  L=45.88                !2ND QW SPLIT ELEMENT
   TFR   5  6   W=0.8  L=0.5  RS=100  F=0     !RES. APPROX ACROSS PORTS 2&3
   MTAPER   5  7  W1=0.3944  W2=0.7244  L=0.4     !APPROX. OF TAPER EFFECT
   MTAPER   6  8  W1=0.3944  W2=0.7244  L=0.4
   MLIN  7  9   W=0.7244  L=36.57                !50 OHM OUTPUT SECTION
   MLIN  8  10   W=0.7244  L=36.57               !50 OHM OUTPUT SECTION
   DEF3P  1  9  10  SPLIT

OUT
  SPLIT  DB[S11]  GR1
  SPLIT  DB[S12]  GR1
  SPLIT  DB[S13]  GR1
  SPLIT  DB[S23]  GR1
FREQ
  SWEEP  2  8  .03

GRID
  RANGE  2  8  .5
  GR1    -50 10 10
```

APPENDIX I

MODE AMPLITUDE FORMULAS AND COUPLER SIMULATION PROGRAMS

Case 2 ($k_L \neq k_C$, $\beta_1 = \beta_2$ and matched terminations): In this case

$$\frac{a_-(0)}{a_-(0)} = \frac{(k_L + k_C)\{j[(\phi_2 - \phi_1)\sin(\theta_1 + \theta_2) + (\phi_2 + \phi_1)\sin(\theta_1 - \theta_2)] - \Delta[\cos(\theta_1 - \theta_2) - \cos(\theta_1 + \theta_2)]\}}{[4(1 + \phi_1\phi_2) - \Delta^2]\cos(\theta_1 + \theta_2) - [4(1 - \phi_1\phi_2) - \Delta^2]\cos(\theta_1 - \theta_2) + j\{[4(\phi_1 - \phi_2) + 2\Delta(\phi_2 - \phi_1)]\sin(\theta_1 + \theta_2) - [4(\phi_1 - \phi_2) - 2\Delta(\phi_1 + \phi_2)]\sin(\theta_1 - \theta_2)\}},$$

$$\frac{a_+(l)}{a_-(0)} = \frac{2\phi_2[2\phi_1\cos\theta_1 + j(2 + \Delta)\sin\theta_1] + 2\phi_1[2\phi_2\cos\theta_2 + j(2 - \Delta)\sin\theta_2]}{\text{DEN of (32)}},$$

$$\frac{b_-(0)}{a_+(0)} = \frac{(k_L + k_C)\{[2\cos(\theta_1 + \theta_2) - 2\cos(\theta_1 - \theta_2)] + j[(\phi_1 + \phi_2)\sin(\theta_1 + \theta_2) + (\phi_2 - \phi_1)\sin(\theta_1 - \theta_2)]\}}{\text{DEN of (32)}},$$

$$\frac{b_+(l)}{a_+(0)} = \frac{2\phi_1[2\phi_2\cos\theta_2 + j(2 - \Delta)\sin\theta_2] - 2\phi_2[2\phi_1\cos\theta_1 + j(2 + \Delta)\sin\theta_1]}{\text{DEN of (32)}}.$$

The coupling is given by

$$C = \left|\frac{b_-(0)}{a_+(0)}\right|,$$

and the directivity is given by

$$D = \left|\frac{b_+(l)}{b_-(0)}\right| = \frac{\left|\begin{array}{l}2(\phi_1\phi_2)(\cos\theta_2 - \cos\theta_1) \\ + j[2(\phi_1\sin\theta_2 - \phi_2\sin\theta_1) \\ - \Delta(\phi_1\sin\theta_2 + \phi_2\sin\theta_1)]\end{array}\right|}{\left(\frac{k_L + k_C}{2}\right)\left|\begin{array}{l}2[\cos(\theta_1 + \theta_2) - \cos(\theta_1 - \theta_2)] \\ + j[(\phi_1 + \phi_2)\sin(\theta_1 + \theta_2) \\ + (\phi_1 - \phi_2)\sin(\theta_1 - \theta_2)]\end{array}\right|}.$$

The input VSWR and impedance may be calculated from

$$\text{input VSWR} = \frac{1 + \left|\frac{a_-(0)}{a_+(0)}\right|}{1 - \left|\frac{a_-(0)}{a_+(0)}\right|}$$

where $a_-(0)/a_+(0)$ is the input reflection coefficient.

```
! THIS PROGRAM IS DESIGNED TO AID IN THE
! CALCULATION OF ODD AND EVEN IMPEDANCES
! FOR MICROSTRIP DIRECTIONAL COUPLED LINES
!
! BY P.ALBERTS SEPTEMBER 1988

! * Definition of variables*
! ZOE - EVEN MODE IMPEDANCE
! ZOO - ODD MODE IMPEDANCE
! ZO - CHARACTERISTIC LINE IMPEDANCE
! W - WIDTH OF LINE (IN mm)
! S - SPACING BETWEEN LINES (IN mm)
! L - LENGTH OF LINE (IN mm)
! ER - RELATIVE PERMEABILTIY OF DIELECTRIC
! H - HEIGHT OF DIELECTRIC (IN mm)
! F - FREE SPACE FREQUENCY (IN Hz)
! * INPUT THE MICROSTRIP VARIABLES

INPUT PROMPT "ER OF BOARD ": ER
INPUT PROMPT "UR OF BOARD(NOMINALLY=1) ":UR
INPUT PROMPT "EREF OF BOARD ": EREF
INPUT PROMPT "HEIGHT OF DIELECTRIC (IN mm) ": H
INPUT PROMPT "CHOOSE CHARACTERISTIC LINE IMPEDANCE ": ZO
INPUT PROMPT "ENTER LENGTH OF LINE (QUARTER WAVELENGTH) ": L
INPUT PROMPT "ENTER SPACING BETWEEN LINES (IN mm) ": S
INPUT PROMPT "ENTER WIDTH OF LINE (IN mm) ": W
INPUT PROMPT "ENTER CENTER FREQUENCY (IN Hz) ": F

! CALCULATING THE FREE SPACE WAVELENGTH

LET C=3E8
LET LO = C / F

! * CALCULATING THE CAPACITIVE AND INDUCTIVE COEFICIENTS

LET A1 = 1 + 0.25*LOG((ER+1)/2)

LET B1 = (SQR(ER+1))/10
LET KC = 0.55*EXP(-(A1*S/H + B1*W/H))

LET A2 = 1 + 0.25*LOG((UR+1)/2)
LET B2 = (SQR(UR+1))/10
LET KL = 0.55*EXP(-(A2*S/H + B2*W/H))

PRINT "KC= ";KC,"KL= ";KL

! * CALCULATING THE PHASE CONSTANT AND THE LENGTH OF THE COUPLING SECTION

LET B = (2*PI*F/C)*(SQR(EREF))*SQR((1-KL*KC)/(1-KL*KL))
LET L = (LO/(4*SQR(EREF)))*SQR((1-KL*KL)/(1-KL*KC))
LET O = B*L

PRINT "LENGTH (IN mm) ";L*1E3

! * CALCULATING THE COUPLING, DIRECTIVITY AND VSWR CONSTANTS

LET C = ((KL+KC)/2)*SIN(O)
LET C = -20*LOG10(C)

LET D = ((KL-KC)/(KL+KC))*O/SIN(O)
LET D = -20*LOG10(D)
```

```
LET A = 1+(KL+KC)*((KL-KC)/4)*((SIN(O))^2+O*(O+SIN(2*O)))
LET VSWR = (1+ABS(A))/(1-ABS(A))

PRINT "C( IN dB)= ";C,"D( IN dB)= ";D,"VSWR= ";VSWR
! * ODD AND EVEN MODE IMPEDANCE

END
```

```
Touchstone (TM) - Configuration( 100 1600 102 16517 1968 1000 1 3294 )
              6GCOUP2.CKT     Tue Sep 26 00:45:17 1989

! THIS PROGRAM DETERMINES THE COUPLING CONSTANTS FOR A COUPLER
! WITH A QUARTER WAVELENGTH COUPLING SECTION. CENTRE FREQUENCY IS 6 GHz

DIM
  FREQ GHZ
  RES OH
  IND NH
  CAP PF
  LNG MM
  TIME PS
  COND /OH
  ANG DEG


CKT
    MSUB   ER=9.6 H=0.635   T=0.034   RHO=0.84   RGH=0
    MCLIN   1 2 3 4   W=.56   S=.4   L=4.86      !SEPAR.=0.4mm
    DEF4P   1   2   3   4    COUP


OUT
  COUP DB[S11]   GR1
  COUP DB[S21]   GR1
  COUP DB[S31]   GR1
  COUP DB[S41]   GR1

FREQ
  SWEEP    2   8   0.5


GRID
  RANGE    2   8   0.5
  GR1    -50   10   10
```

```
Touchstone (TM) - Configuration( 100 1600 102 16517 1968 1000 1 3294 )
              6GCOUP3.CKT     Tue Sep 26 00:48:04 1989

! THIS PROGRAM DETERMINES THE COUPLING CONSTANTS FOR A COUPLER
! WITH A QUARTER WAVELENGTH COUPLING SECTION. CENTRE FREQUENCY IS 6 GHz

DIM
  FREQ GHZ
  RES OH
  IND NH
  CAP PF
  LNG MM
  TIME PS
  COND /OH
  ANG DEG


CKT
    MSUB   ER=9.6 H=0.635   T=0.034   RHO=0.84   RGH=0
    MCLIN   1 2 3 4   W=.492   S=.468   L=4.86      !SEPAR.=0.4mm
    DEF4P   1   2   3   4    COUP


OUT
  COUP DB[S11]   GR1
  COUP DB[S21]   GR1
  COUP DB[S31]   GR1
  COUP DB[S41]   GR1

FREQ
  SWEEP    2   8   0.5


GRID
  RANGE    2   8   0.5
  GR1    -50   10   10
```

APPENDIX J

AVANTEK VTO-8100 OSCILLATOR CHARACTERISTCS

LIMITED FREQUENCY RANGE VARACTOR-TUNED OSCILLATORS

COMMERCIAL VARACTOR TUNED OSCILLATORS

Avantek VTO-8000 Series oscillators use a silicon transistor chip as a negative resistance oscillator. The oscillation frequency is determined by a varactor diode acting as a voltage-variable capacitor in a thin-film microstripline resonator. This provides extremely fast tuning speed, limited primarily by the internal impedance of the user-supplied voltage driver.

A typical oscillator can be swept across its frequency band in less than one microsecond.

The VTO-8000 Series varactor-tuned oscillators are packaged in TO-8 transistor cans for simple installation in a conventional 50-Ohm microstripline PC board. They are ideal for the most compact, lightweight commercial and military equipment designs.

VTO-8000 SERIES

Guaranteed Specifications at 25° C Case Temperature (0 to 65° C Operating Temperature) PC6

Model	Frequency Range (GHz)	Power Output into 50 Ohms, Min. (dBm)	Power Output Variation Maximum (dB)	Tuning Voltage Limits (at each end of specified freq. range) +VDC @ Low Freq.	+VDC @ High Freq.	Input Power (±1% Reg.) Voltage (VDC)	Current (mA) Maximum	All Harmonics Typical (dBc)	Case Type
VTO-8030	0.3-0.45	-10	±1.5	5±4	50±10	+15	50	-15	TO-8V
VTO-8040	0.4-0.6	-13	±1.5	3±1	40±8	+15	50	-15	TO-8V
VTO-8060	0.6-1.0	-13	±1.5	3±1	40±8	+15	50	-15	TO-8V
VTO-8080	0.8-1.4	+13	±1.5	2±1.5	35±10	+15	50	-15	TO-8V
VTO-8090	0.9-1.6	+13	±1.5	2±1	48+8; -10	+15	50	-15	TO-8V
VTO-8100	1.0-1.4	+10	±1.5	2±1	48±8	+15	50	-15	TO-8V
VTO-8150	1.5-2.5	-10	±1.5	2.5±1	47±8	+15	50	-18	TO-8V
VTO-8200	2.0-3.0	-10	±1.5	2+2; -1	30±8	+15	50	-18	TO-8V
VTO-8240	2.4-3.7	-10	±1.5	2+2; -1	30±8	+15	50	-18	TO-8V
VTO-8300	3.0-3.5	-10	±1.5	3.5 min.	11 max.	+15	50	-18	TO-8V
VTO-8350	3.5-4.5	+10	±1.5	5 min.	35 max.	+15	50	-20	TO-8V
VTO-8360	3.6-4.3	-10	±1.5	8±2	24±4	+15	50	-25	TO-8V
VTO-8400	4.0-4.5	-10	±1.5	2 min.	14 max.	+15	50	-25	TO-8V
VTO-8420	4.2-5.0	-10	±1.5	7.5±2.5	25+2.5; -4	+15	50	-25	TO-8V
VTO-8430	4.3-5.8	-10	±1.5	5.5±2	24+3	+15	50	-25	TO-8V
VTO-8490	4.9-5.9	+10	±1.5	5.5±2	24+3; -4	+15	50	-25	TO-8V
VTO-8520	5.2-6.1	+10	±1.5	5.5±2	24±3	+15	50	-25	TO-8V
VTO-8540	5.4-5.9	+10	±1.5	8 min.	28 max.	+15	50	-15	TO-8V
VTO-8580	5.8-6.6	+7	±1.5	5±2.5	24+3; -5	+15	50	-25	TO-8V
VTO-8650	6.5-8.6	+10	±1.5	2±1	20±5	+15	100	-20	TO-8V
VTO-8790	7.9-10.1	+10	±2	3±2	26±4	+15	150	-10	TO-8V
VTO-8810	8.1-9.1	+10	±2	2 min.	16 max.	+15	100	-15	TO-8V
VTO-8850	8.5-9.6	+10	±1.5	5±2	13±5	+15	100	-25	TO-8V
VTO-8950	9.5-10.5	+10	±1.5	4±1	10 max.	+15	100	-20	TO-8V
VTO-81000	10.0-10.25	+10	±1.5	0 min.	15 max.	+15	100	-15	TO-8V

COMMERCIAL HYPERABRUPT VARACTOR TUNED OSCILLATORS

This family of oscillators is similar to the standard commercial VTO-8000 Series except for the incorporation of a silicon hyperabrupt varactor tuning diode. This enables the oscillator to be tuned over the specified range in less than 20 volts rather than 40-50 volts in conventional oscillators. They feature extremely fast tuning speed, limited primarily by the internal impedance of the user-supplied voltage driver.

VTO-9000 SERIES

Guaranteed Specifications at 25° C Case Temperature (0° to 65° C Operating Temperature) PC8

Model	Frequency Range (GHz)	Power Output into 50 Ohms, Min. (dBm)	Power Output Variation Maximum (dB)	Tuning Voltage Limits (at each end of specified freq. range) +VDC @ Low Freq.	+VDC @ High Freq.	Input Power (±1% Reg.) Voltage (VDC)	Current (mA) Maximum	All Harmonics Typical (dBc)	Case Type
VTO-9032	0.32-0.64	-10	±2	0 min.	+20 max.	+15	50	-14	TO-8V
VTO-9050	0.5-0.9	-10	±2	0 min.	+20 max.	+15	50	-10	TO-8V
VTO-9068	0.68-1.38	+10	±2	0 min.	+20 max.	+15	50	-14	TO-8V
VTO-9090	0.9-1.6	-10	±2	+2 min.	+18 max.	+15	50	-14	TO-8V
VTO-9120	1.2-2.0	+10	±2	+2 min.	+14 max.	+15	50	-14	TO-8V
VTO-9130	1.3-2.3	-10	±1.5	+2 min.	+20 max.	+15	50	-15	TO-8V
VTO-9140	1.4-2.1	-10	±1.5	+4±2	+10±2	+15	50	-15	TO-8V

Avantek, Inc. • 3175 Bowers Ave., Santa Clara, Ca 95054 • Phone: (408) 727-0700 • FAX: (408) 727-0539 • TWX: 310-371-6717 or 310-371-6478 • TELEX 34-6337

VARACTOR TI
Avantek MTO-
temperature
VTO-8000 Ser
lators. They a
guaranteed to
of -54° to +85
higher reliabi

MTO-8000 SI
Guaranteed Spec

Model
MTO-8040
MTO-8060
MTO-8090
MTO-8240
MTO-8360
MTO-8650
MTO-8950

CASE DRAWING
CASE DRAWING

BUFFERED V
The VTD Ser
gral buffer am
in-line packag
than 0.2 oz.
fabricated or
using advanc
silicon transis
Internal buffe
in load impec
producing +1
VTD to be us
wideband isc
lightly-loadec

VTD SERIES
Guaranteed Spe

Model
VTD-600
VTD-2000
VTD-2800
VTD-3800
VTD-4900

Avantek, Inc. •

broadband linear

Power Amplifiers

up to 1 Watt (+30 dBm)

700 MHz to 4.2 GHz

case style selection

outline drawings see section 1

RF-IF signal processing guide
Mini-Circuits

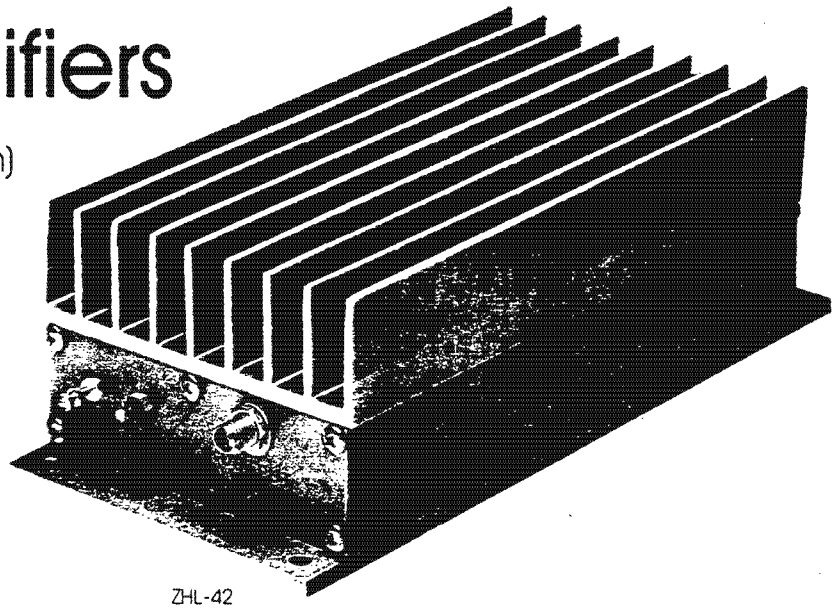

ZHL-42

	MODEL NO.	FREQUENCY GHz	GAIN, dB Min.	GAIN, dB Flatness Max	MAXIMUM POWER, dBm Output (@dB) Compression	MAXIMUM POWER, dBm Input (no damage)	DYNAMIC RANGE NF, dB Typ.	DYNAMIC RANGE Intercept pt., dBm 3rd order Typ.	VSWR In	VSWR Out	DC POWER Volt.	DC POWER Current	PRICE $ Ea.	PRICE $ Qty.
ZHL-42 case U 36	ZHL-42	0.7-4.2	30	±1.0	+29	+10	10	+38	2.5:1	2.5:1	15	0.69A	895	(1-9)
	ZHL-4240	0.7-4.2	40	±1.5	+29	0	4	+33	2.5:1	2.5:1	15	0.7A	1395	(1-9)

NOTES:

1. Operating temperature −20°C to +65°C
   Storage temperature −55°C to +100°C
2. With no load output, derate maximum input power (no damage) by 10dB.
3. Prices and specifications subject to change without notice.

FEATURES

- up to 1w, covers 700 MHz to 4.2 GHz
- ultra-linear Class A design provides unconditional stability
- any load impedance can be connected without concern for damage or oscillation
- ideally suited for TACAN, mobile radio, telemetry, anti-collision, and satellite communications systems
- use to boost signal/sweep generator output, achieve broadband isolation, and provide up to four test set ups with a four-way splitter
- exceptionally low price
- one-year guarantee
- immediate delivery

ZHL-42

FREQ. (MHz)	GAIN, dB Forward	GAIN, dB Reverse	LINEARITY Comp. (dB)	LINEARITY P_{out} (dBm)	NOISE FIGURE (dB)	VSWR in	VSWR out
700.25	33.56	47.42	1.18	28.91	7.3	1.57	1.98
845.84	33.44	47.61	1.05	28.82	7.17	1.54	1.67
991.85	33.61	47.66	0.86	29.29	7.17	1.51	1.42
1137.60	34.37	47.97	0.93	29.98	7.17	1.46	1.37
1283.50	34.54	47.96	0.61	30.42	7.20	1.43	1.36
1429.70	34.09	48.08	0.07	30.65	7.17	1.60	1.33
1575.50	34.06	48.00	0.16	30.53	7.19	1.67	1.47
1720.90	34.65	48.03	0.80	30.65	7.21	1.72	1.43
1866.60	35.05	48.15	1.41	30.46	7.24	1.62	1.32
2013.10	35.42	48.30	1.75	30.57	7.28	1.57	1.20
2158.00	35.21	48.36	1.40	30.53	7.33	1.47	1.21
2304.20	34.72	48.35	1.30	30.13	7.42	1.48	1.16
2448.60	34.42	48.27	1.22	29.77	7.39	1.49	1.15
2595.20	34.55	48.36	1.05	29.91	7.38	1.51	1.18
2741.40	33.78	48.26	0.31	30.01	7.38	1.37	1.24
2887.60	34.03	48.29	0.32	30.35	7.39	1.34	1.52
2999.40	34.25	48.39	0.49	30.38	7.40	1.28	1.94
3033.30	34.05	48.50	0.29	30.50	7.41	1.24	1.99
3179.70	33.85	48.35	0.36	30.27	7.43	1.24	1.74
3324.30	34.01	48.62	0.77	30.04	7.43	1.30	1.56
3470.30	34.34	48.51	0.79	30.19	7.47	1.39	1.43
3616.70	34.49	48.76	1.07	29.91	7.52	1.58	1.28
3763.00	34.65	48.61	0.72	29.73	7.58	1.67	1.11
3909.00	32.36	48.49	0.33	29.69	7.62	1.54	1.21
4053.50	33.32	48.74	0.05	30.30	7.96	1.39	1.39
4199.90	34.60	48.69	0.08	30.04		1.44	1.84

ZHL-4240

700.00	45.20	1.18	28.91	3.9	1.23	1.65
875.00	45.38	1.05	28.82	3.9	1.20	1.29
1050.00	44.65	0.86	29.29	3.9	1.23	1.22
1225.00	44.40	0.93	29.98	3.8	1.22	1.37
1400.00	44.47	0.61	30.42	3.8	1.34	1.33
1575.00	44.93	0.07	30.65	3.8	1.50	1.20
1750.00	45.46	0.80	30.65	3.9	1.30	1.20
1925.00	45.48	1.75	30.57	3.9	1.26	1.22
2100.00	44.99	1.30	30.13	3.9	1.23	1.22
2275.00	44.57	1.22	29.77	3.8	1.40	1.18
2450.00	44.37	1.05	29.91	3.6	1.49	1.20
2625.00	44.45	0.31	30.01	3.6	1.64	1.41
2800.00	44.70	0.32	30.35	3.6	1.59	1.76
2975.00	44.88	0.49	30.38	3.6	1.52	1.90
3150.00	45.64	0.36	30.27	3.6	1.32	1.98
3325.00	46.25	0.77	30.04	3.6	1.28	1.73
3500.00	45.92	0.79	30.19	3.6	1.37	1.32
3675.00	45.19	1.07	29.91	3.8	1.41	1.24
3850.00	44.85	0.33	29.69	3.8	1.56	1.48
4025.00	45.18	0.05	30.30	3.8	1.41	1.55
4200.00	46.71	0.08	30.04	4.1	1.66	1.96

Mini-Circuits P.O. BOX 166, Brooklyn, New York 11235 (718) 934-4500

APPENDIX K

LINE IMPEDANCES FOR SINGLE ENDED MIXER

The figure below indicates a microstrip single ended mixer with RF choke and RF bypass. The RF choke is the shorted quarter wavelength line. It is used to provide a path for the IF rectified current, while being a high impedance to RF signals. The RF bypass is the low impedance, open circuit patch on the IF output. It ensures that the RF signals are applied across the diode, and that the IF component is sent to the IF output port. The following section proves these principles.

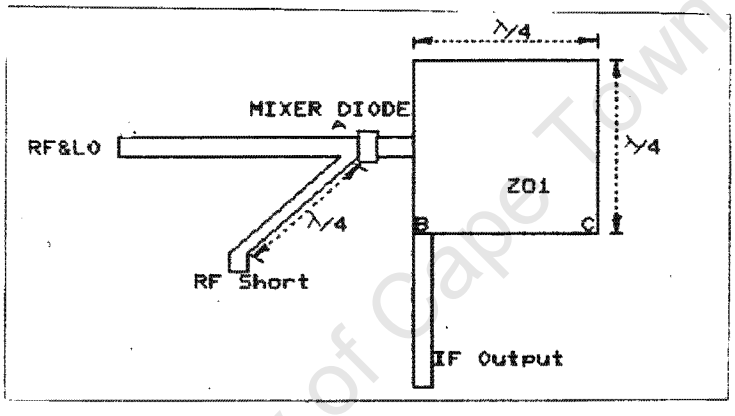

The RF bypass

At a : $Z_{in} = \frac{Z_o * Z_1 + j * Z_o * \tan \beta l}{Z_o + j * Z_1 * \tan \beta l}$

now : $\beta = \frac{2 * \pi}{\lambda}$

For the case of the RF signals $l = \lambda/4$

then : $Z_{in} = \frac{Z_o * Z_1 * \cos\pi/2 + j * Z_o * \sin\pi/2}{Z_o * \cos\pi/2 + j * Z_1 * \sin\pi/2}$

$= \frac{Z_o^2}{Z_1}$

The load is a short circuit, thus $Z_1=0$ and hence $Z_{in} = 50^2/0 \longrightarrow \infty$
Therefore at RF frequencies, the RF bypass acts as a high impedance. The stub will now be analysed at IF frequencies.
The wavelength at 6 GHz is $\lambda_1 = 0.05$ m (RF signal)
at 10.7 MHz $\lambda_2 = 28.04$ m (IF component)

As can be seen the at 10.7 MHz the short circuit stub is not /4 long, but rather $\frac{\lambda * 28.04}{4*0.05} = \frac{\lambda * 560.8}{4}$ long.

Now at 6 GHz $\lambda/4 = 0.05/4 = \underline{0.0125 \text{ m}}$
The length of the stub at 10.7 MHz, in terms of wavelengths, is thus: $\frac{0.0125*\lambda}{28.04} = \underline{4.458*10^{-4} * \lambda}$

Thus the impedance of the stub at 10.7 MHz is:

$$Z_{in} = \frac{Z_o*Z_1*\cos(2*\pi*4.458*10^{-4}) + j*Z_o*\sin(2.8*10^{-3})}{Z_o*\cos(2.8*10^{-3}) + j*Z_1*\sin(2.8*10^{-3})}$$

$$= \frac{Z_o*Z_1*0.999 + j*Z_o*2.8*10^{-3}}{Z_o*0.999 + j*Z_1*2.8*10^{-3}}$$

$$|Z_{in}| = Z_o * \frac{(Z_1*0.999)^2 + (Z_o*2.8*10^{-3})^2}{(Z_o*0.999)^2 + (Z_1*2.8*10^{-3})^2}$$

letting $Z_o = 50\Omega$, $Z_1 = 0$

$$|Z_{in}| = \underline{0.14\Omega}$$

Thus, at an IF frequency of 10.7 MHz, the stub has a low impedance of 0.14Ω .
The stub thus provides a DC return for the rectified RF current.

<u>The RF bypass</u>
Similiar to the previous analysis, the impedance of the patch to the RF and IF signals can be calculated and the operation as a RF bypass confirmed.

The impedance looking in at b can be calculated as follows. The

impedance at c is an open circuit, the characteristic impedance of the patch Z_{o1} is low since the patch is wide. The impedance at b is given by:

$$Z_b = Z_{o1}^2/Z_1 \longrightarrow 0 \text{ since } Z_1 \rightarrow \infty$$

Thus there is very little impedance to RF signals through this patch. This patch thus also provides isolation of the RF signals from the IF output. An important quantity in single ended mixer design. The higher the isolation, the better.

At 10.7 MHz the λ(6 GHz)/4 section is $4.458*10^{-4}*\lambda$(10.7 MHz). The impedance looking in at b is then given by:

$$Z_{in}(\text{at b}) = \frac{Z_{o1}*Z_1*0.999 + j*Z_{o1}*2.8*10^{-3}}{Z_{o1}*0.999 + j*Z_1*2.8*10^{-3}}$$

letting X = 0.999 and Y = $2.8*10^{-3}$, and inserting into the equation above, gives.

$$Z_{in}(\text{at b}) = \frac{Z_{o1}*Z_1*X + j*Z_{o1}*Y}{Z_{o1}*X + j*Z_1*Y}$$

Using L'hospitals rule:

$$= \lim_{Z_1 \rightarrow \infty} Z_{o1}*\frac{(Z_1*X + j*Z_{o1}*Y)}{(Z_{o1}*X + j*Z_1*Y)}$$

$$= \lim_{Z_1 \rightarrow \infty} Z_{o1}*\frac{\frac{\partial}{\partial Z_1}(Z_1*X + j*Z_{o1}*Y)}{\frac{\partial}{\partial Z_1}(Z_{o1}*X + j*Z_1*Y)}$$

$$Z_{in}(\text{at b}) = \lim_{Z_1 \rightarrow \infty} \frac{Z_{o1}*X}{j*Y}$$

$$= \frac{Z_{o1}*356.8}{j}$$

Therefore $|Z_{in}(\text{at 10.7 MHz})| = |Z_{o1}*356.8|$

This is still a reasonably high resistance, eventhough Z_{o1} is a low characteristic impedance. The IF signals will travel down the low impedance IF output line, rather than through the open circuit quarter wavelength patch.

APPENDIX L

SCEMATIC OF COUNTER CIRCUIT

AND ANZAC MD 162 BALANCED MIXER CHARACTERISTICS

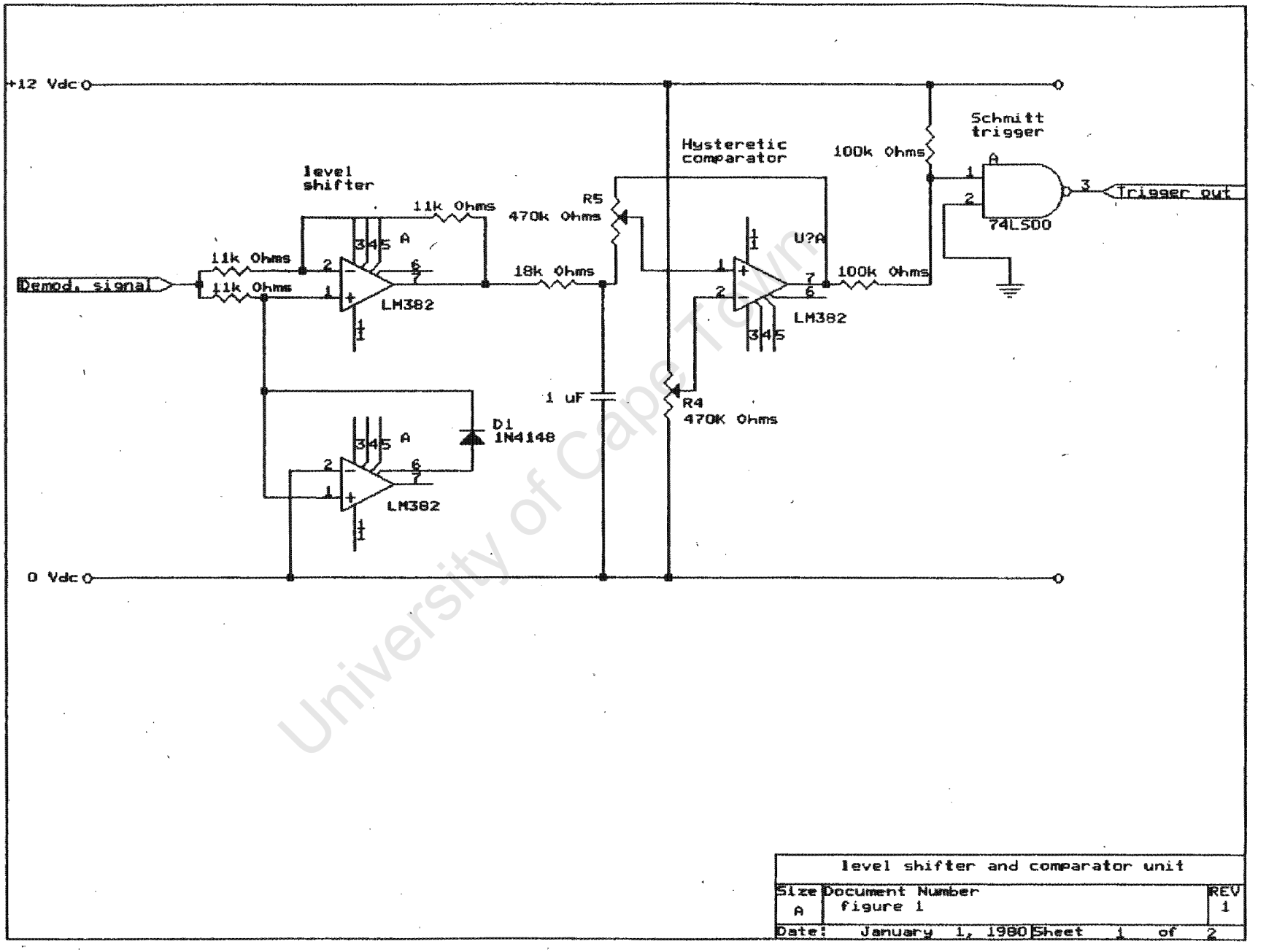

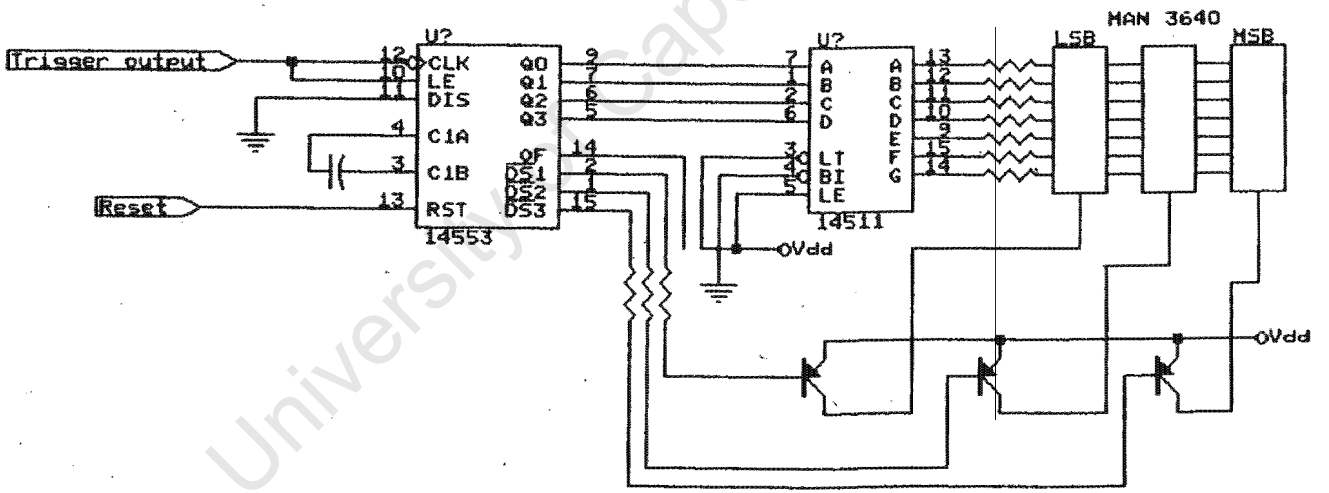

counter unit and display		
Size A	Document Number figure 2	REV 1
Date: January 1, 1980	Sheet 2 of 2	

OPERATING CHARACTERISTICS

The MC14553B three-digit counter, shown in Figure 3, consists of three negative edge-triggered BCD counters which are cascaded in a synchronous fashion. A quad latch at the output of each of the three BCD counters permits storage of any given count. The three sets of BCD outputs (active high), after going through the latches, are time division multiplexed, providing one BCD number or digit at a time. Digit select outputs (active low) are provided for display control. All outputs are TTL compatible.

An on chip oscillator provides the low frequency scanning clock which drives the multiplexer output selector. The frequency of the oscillator can be controlled externally by a capacitor between pins 3 and 4, or it can be overridden and driven with an external clock at pin 4. Multiple devices can be cascaded using the overflow output, which provides one pulse for every 1000 counts.

The Master Reset input, when taken high, initializes the three BCD counters and the multiplexer scanning circuit. While Master Reset is high the digit scanner is set to digit one; but all three digit select outputs are disabled to prolong display life, and the scan oscillator is inhibited. The Disable input, when high, prevents the input clock from reaching the counters, while still retaining the last count. A pulse shaping circuit at the clock input permits the counters to continue operating on input pulses with very slow rise times. Information present in the counters when the latch input goes high, will be stored in the latches and will be retained while the latch input is high, independent of other inputs. Information can be recovered from the latches after the counters have been reset if Latch Enable remains high during the entire reset cycle.

FIGURE 3 — EXPANDED BLOCK DIAGRAM

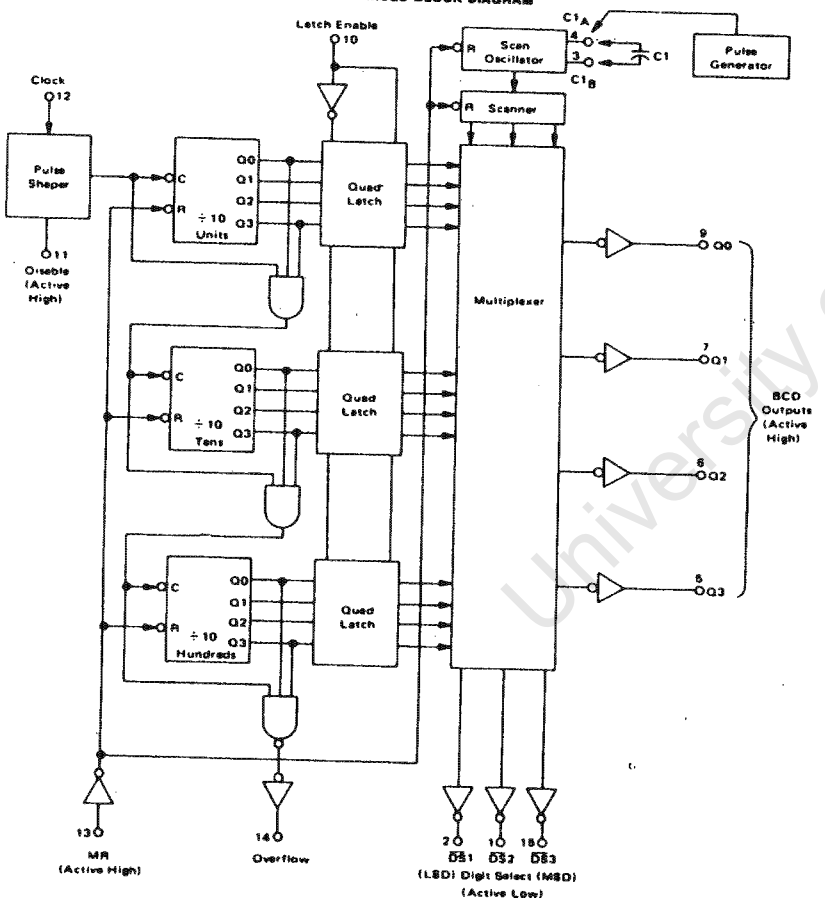

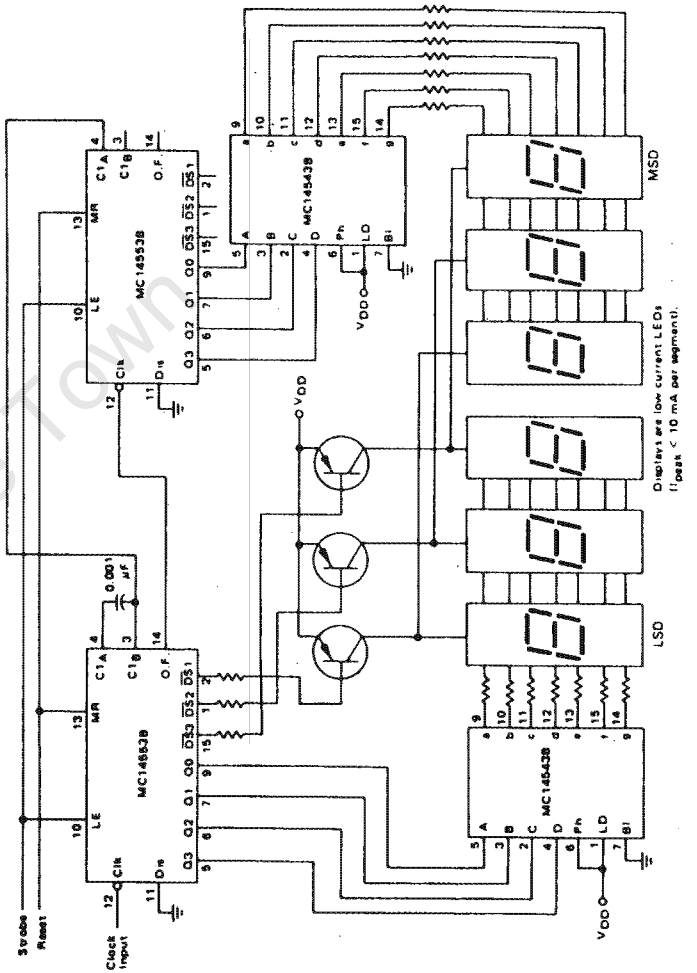

FIGURE 4 — SIX-DIGIT DISPLAY

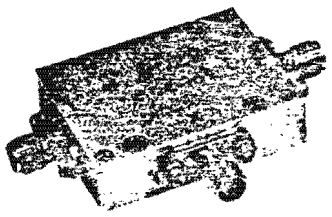

TERMINATION-INSENSITIVE MICROWAVE MIXER

1-7 GHz

- Intermodulation Ratio Insensitive to IF Port Mismatches
- 6 dB Typical Midband Conversion Loss

Guaranteed Specifications*

(From -55°C to +85°C)

Frequency Range:		
RF, LO Ports		1-7GHz
IF Port		10-2000 MHz
Conversion Loss:**		
1.5-5.5 GHz		7.5 dB Max
1-7 GHz		8.5 dB Max
Isolation:		
LO to RF	(1-3 GHz)	15 dB Min
	(3-7 GHz)	17 dB Min
LO to IF	(1-3 GHz)	20 dB Min
	(3-7 GHz)	13 dB Min
RF to IF	(1-3 GHz)	17 dB Min
	(3-7 GHz)	12 dB Min

Operating Characteristics

Impedance:	50 Ohms Nominal
Maximum Input:	
Total Power	350 mW Max @ 25°C Derated 3.5 mW/°C
RF Input:	
1 dB Compression	+8 dBm Typical
1 dB Desensitization	+6 dBm Typical
SSB Noise Figure:	Within 1 dB of Conversion Loss Max
3rd Order Input Intercept:	
2.0 GHz	+16.5 dBm Typical
7.0 GHz	+18.0 dBm Typical
3rd Order Intercept Degradation:	1.5 dB Typical @ IF Termination VSWR 3:1

* All specifications apply when operated at +13 dBm available LO power with 50 ohm source and load impedance.

** For IF frequencies of 10-500 MHz and an RF of -10 dBm or lower.

† Independent of sum frequency match.

This product contains elements protected by United States Patent Number 4,224,572.

Typical Performance**

CONVERSION LOSS

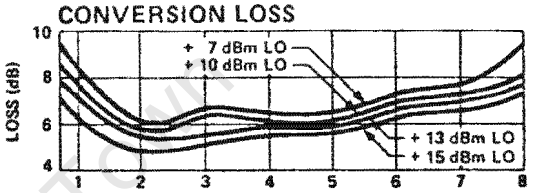

CONVERSION LOSS VS IF PORT TERMINATION†

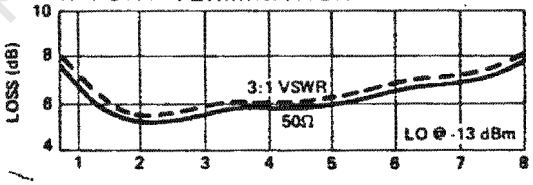

3rd ORDER INTERCEPT

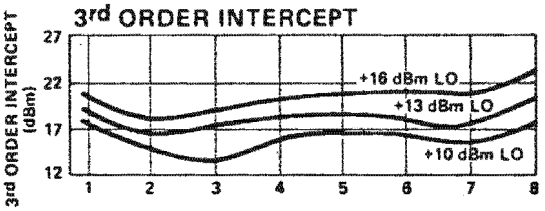

3rd ORDER INTERCEPT VS IF PORT TERMINATION†

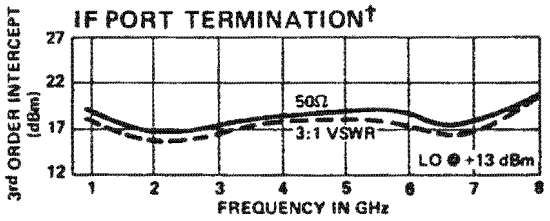

Environmental

This unit has been designed to meet or exceed the following environmental criteria:

Governing Document: MIL-STD-202E		
Test	Method	Condition
Visual Inspection	Anzac Workmanship Manual	
Mechanical Inspection	Device Outline Dwg.	
Hermetic Seal *	112	D
Shock	213	C
Acceleration	212	A
Vibration	204	D
Resistance to Soldering *	210	C
Thermal Shock	107	A
Moisture Resistance	106	

Specific device testing to these and other environmental tests is available at additional cost.

* These tests apply to MD-162 only

Schematic

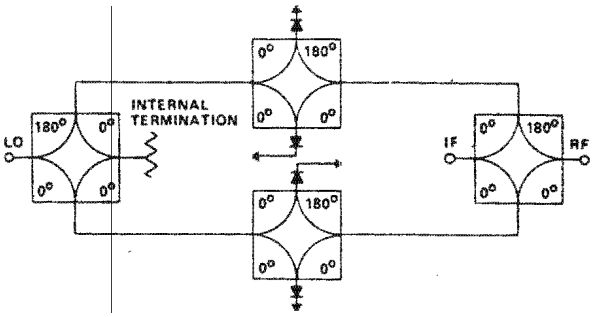

Typical Performance

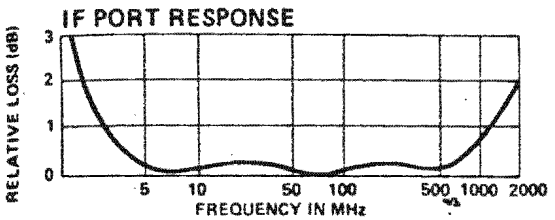

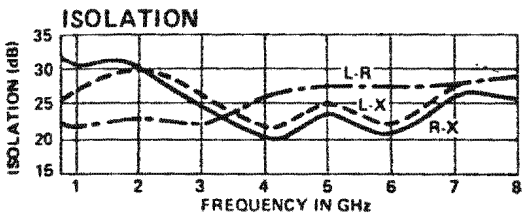

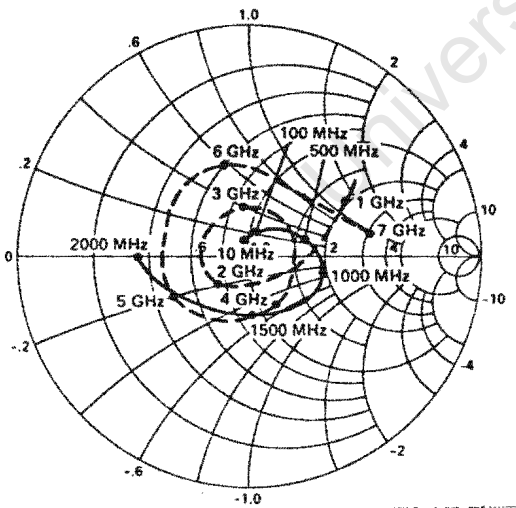

RF & LO IMPEDANCE

IF IMPEDANCE

Mechanical Data

MDC-162

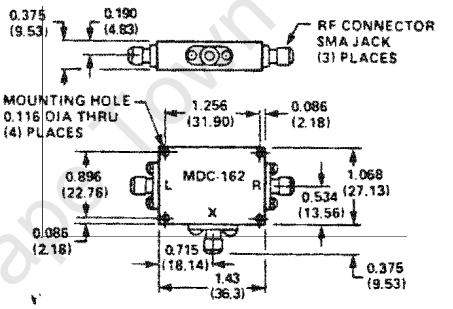

UNLESS OTHERWISE NOTED, .XXX = ± 0.020 °(.X = ± 0.5)
WEIGHT (APPROX.): 1.2 OUNCES 34.5 GRAMS
*DIMENSIONS IN ( ) ARE IN MM
FINISH: CHEMICAL CLEAR PER MIL-C-5541 B, CLASS 3.

MD-162

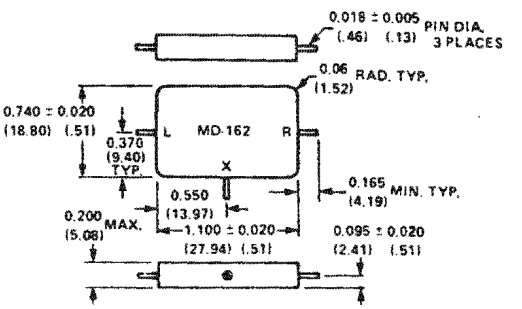

UNLESS OTHERWISE NOTED, .XXX = ± 0.010 °(.X = ± 0.03)
WEIGHT (APPROX.): 0.35 OUNCES 9.9 GRAMS
*DIMENSIONS IN ( ) ARE IN MM
FINISH: CASE AND LEADS - GOLD ELECTROPLATED PER MIL-G-45204 TYPE 3, CLASS 2
LEADS: WELDABLE AND SOLDERABLE PER MIL-STD-12768

Ordering Information

MODEL NO.	PART NO.	CONNECTORS	UNIT PRICE (1-9 UNITS)
MD-162	9149	—	$380
MDC-162	9144	SMA	475

Delivery is from stock.

80 Cambridge Street, Burlington, Mass. 01803 (617) 273-3333 TWX 710 • 332 • 0258